Experimental Performance Investigation of Double Pass Solar Air Heater with Baffles for Red Chilli Drying

By

Abdu Yasin Kerse

A Thesis Submitted to Department of Thermal and Aerospace Engineering

School of Mechanical, Chemical and Materials Engineering

Office of Graduate Studies

Adama Science and Technology University

August, 2021

Adama, Ethiopia

Experimental Performance Investigation of Double Pass Solar Air Heater with Baffles for Red Chilli Drying

By

Abdu Yasin Kerse

Advisor: Dr. Dawit Gudeta

A Thesis Submitted to Department of Thermal and Aerospace Engineering

School of Mechanical, Chemical and Materials Engineering

Office of Graduate Studies

Adama Science and Technology University

August, 2021

Adama, Ethiopia

DECLARATION

I hereby declare that this Master Thesis entitled "Experimental Performance Investigation of Double Pass Solar Air Heater with Baffles for Red Chilli Drying" is my original work and has not been submitted for the award of any academic degree, diploma, or certificate in any other university. All sources of materials that are used for this thesis have been duly acknowledged through citation.

______________________	________________	______________
Name of the student	Signature	Date

RECOMMENDATION

I, the advisor of this thesis, hereby certify that I have read the thesis entitled "Experimental Performance Investigation of Double Pass Solar Air Heater with Baffles for Red Chilli Drying" prepared under my guidance by Abdu Yasin submitted in partial fulfillment of the requirements for the degree of Master of Science in Thermal Engineering. Therefore, I recommend the submission of the thesis to the department following the applicable procedures.

______________________	____________________	________________
Advisor	Signature	Date

APPROVAL PAGE

I, the advisor of the thesis, hereby certify that the recommendation and suggestions given by the board of examiners are appropriately incorporated into the final thesis entitled "Experimental Performance Investigation of Double Pass Solar Air Heater with Baffles for Red Chilli Drying" by Abdu Yasin.

Advisor	Signature	Date

We, the undersigned, members of the Board of Examiners of the thesis open defense by Abdu Yasin have read and evaluated the thesis entitled "Experimental Performance Investigation of Double Pass Solar Air Heater with Baffles for Red Chilli Drying" and examined the candidate. This is, therefore, to certify that the thesis is accepted for partial fulfillment of the requirement of the degree of Master of Science in Thermal Engineering.

Chairperson	Signature	Date
Internal Examiner	Signature	Date
External Examiner	Signature	Date

Finally, approval and acceptance of the thesis is contingent upon submission of its final copy to the Office of Postgraduate Studies (OPGS) through the Department Graduate Council (DGC) and School Graduate Committee (SGC).

Department Head	Signature	Date
School Dean	Signature	Date
Office of Postgraduate Studies, Dean	Signature	Date

ACKNOWLEDGMENT

First and foremost, my deepest gratitude goes to the almighty ALLAH for giving me the patience, courage, and strength to do this thesis. I would like to express my sincere gratitude to my advisor Dr. Dawit Gudeta for his constant support and guidance throughout this thesis work. Without his precious help this thesis could have never achieved its current form. I would also like to express my deep feeling of happiness to all my families especially my mom, who encourages me to finish this study with full of commitment and everyone who helped me finish this thesis.

Finally, I would like to thank Dr. Addisu Bekele for his encouragement, suggestion, and guidance during my master's study. I would like to thank Adama science and technology university for giving me the chance to join the master's program with full sponsorship.

ABSTRACT

Drying is an important form of food preservation method used to remove the excess moisture content from products for long-term storage without compromising quality. Food preservation by solar drying has become a widespread practice in developing countries to overcome the drawbacks associated with traditional open air drying but developing cheap and energy-efficient solar dryers is still a challenge hence studying a way to improve the efficiency of solar dryers are becoming increasingly important. The main aim of this thesis is to design, develop and experimentally investigate the performance of solar dryer using double pass solar air heater (DPSAH) integrated with baffles and thermal energy storage inside the drying chamber by drying red chilli. The dryer is designed based on requirements to dry 5kg of red chilli and has a double pass solar air heater integrated with baffles to enhance the efficiency of the solar air heater, drying chamber with latent heat storage unit, and a blower. A comparative study of the performance of a DPSAH with and without baffles was conducted, and the result shows that integrating the baffles increases change in air temperature, thermal and exergy efficiency of the solar air heaters by an average value of 6 ℃, 7% and 0.53%, respectively. The effects of mass flow rate on the performance of the enhanced DPSAH is also studied and maximum change in air temperature of 35.8 ℃, 26.7 ℃ and 21.2 ℃ and an average thermal efficiency of 34.80%, 46.99%, and 56.97% were obtained for a mass flow rate of 0.0186 kg/s, 0.037 kg/s and 0.056 kg/s, respectively. The addition of PCM in the drying chamber reduces the air temperature fluctuation and the air is supplied at nearly constant temperature to the drying chamber. Red chilli was dried within 29 h and 56 h, reducing the moisture content from an initial value of 81% (w.b.) to a final value of 11.7% (w.b.) and 14.32%, in the solar dryer and open-air sun drying, respectively. The specific energy consumption of the dryer was 7.52 kWh per kilogram of moisture removed, while the electrical energy consumption of the blower was 7.4% of the total energy. The overall efficiency of the drying system was 8.75%. Finally, an economic analysis was carried out and the pay-back period of the dryer was found to be 2.04 years.

Keywords: Double pass solar air heater, baffles, PCM, paraffin wax, solar drying of red chilli.

TABLE OF CONTENTS

LIST OF FIGURES

LIST OF TABLES

ABBREVIATIONS

FPC	Flat plate collector	CD	Cabinet dryer
TES	Thermal energy storage	MSD	Mixed solar dryer
LHS	Latent heat storage	ISD	Indirect solar dryer
SHS	Sensible heat storage	DPSD	Double pass solar dryer
PCM	Phase change material	PBMs	Packed bed materials
SAH	Solar air heater	EHC	Effective heat capacity
DPSAH	Double pass solar air heater	db	Dry basis
OSD	Open sun drying	wb	Wet basis

NOMENCLATURE

I_{sc} Solar constant (W/m^2)

n Day of the year

I_{ext} Extraterrestrial radiation (W/m^2)

I_0 Extraterrestrial solar radiation on a horizontal surface (W/m^2)

H_0 Extraterrestrial radiation on a horizontal surface (kW/m^2/day)

$\overline{H}$ Monthly average daily global solar radiation on horizontal surface (kW/m^2/day)

$\overline{H}_o$ Monthly average daily extraterrestrial solar radiation a horizontal surface (kW/m^2/day)

$\bar{n}_s$ Monthly average daily hours of bright sunshine

$\overline{N}_s$ Monthly average of the maximum possible daily hours of bright sunshine

$\overline{H}_b$ Monthly average daily beam radiation on a horizontal surface (kW/m^2/day)

$\overline{H}_d$ Monthly average daily diffuse radiation on a horizontal surface (kW/m^2/day)

$\bar{I}$ Monthly average hourly global solar radiation on horizontal surface (W/m^2)

$\bar{I}_b$ Monthly average hourly beam radiation on a horizontal surface (W/m^2)

$\bar{I}_d$ Monthly average hourly diffuse radiation on a horizontal surface (W/m^2)

I_T Total hourly irradiance on a tilted surface (W/m^2).

R_b Beam radiation factor

m Mass (kg)

h_{fg} Latent heat of vaporization of water (kJ/kg)

Q_r Energy required for the drying process (kJ)

T Temperature (°C)

$\dot{m}$ Mass flowrate (kg/s)

V Volume (m^3)

$\dot{V}$ Volume flowrate (m^3/s)

t_d Drying time per day (hr)

Q Heat (KJ)

A Area (m^2)

L Length (m)

W Width (m)

$\dot{Q}$ Rate of heat (kW)

$\dot{E}x$ Exergy rate (kW)

FC Fixed cost

PP Payback period

GREEK SYMBOLS

ρ	Density (kg/m^3)	α_s	Solar altitude angle (º)
ϕ	Latitude (°)	γ_s	Solar azimuth angle (º)
θ	Angle of incidence (°)	ε	Emissivity
β	Tilt angle (°)	τ_g	Transmissivity of the glass cover
ω	Hour angle (°)	α_a	Absorptivity of the absorber plate
γ	Surface azimuth angle (°)	ξ	Porosity (%)
δ	Declination (°)	η	Efficiency (%)
θz	Zenith angle (°)		

SUBSCRIPTS

p	Product	c	Collector
i	Initial	T	total
f	Final	t	tray
a	Air	b	Bulk
o	Outlet	ch	Charging
amb	Ambient	dich	Discharging
u	Useful	dc	Drying chamber

CHAPTER ONE

INTRODUCTION

1.1 Background of the Study

Ethiopia has great solar energy potential like other countries located in the tropical region and receives a solar irradiation of 5000 – 7000 Wh/m^2 according to region and season. The average solar radiation of the country is 5.2 kWh/m^2/day with a variation from 4.55-5.55 kWh/m^2/day seasonally and from 4.25 to 6.25 kWh/m^2/day based on location (MoWIE, 2017). Despite of such potentials, the utilization of solar energy is insignificant.

One of the applications of solar energy is drying. Drying is an important form of food preservation that is often carried out at farm level right after harvest for the removal of excess moisture to a level that is safe for long time storage without affecting the quality of the final product (Menya and Komakech, 2013). Up to 70 % of agricultural products spoil during the traditional process of open-air drying, especially in tropical and sub-tropical regions (INNOTECH, 2012).

Like many developing countries, most of the population of Ethiopia engaged in farming and about 80% the countries food products cultivated by small farmers, these farmers do not use proper postharvest management technologies, but the traditional open-air dryer techniques (Mengesha, 2020) In this regard, the development and introduction of solar drying as post-harvest technologies are significantly important in improving livelihood development of developing countries.

Solar drying is in practice since the time in memorable for preservation of food and agriculture crops. This was done particularly by open sun drying and has several disadvantages like spoilage of product due to adverse climatic condition like rain, wind, moist, and dust, loss of material due to birds and animals, deterioration of the material by decomposition, insects, and fungus growth. Also, the process is highly labor intensive, time consuming and requires large area. With cultural and industrial development artificial mechanical drying came into practice. This process is highly energy intensive and expensive which ultimately increases product cost. Solar energy is one of the most promising renewable energy sources in the world compared to nonrenewable sources for the purpose of drying of agriculture and industrial products (Toshniwal and Karale, 2013).

Also, as rising populations place pressure on food sources, about one-third of the total food produced for the human consumption are lost, with most of the loss occurring between a harvest and the user in developing countries. Controlling product dryness is the most critical factor for maintaining quality in stored non-perishable foods (Bradford *et al*., 2020). Thus, the solar dryer can be seen as one of the solutions to the food and energy shortages of the nation.

In Ethiopia, different pepper types such as bell (sweet) pepper which is non-pungent, chili (mitimita) and hot pepper (berbere) which is pungent are produced. Capsicum is grown in different agro-ecological areas in which hot pepper predominates. Small scale farmers in various regions especially in Southern and Western Ethiopia extensively produce it. The fruits are consumed as fresh, dried or processes products as vegetable and as a spice (Gebretsadik, 2016). The crop is also one of the important spice cash crops that serve as the source of income particularly for smallholder producers in many parts of the country.

Traditionally, open sun drying is used to obtain the dried chilli and it requires 7 - 20 days to reduce the moisture content to 10-15 % depending on the weather condition (Oberoi *et al*., 2005 and Gupta *et al*., 2018). The process is highly labor intensive, time consuming and requires large area. Thus, Solar drying is the best alternative to produce high-quality dried products within a relatively short period of drying time. On the other hand, the gap between solar energy availability and operating time is the main draw back in solar drying. Thermal energy storage can be used to overcome this problem. Thermal energy storages have been placed at the bottom of the absorber plate in most research works which results side and bottom heat loss. This heat loss can be minimized by placing the thermal energy storage at the inner bottom of the drying compartment.

1.2 Statement of Problem

The agricultural sectors in Ethiopia have the problem of using proper and effective postharvest drying mechanism. Instead, they use traditional method which is open sun drying system and has several disadvantages like poor product quality and high time consumption. As a result, other alternatives which are economical and environmentally friendly should be developed and solar drying is the best alternative. Like sun drying, solar drying also uses the sun as the source of energy. In comparison to the traditional way of drying in an open field, they prevent contamination and high time consumption. However, it is still a challenge to develop cheap and energy-efficient dryers to produce high-quality foods and the efficiency of the solar dryer is a function of the performance of its components. Solar air heater is a part where the solar radiation is converted to heat energy in the solar dryers and conventional solar air heaters have poor thermal efficiency. Also, the gap between solar energy availability and operating time is the main draw back in solar drying. Thermal energy storage can be used to overcome this problem. Thermal energy storages have been placed at the bottom of the absorber plate in most research works which results side and bottom heat loss. This heat loss can be minimized by placing the thermal energy storage at the inner bottom of the drying compartment. Thus, the performance of an indirect solar dryer by integrating baffles into the constructed double pass solar air heater and phase change material inside the drying chamber as a thermal energy storage was evaluated for the purpose of red chilli drying to identify better opportunities to save time and enhance the efficiency.

1.3 Objectives

This section describes the general and specific objective of the study.

1.3.1 General Objective

The general objective of this thesis is experimentally investigating the performance of solar dryer using double pass solar air heater integrated with baffles and thermal energy storage inside the drying chamber for red chilli drying application.

1.3.2 Specific Objectives

- Sizing and fabricating of double pass solar air heater, drying chamber, and thermal energy storage.
- Conducting experiment to evaluate the performance of double pass solar air heater with and without baffles.
- Evaluating the performance of the developed drying system experimentally.
- Comparing the developed solar drying system with that of open sun drying system for red chilli drying.

1.4 Significance of the Study

The significance of this study is providing inexpensive solar air dryer with better performance to substitute the traditional open sun drying. The dryer reduces post-harvest losses due to spoilage of product, loss of material due to birds and animals, deterioration of the material by decomposition, insects, and fungus growth. It also reduces the time required for the process, labor intensity and required area. Additionally, compared to open sun drying, the proposed solar air dryer improves the product quality significantly which as a result produce better income and contributes to the prosperity of the farmers as well as for the country.

1.5 Scope of the Study

This research mainly focuses on experimental analysis of active, indirect solar air dryer for red chilli drying application. This includes analysis of parameters, sizing of the enhanced double pass solar air heater by integrating baffles, drying chamber and thermal energy storage, selection of material, developing the prototype, performing experiment on the dryer, and comparing the experimental result with that of open sun drying. Additionally, energy and exergy analysis for the solar air heater and drying chamber is included. Since this study mainly focuses on experimental analysis, numerical investigation using software is not included in the study.

1.6 Organization of the Study

This thesis is organized in to seven chapters. Chapter one presents introduction of the thesis including background about drying, statement of problem, the general and specific objectives, significance, and scope of the study. The second chapter presents literature reviews about classifications of solar dryer, solar air heater, thermal energy storage and previous works related to solar dryer, summary, and gap for the literature review. Chapter three discusses the methodology for the thesis work that include methods of data collection, material and equipment's and solar radiation estimation. The fourth chapter is about theoretical analysis of the solar dryer which include sizing of its components and energy and exergy analysis of the components of the dryer. Conceptual model, working principle, Manufacturing process, experimental setup and procedure of the solar dryer is presented in chapter five. Chapter six is about discussion of the result and findings obtained from experimental test and chapter seven, the last chapter, presents conclusion of the study and recommendation for further study.

CHAPTER TWO

LITERATURE REVIEW

2.1 Introduction

Considering the growing energy crisis, the demand for green energy alternatives is imminent. The food industry must consider using renewable energy to replace traditional energy-intensive processes; especially drying. In terms of energy efficiency, economy and applicability in rural areas, the use of solar energy to dry food remains attractive. However, there is a huge technological gap (Mohana *et al.*, 2020). It is a challenge to develop cheap, energy-efficient dryers for high-quality food production. The correct design and selection of solar dryer components are essential for the effective use of heat energy.

Many research has been done in solar energy utilization in the past years for food drying applications. In this chapter, classification of solar dryer, enhancement techniques and previous works associated with the solar drying systems are discussed.

2.2 Classification of Solar Dryers

Solar dryers can be classified as high and low temperature dryers based on operating temperature, direct, indirect, mixed and hybrid dryers based on utilization of solar energy. And as forced and natural convection dryers based on the mode of air flow.

2.2.1 Classification According to Operating Temperature

All drying systems can be classified primarily according to their operating temperature ranges into two main groups of high temperature dryers and low temperature dryers. High temperature dryers are necessary when very fast drying is desired and employed when the products require a short exposure to the drying air (Akarslan, 2012). Because of their temperature ranges, most known designs are electricity or fossil-fuel powered. Only a very few practically realized designs of high temperature drying systems are solar-energy heated.

In low temperature dryers, the moisture content of the product is usually brought in equilibrium with the drying air by constant ventilation. Thus, they do tolerate variable heat input. They enable products to be dried in bulk and most suited for long term storage systems. Thus, they are usually known as bulk or storage dryers and practically realized solar energy applications are of this type.

2.2.2 Classification According to the Utilization of Solar Power

According to the utilization of solar power, the drying system is also classified into two groups; open sun drying (OSD) and controlled solar drying (Lingayat *et al*., 2020). Figure 2.1 shows the main classification of solar drying system.

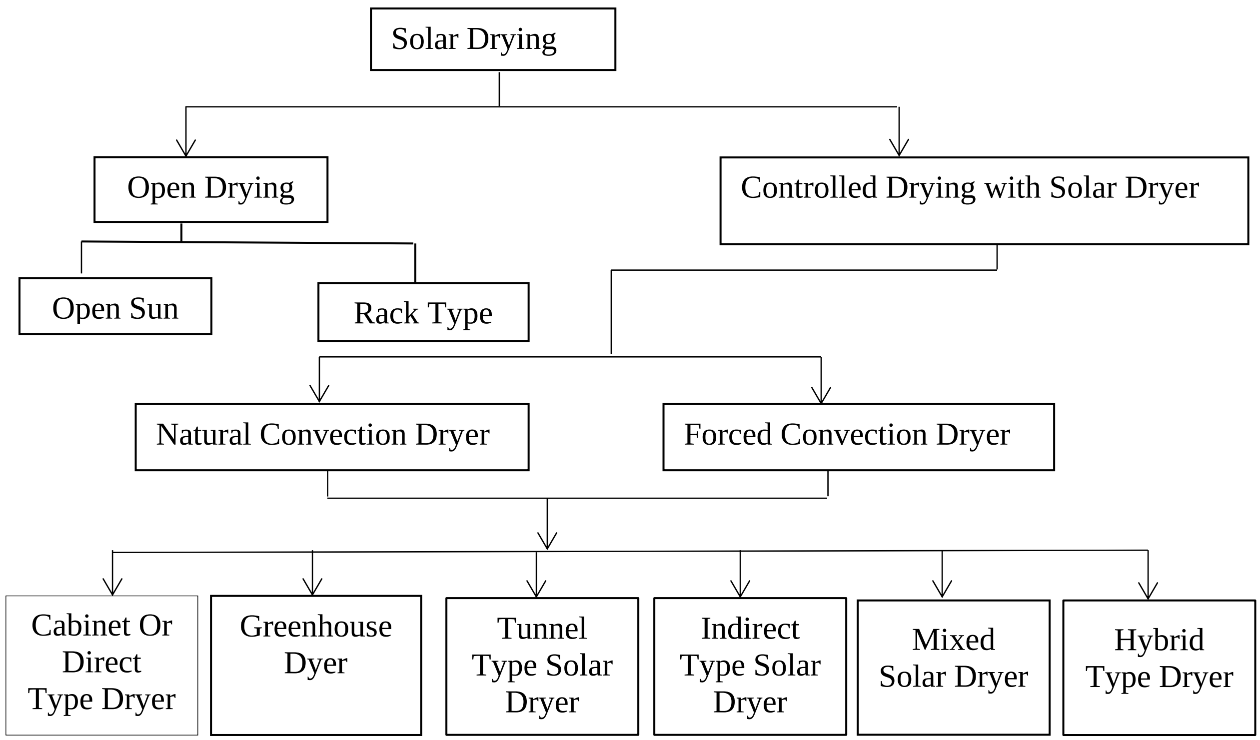

Figure 2.1 Classification of solar dryer system (Lingayat *et al*., 2020)

2.2.2.1 Open sun drying

In open sun drying, the drying products are directly placed under solar radiation to reduce the moisture content. The density difference of atmospheric air creates the movement of air. This way to dry the product involves a thin layer of drying product spread over large space to expose the solar radiation (Kumar and Singh, 2020).

It is well known that the open solar drying is one of the oldest methods used for many years for the preservation of food due to its simple and cost-effective nature. However, there are more possibilities for the contamination of dried products with dust, insects and excreta of wandering animals or insects and the direct exposure to the open atmosphere can greatly reduce the level of nutrients such as vitamins in the dried product which in turn may cause low financial return

(Rakshamuthu *et al*., 2021). Figure 2.2 shows the working principle of open sun drying by using solar energy.

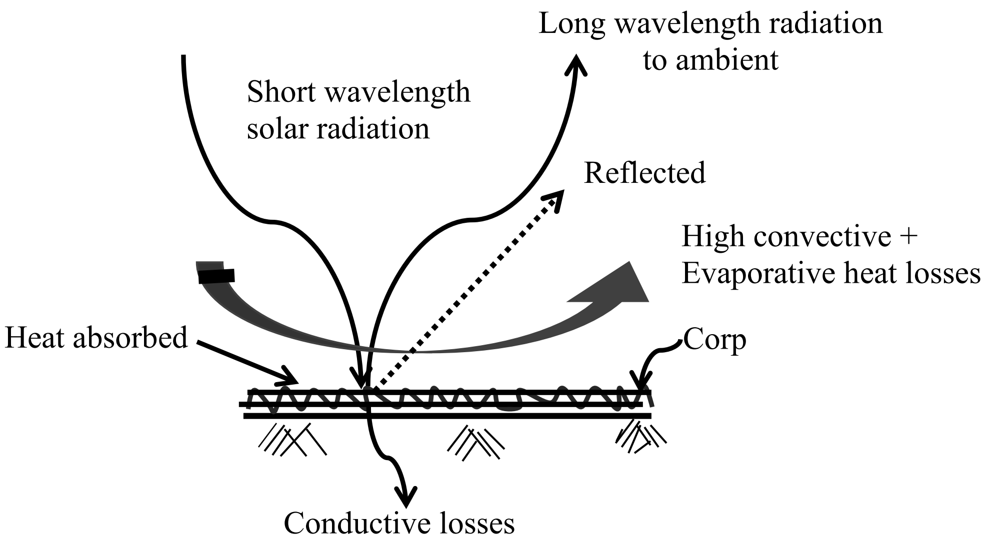

Figure 2.2 Working principle of open sun drying (Akarslan, 2012)

2.2.2.2 Controlled drying with solar dryers

With the awareness of inadequacies involved in open sun drying, a more scientific method of solar-energy utilization for drying has emerged termed as controlled drying with solar dryers (Akarslan, 2012). These controlled solar drying systems are classified as follows.

Based on the incidence of solar radiation on the product, solar dyers can be direct, indirect, or mixed mode.

A. Direct mode solar dryer

In a direct mode solar dryer, the product is directly exposed to solar radiation. For this to occur the structure containing the product must be covered with a transparent material. The solar radiation passes through the glazing and is absorbed by the product and its immediate surroundings (Mohana *et al*., 2020). Most of the solar radiation is converted into heat, thus raising the temperature of the product and its surroundings. The direct absorption of solar radiation by the product is the most effective way of converting solar radiation into useful heat for drying.

This type of dryer is very simple in construction, cost-effective, less maintenance required and easy to handle. After drying, the quality of the product is not in good condition in terms of color, texture, and nutrition (Kumar and Singh, 2020).

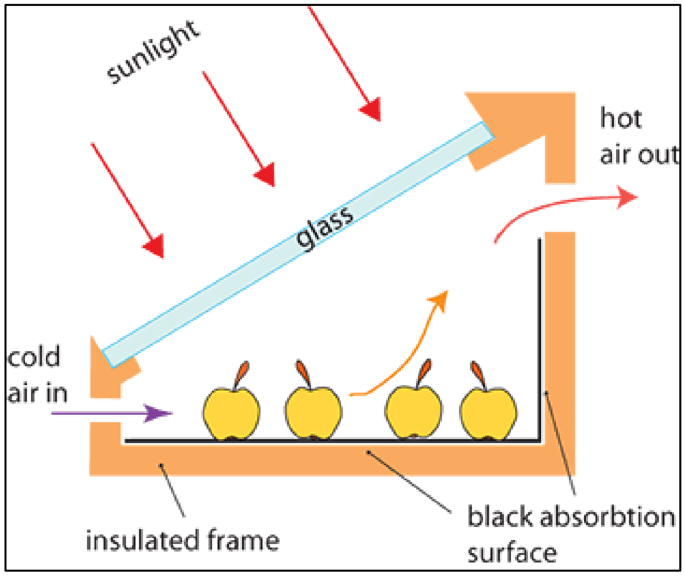

Figure 2.3 Direct type solar dryer (https://www.meatsandsausages.com/drying-preservation/drying-food/solar-drying)

Direct type solar dryers are being used for drying of fruits and vegetables like red peppers and mangoes, and meat (Kumar *et al*., 2016). Some direct solar dryers are box type or solar cabinet dryer or glass roof solar dryer and greenhouse dryer.

Mursalim and Dewi (2002) conducted an experiment to compare the performance of direct solar dryer and open sun drying. The results showed the solar dryer is better in terms of drying rate and product quality. Similarly, **Eke (2013)** developed a natural convection direct type solar dryer to study the drying performance of tomato (S. lycopersicum), okra (Abelmoschus esculentus), and carrot (Daucus carota) which are sliced in 15 mm thickness. At an average drying temperature of 60 °C, 50% reduction in drying time was achieved compared to that of open sun drying.

Dissa *et al*. (2011) experimentally studied drying characteristics of Amelie and Brooks mangoes using a direct solar dryer with final moisture content of 24.83% and 66.32%, respectively. Results showed that, drying rate and efficiency were observed to decrease with drying time progression.

Tefera *et al*. (2013) evaluated the performance of a pyramidal and wooden direct solar dryer for drying potatoes and compared it to drying in the sun. The result showed that 2-3 h was saved compared to open sun drying. From the two dryers, pyramid dryer was better in creating conducive drying environment and in economic feasibility than box dryer. **Eke and Arinze (2011)** also developed a prototype natural convection direct solar dryer drying maize. moisture content was observed to drop from 29% to 12% on a wet basis. The dryer saves 55% of drying time compared to drying in the open sun. Drying efficiency of 45.6 % and 22.7 % were found for the dryer and open sun drying, respectively. Similarly, **Gbaha *et al*. (2007)** designed and tested experimentally a direct, natural convection type solar dryer for drying cassava, bananas, mango. It is about an experimental approach which consists in analyzing the behavior of the dryer. The moisture content of cassava and sweet banana reduced to 13% from 80% in 19 and 22 h, respectively. The newly developed dryer had achieved better thermal performance compared to open sun drying. **Sanusi *et al*. (2013)** also investigated the performance of open, direct, and indirect solar dryers for tomato (Solanum lycopersicum) drying. From the result, it was observed that the direct solar dryer achieved the highest reduction in moisture content and the highest temperature variation followed by the indirect dryer then the open sun drying.

B. Indirect type solar dryer

The limitations of direct-type solar dryers in terms of product quality and low thermal efficiency can be overcome with indirect-type solar dryers (Mohana *et al*., 2020) Indirect type solar dryer (ITSD) differs from the direct type of solar dryer in terms of moisture removal and heat transfer. The crops in these dryers are placed in trays or shelves inside an opaque drying cabinet and solar collector is used for heating of the entering air into the cabinet. The heated air is allowed to flow through/over the wet crop that provides the heat for moisture evaporation by convective heat transfer between the hot air and the wet crop (Tiwari, 2016).

The main advantages of indirect solar drying are its fast drying, better quality, and color of dried product as the product is not exposed to the sun radiation directly, better performance than the other conventional type dryers and higher efficiency than solar drying. However, the additional cost and complexity involved in construction are its disadvantages. Like direct mode dryers, the capacity can range from kilograms to several metric tons.

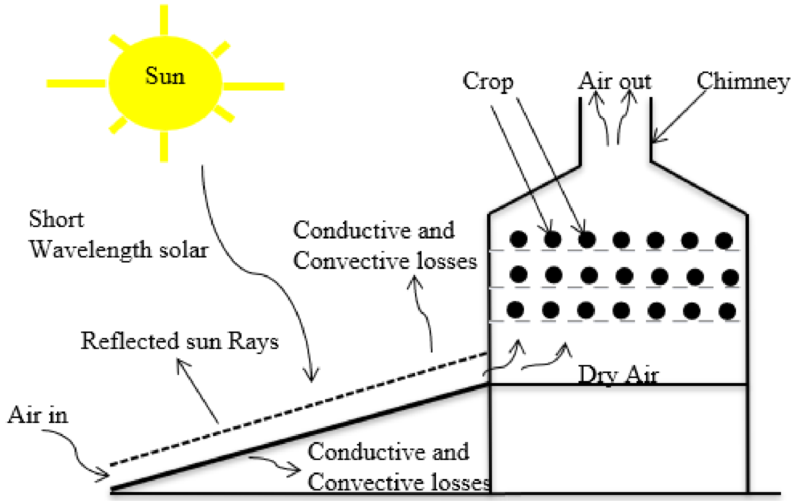

Figure 2.4 Schematic view of the indirect type of solar dryer (ITSD) (Lingayat *et al*., 2020)

Kumar *et al*. (2016) did a review on various types of solar dryers namely, direct, indirect, hybrid solar dryers and their diverse drying applications. from reviewed literatures, an indirect mode forced convection dryers have been reported better in drying speed and quality drying compared to the others.

Tesfamichael (2004) conducted an experimental analysis for the performance evaluation of natural convection indirect solar dryer for potato drying. The main components of the dryer were flat plate solar collector, drying chamber and connecting ducts. From the result, the drying time required by traditional open sun drying is reduced by 3 h (about 19%) to reach a final moisture content of 2.62-2.93%. similarly, **Tiris *et al*. (1995)** also constructed and studied the performance of a natural convection indirect solar dryer. The dryer consists of a solar air heater and a drying chamber. The experiment was done for different food products at different airflow rates and the thermal efficiencies of the solar air heater, and the drying chamber were discussed. The result shows that thermal efficiencies were between 30% and 80% during drying experiments and the overall drying performance and efficiency increase as the airflow rate increases. **Bolaji (2005)** also investigated the performance of an indirect solar dryer using a box type collector. The components of the dryer were a solar air heater, an opaque crop bin and a chimney. The collector was made of a glass cover and black absorber plate and was inclined at an angle of 20° to the horizontal. The result shows that the maximum efficiency of the system was 60.5% and the maximum average temperatures were 64 and 57 °C inside the collector and drying chamber, respectively.

Goud *et al*. (2019) developed an indirect solar dryer (ISD) and fans that operated by solar photovoltaic (PV) panels were used. The moisture content of green chilli and okra were reduced from 8.3984 and 10.1234 kg/kg (db) to 0.01001 and 0.12675 kg/kg (db) in 18 and 9 h, respectively. Solar air collector efficiency of 74.13 % and 78.30 % and drying efficiency of 9.15 % and 26.06 % were achieved for green chilli and okra, respectively. The total heat supplied (Qs) to the drying chamber was 817.08 W and 885.03 W during complete drying of green chilli and okra, respectively. **Lingayat *et al*. (2017)** also conducted an experiment by designing and developing indirect type solar dryer. The dryer is composed of flat plate air collector with V corrugated absorption plate, insulated drying chamber, and chimney for exhaust air. The result showed that, the average thermal efficiency of the collector and drying chamber efficiency were 31.50% and 22.38%, respectively. It was also observed that, the temperature of drying air, humidity of air and air velocity highly affect the drying rate.

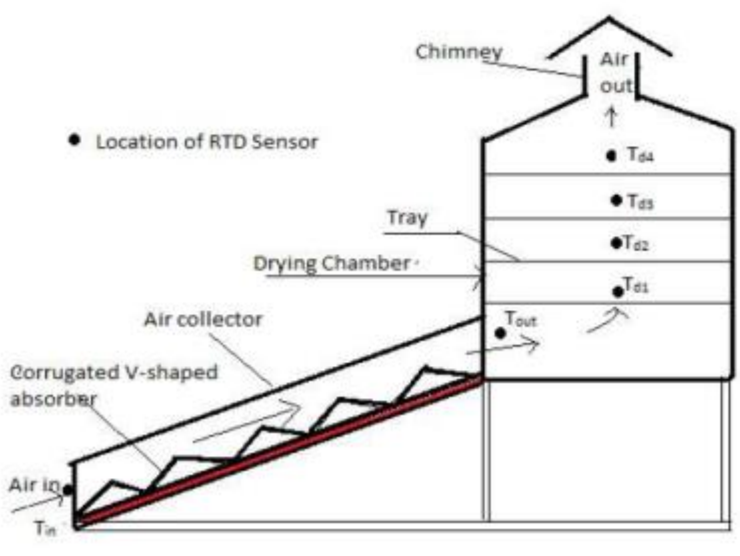

Figure 2.5 indirect type solar dryer consists of V corrugated absorption plate

Castillo *et al*. (2017) performed experimental study at controlled temperatures of 45 C, 55 C and 65 C, using a laboratory oven and an indirect tunnel-type solar dryer for dehydration of a red chilli. The drying kinetics between 55 C and 65 C are similar, with drying times of 2.75 h and 3.0 h, respectively, while at 45 C, the drying time was 6.25 h. high and low velocity of between 1.4 and 2.6 m/s, and 0.7 and 1.48 m/s were established, respectively. In both cases, a temperature between 31 C and 45 C was obtained. drying time of 16 h with final MC between 0.057 and 0.90 kg water/kg (db) and 21 h with a MC of 0.0611- 0.109 kg of water/kg (db) for the first and second range, respectively was found. An indirect forced convection solar dryer was developed and tested by **Al-Juamily *et al.* (2007)** for drying fruit and vegetable. The dryer consisted of a solar collector, blower, and a solar drying cabinet. Two identical solar collectors with V-groove absorber plates and two air passes were used. Grapes, apricots, and beans with initial moisture contents of 80%, 80% and 65% dried to a final moisture content of 18%, 13% and 18% within two and a half days, one and a half of days and one day, respectively. And also, its observed that, the most effective factor on the drying rate is the temperature of the air inside the cabinet.

C. Mixed-type solar dryers

Mixed-type solar dryers work on the combined principle of both direct and indirect-type solar dryers, i.e., they have a transparent drying chamber and a provision to pre-heat the air (Shalaby and Bek, 2014). In such dryers, heat transfer takes place by convection from the dry air to the food surface and by radiation in the drying chamber.

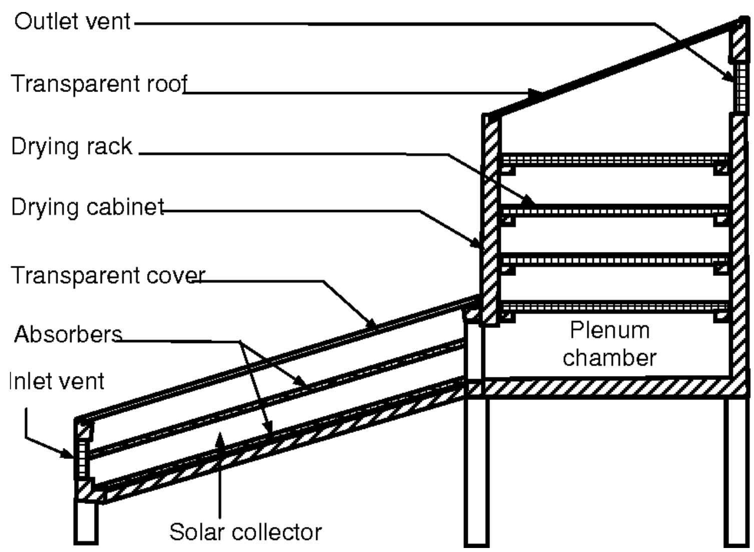

Figure 2.6 Sectional view of the mixed-mode solar dryer (Bolaji and Olalusi, 2008)

Mixed type solar dryers have a relatively higher thermal efficiency than the previously mentioned systems. Mixed-type solar dryers have been used for drying of beans, tomato, banana, red pepper, turmeric, and seafood (Pardhi and Bhagoria, 2013). Less drying time is required in mixed mode as compared to direct and indirect type solar dryer. But the product quality is less compared to that of indirect type.

Bolaji and Olalusi (2008) designed and built a mixed mode solar dryer using local materials. The temperature rises inside the drying cabinet reached 24 ℃ (74%) for about three hours just after solar noon. Drying rate, collector efficiency and percentage of moisture removed (in terms of dry matter) when drying the yam were 0.62 kg / h, 57.5 and 85.4%, respectively.

Husainy *et al*. (2018) conducted an experiment to study drying time of turmeric on forced convection mixed mode solar dryer. The experiment was conducted having incident solar radiation and wind speed 5.12 W/m2 /day and 5 km/hr, respectively. It has been experimentally found that, the complete drying process could be attained with 47 hours (considering sunshine hr.) which reduced the drying time up to 7 days as compared to a conventional method which requires 13 - 15 days. Forced convection mixed mode solar dryer was evaluated by **Mengesha (2020)** under Jimma (Ethiopia) condition. Efficiency of Bottom and upper Tray is 10.4 and 12.27%, respectively for parchment coffee bean drying and 29.07 and 30.5 %, respectively for red pepper. It took 71 h to dry red pepper of 9.1 kg with final MC of 9.22% and 8.24% and 26 h for parchment coffee bean of 18.2kg with final MC of 13% and 9%, respectively. But the drying in open sun takes much more time. Similarly, A forced convection mixed-mode solar dryer with paraffin based thermal energy storage was experimentally analyzed by **Baniasadi *et al*. (2017).** A photovoltaic panel and battery storage were integrated with the dryer to supply the required electrical energy. The result showed that, using the thermal energy storage improved performance of the collector and reduced drying time by 50 %. The moisture pick-up efficiency and the overall thermal efficiency of the dryer were found to be 10% and 11%, respectively. **César *et al*. (2020)** also evaluated a passive, mixed-type solar dryer which has the option of working as MSD or ISD. Drying of tomato in ISD (26 h) took longer than the MSD (17 h). The efficiency of the solar collector was between 52.30% and 55.45%. The overall dryer efficiency in MSD and ISD mode were between 10.66% and 8.80%, while the drying efficiency was in a range of 5.47% and 4.48%, respectively.

Das and **Akpinar (2020)** investigated the thermal performance of a solar air dryer provided with solar tracking feature. Depending on fan speed, in the moving and fixed SACD, the activation energy and effective moisture diffusivity values ranged from 0.062 × 10- 7 to 0.084 × 10- 7 m2/s and 33.2–40.01 kJ/mol and 0.031 × 10- 6 to 0.049 × 10- 6 m2/s and 16.4–22.9 kJ/mol, respectively. The solar air collector thermal efficiency was calculated as 75.7% and 51.7% about in the moving and fixed SACD, respectively.

D. Hybrid solar dryer

In a hybrid solar dryer, solar energy with a conventional or some auxiliary source of energy such as electricity, biomass, etc. can be used in combined or single mode. It combines both the actions, direct solar radiation heating as well as preheating of air using an auxiliary energy source (Kumar *et al*., 2016). For that reason, drying is completed without stopping and product is saved without spoilage by microbial infestation through adverse weather or off sunshine hours (Amer *et al*., 2018).

Bena and Fuller (2002) combined a direct natural convection solar dryer and a simple biomass burner for drying fruits and vegetables where no electricity is used. The overall drying efficiency was found to be 9% with a capacity of the dryer about 20–22 kg fresh pineapple (Ananas comosus) arranged in a single layer of 0.01 m thick slices. Similarly, **Tarigan and Tekasakul (2005)** developed a mixed mode solar dryer with natural convection and integrated with biomass burner for drying agricultural products. Drying efficiency of 23% and 40% were observed for the solar component with and without the heat storage, respectively. uniform drying across the drying tray and acceptable thermal efficiency were achieved for the combined unit.

Khalifa *et al*. (2012) experimentally studied the performance of a solar drying system with forced convection, equipped with an additional heater for drying moringa and peas with an air flow rate of 0.0383, 0.05104, 0.0638 and 0.07655 m / s. Drying time was reduced from 56 hours for natural drying to 14 and 9 hours for solar and mixed drying (solar and auxiliary), respectively. It is reported that the efficiency of the mixed-mode drying system has increased by 15%, from 25 to 40 %.

2.2.3 Classification According to the Mode of Air Flow

According to the mode of air flow, solar dryers also classified into natural convection (passive type) and forced convection (active type) solar dryer.

Natural convection – In this dryer natural movement of air takes place thus called as passive dryers. The heated air flow is induced by thermal gradient (Toshniwal and Karale, 2013). It takes more time for drying the food, compared to active type. As the air flow is natural, there is no need of external power supply as a result it has low cost, but it is drying rate is limited.

Forced convection- In this type of dryer, air is forced through the solar collector and the product floor by a fan or blower, commonly known as an active dryer. It is best alternative for processing large quantities of fresh products. One basic disadvantage is their requirement of electrical power to run the fan or blower. Since the rural or remote areas of many developing countries are not connected to electric grids, the use of these dryers is limited to electrified urban areas. But it is also possible to use solar PV to drive the fan or blower to overcome this problem.

Patil and Gawande (2016) developed two cabinet solar dryers of same dimensions with flat plate solar collector to test the performance of natural and forced mode convection while drying tomato. The moisture content of tomato slices was reduced from 94 % to 10 % in wet basis with in 12 and 9 h in natural and forced convection mode, respectively. collector efficiency of the cabinet dryer in natural and forced convection mode were 17.2% and 32.96 %, respectively. Dryer efficiency in forced convection mode was higher (11.24%) than natural convection mode (9.94%) for the same drying condition. **Asl *et al.* (2017)** also constructed an indirect cabinet solar dryer to evaluate the performance of natural and forced convection method by drying mint leaves and compared their value with that of traditional shade drying. The results showed that total drying time required was 3.5 to 15 h for natural and forced convection mode, respectively while it was approximately 5 days in traditional method. Drying time in forced convection was 29.7% less than that of natural convection. Similarly, A solar dryer powered by a photovoltaic module was evaluated to study the performance of natural and forced convection by **Hidalgo *et al*. (2021)**. The average solar dryer efficiency and specific energy consumption were 34.2%, 18.3 kWh / kg and 38.3%, 16.4 kWh / kg in natural and forced drying, respectively. slight color differences were observed between fresh and dried green onions under the two operating conditions in accordance with the need to preserve the green color of the material.

2.3 Solar Air Heater

A solar air heater (SAH) is a device that absorb solar energy from the sun by absorbing material and extracts the thermal energy by the air flowing over the surface of the absorbing material. SAH is the cheapest form of solar energy conversion, and it can be used for many purposes, such as space heating, crop drying, and other industrial applications. (Singh and Singh, 2018). A typical solar air heater has many advantages like low fabrication, installation, and operational costs, and can be constructed by using cheaper and lesser amount of material. However, they have low efficiency because of poor heat transfer characteristics of air, and also the air cannot be used as storage fluid due to low thermal capacity (Sharma and Kalamkar, 2015).

2.3.1 Components of Solar Air Heater

The main components of solar air heater are cover plate, absorbing plate and insulation. As the solar radiation passes through the translucent cover of solar air heater, its absorbed by the absorbing plate and this absorbing plate transfers this heat to the air.

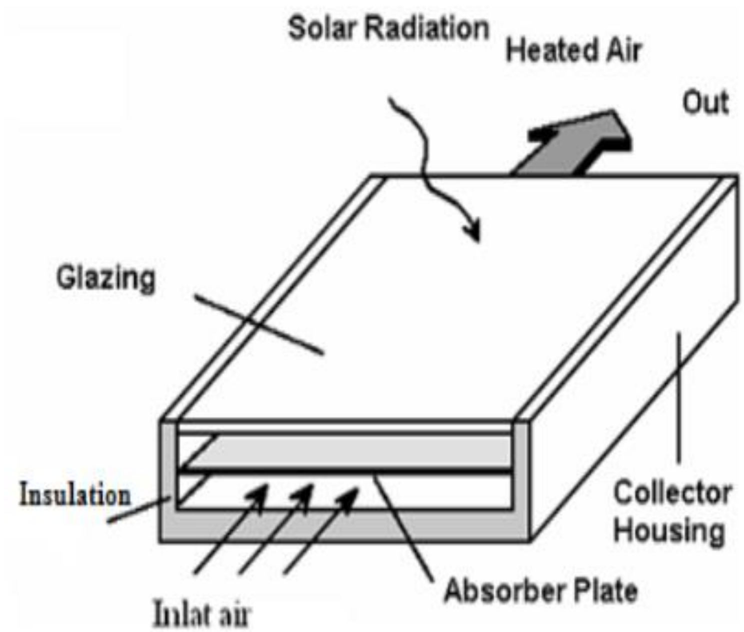

Figure 2.7 Schematic layout of SAH (Ikem *et al.*, 2017).

A. Cover plate

Cover plate (glazing) is most important part of solar air heater, which transmits the maximum amount of solar radiation to the absorbing plate. It performs three major functions in particular: (i) to transmit the incident solar radiation to the absorber plate with minimum loss, (ii) to minimize convective and radiant heat loss from absorber, and (iii) to protect the absorber plate from outside environment. Other important characteristics of glazing materials are reflection (r), absorption (α), and transmission (τ). For maximum efficiency, reflection and absorption should be as low as possible, whilst transmission should be as high as possible. Additionally, strength of material, durability, non-degradability when exposed to the ultraviolet light (UV), and costs are factors to be consider while selecting cover plate material. Usually, glass and plastics are the common materials used as glazing (Bakari *et al.*, 2014 and Tyagi *et al.*, 2018).

B. Absorber plate

Absorber plate is a flat plate made of materials, which have high thermal conductivity, better tensile strength, and non-corrosive (e.g., copper). The function of the absorber plate is absorbing the incident solar radiation and transfers it to the working fluid in solar air heater. The solar collector is made of steel or galvanized iron, aluminum, and types of thermoplastics. For fabrication of absorber plate, a thin sheet of metal (Cu or Al) may be taken with insulations, i.e., to non-flow sides (Tyagi *et al*., 2018). Absorptivity of the material highly affect the amount of solar radiation absorbed. Thus, absorber plate usually painted black to increases absorbance percentage.

C. Insulation

Preventing heat losses from absorbing plates either in the form of conduction or convection is essential for better performance of solar air heater. Insulation minimizes this loss by providing the best heat resistance. The most used insulations nowadays are fiber glass, mineral wool, glass wool and thermo foam.

2.4 Double Pass Solar Air Heater

Thermal efficiency of the conventional SAH is poor due to low convective coefficient between heat collecting surface and working fluid. So, it becomes essential to increase the convection coefficient to increase the thermal performance of the system. The performance of a conventional solar air heater can be effectively improved by reducing the losses from the collector surface by providing the proper insulation and increasing the convective coefficient between heat collecting surface and working fluid by enhancing the heat transfer area which can be increased by double pass design (Ravi and Saini, 2016).

The double pass solar air heaters are of mainly two types depending on the fluid flow direction namely counter or return flow double pass solar air heater and parallel pass double duct solar air heater (Chamoli *et al*., 2012). In both cases, the design consists of glazing, absorber plate and bottom plate with insulation. There are two air flow channels, one between the glazing and absorber plate and the other between the absorber and the bottom insulated plate. In counter flow type, air flows above and below the absorber plate in opposite direction while in parallel flow type, air flows both above and below the absorber plate in same direction as shown in Fig. 2.8 (a) and (b).

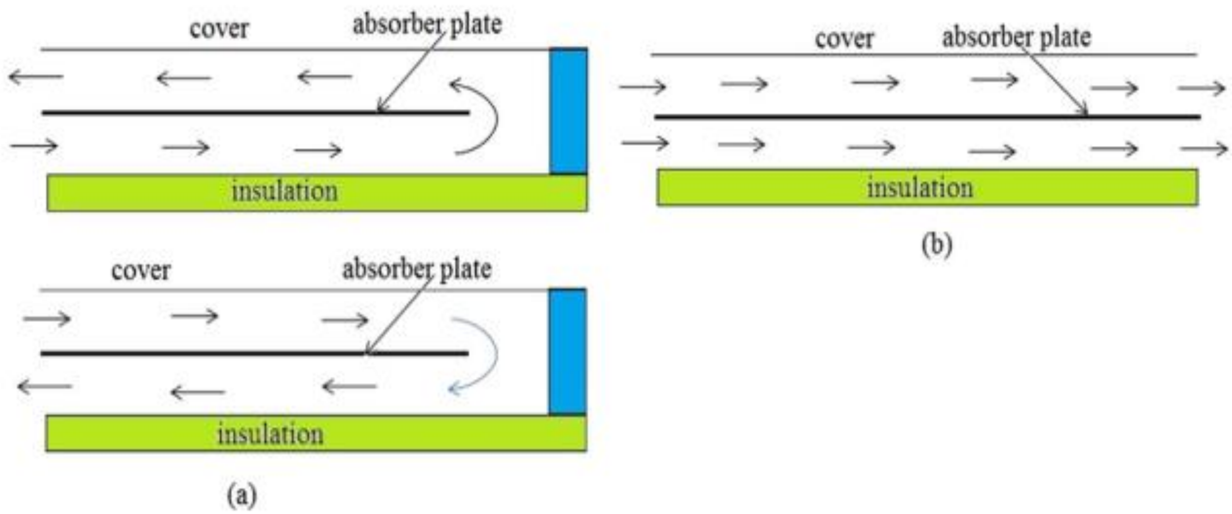

Figure 2.8 Double-pass SAH a) counter flow, b) parallel flow (Kabeel *et al*., 2017).

Banout *et al*. (2011) compared Performances of Double-pass solar drier (DPSD) with a typical cabinet drier (CD) and open-air sun drying for drying of red chilli in central Vietnam. The drying times (including nights) to reach MC of 10% (wb) were 32 h, 73 h and > 93 h respectively. The overall drying efficiencies were 24.04% and 11.52% for DPSD and CD, whereas for open sun drying 15% (wb) was 8.03%. The drying cost per one kilogram of chilli was 39% lower in case of DPSD (0.077 US$/kg) as compared to CD (0.126 US$/kg). similarly, **Aldabbagh *et al*. (2010)** experimentally investigated the performance of single and double pass solar air heaters that use steel wire mesh layer instead of flat absorber plate. Effects of mass flowrate on the outlet temperature and thermal efficiency were also studied. The efficiency of double pass was 34-45 % higher than that of single pass for the same flowrate and with increasing mass flowrate, the efficiency increased for both type of solar air heater. An efficiency of 45.93 and 83.65 % was obtained for single and double pass air heater, respectively. Moreover, the result showed substantial enhancement in thermal efficiency for packed bed collector when compared to conventional solar collectors.

Wang and Hong (2015) studied the effect of collector tilt angle on the thermal performance of a solar collector. It was reported that solar energy reaching the solar collector surface changes with the tilt angle and orientation of the collector. Maximum radiation on the surface of the collector is obtained when the collector is installed at an optimum tilt angle and with proper orientation. It was also reported that collectors installed in the northern hemisphere oriented to the south and are tilted at a certain angle. Similarly, **Ahmad and Tiwari (2009)** also investigated the effect of tilt angle on the performance of flat plate collectors. The result shows that the collector energy loss is almost 1% when the collector tilt angle was adjusted seasonally instead of adjusting each month.

2.4.1 Performance Enhancement Techniques for Double Pass SAH

Various experimental and theoretical investigations have been considered to enhance the performance of double pass solar air heaters (DPSAHs) provided with performance enhancement techniques such as using packed bed materials (PBMs), extended surfaces, corrugated/grooved absorbing surfaces and obstacles in the flow channel.

A. DPSAHs with packed bed materials

There are two main reasons for the low thermal efficiency of SAH: one is the low convection coefficient between the collector plate and the working fluid (air) due to the low thermal conductivity of the air and the other one is related to the thickness of the absorption plate, which can be improved by using a packed bed absorbing surface. Packed bed materials (PBMs) used in SAH acts as thermal energy storage media. A packed bed is a volume of porous media attained by packing particles of selected material into a box. The packaging material increases turbulence, thereby increasing the heat transfer rate. (Ravi and Saini, 2016).

B. DPSAHs with extended surface

As described earlier, the heat transfer between absorber plate and air is poor due to low convection coefficient which result thermal losses to the environment. This loss can be reduced by increasing the heat transfer coefficient and extended surface in the form of fins can be fitted in the solar air heater flow channel to increase the heat transfer rate from heated surface to the air stream and thus efficiency of the SAH. These fins have two functions: the first one is to interrupt the air flow which generate turbulence and increase the heat transfer coefficient. Secondly, they provide a large heat transfer area. A common problem with this type of air heater design is the high coefficient of friction, which is also an important factor when choosing SAH (Kumar and Kim, 2017).

C. DPSAHs with artificial roughness

Another reason for poor heat transfer between the absorber surface and air in the SAH duct is the laminar sub layer created near the wall of the heat absorbing surface. This layer provides the resistance to heat flow and breaking this layer is necessary to achieve better heat transfer rate. Artificial roughness in the form of repeated ribs on the absorber plate disturb laminar sublayer in and creates turbulence in the fluid flowing just near to the absorbing surface (Yadav and Thapak, 2014). On the other hand, artificial roughness produces an increase in pressure drop. Therefore, it is important that the SAH design meets the goals of maximizing the convection coefficient and minimizing the increase in pressure drop.

D. Placing obstacles in the flow channel

Obstacles attached to the heat absorber plate are generally known to increase the heat transfer by enlarging the heat transfer area and enhancing turbulence intensity. However, as the area of the obstacles attached to the heat absorber plate increases, the pressure drop through the SAH also increases (Ahn and Kim, 2020). Therefore, many studies have been conducted on the shape of the obstacles to enhance the overall heat transfer performance by increasing the heat transfer while minimizing the pressure drop.

Kulkarni and Kim (2016) performed numerical analysis to find the optimum shape of obstacles from four different obstacle shapes (U-shaped, rectangular, trapezoidal, and pentagonal) and three arrangements of obstacles were tested to determine their effects on performance of the solar air heater. It's observed that, the shape and arrangement of the obstacles highly influenced the Nusselt number and friction coefficient and among the tested shapes, pentagonal obstacle shape showed the highest performance factor (defined by a ratio of thermal to aerodynamic performance) regardless of the Reynolds number.

Bekele *et al*. (2014) designed and experimentally investigated the effects of delta-shaped obstacles mounted on the absorber plate on the performance of solar air heater by collecting heat transfer and flow friction data. The absorber plate is exposed to a uniform heat flux of 800 W/m^2. The experiment was conducted for the range of Reynolds number from 2100 to 30,000, relative obstacle height (ratio of obstacle to duct height) from 0.25 to 0.75, and the angle of incidence from

30° to 90°. To obtain the optimum thermo-hydraulic performance, experiments were carried out for various values and combinations of parameters and was found at parameters value of Pl/e (relative obstacles longitudinal) = 3/2, Pt/b (relative obstacles transversal pitch) = 7/3, e/H = 0.50 and α = 30° over all range of Reynolds number investigated. Superior thermal performances have been found compared to smooth solar air heater for the same operating conditions but with high pressure drop.

Alam and Kim (2017) studied heat transfer techniques used to increase the performance of double-pass SAHs. Incorporation of various features, such as extended surfaces, corrugated surfaces, artificial roughness, and packed beds. Packed bed increases the heat transfer rate along with reduction in losses to environment because insolation is absorbed in the depth of packing material cause to lower the top layer temperature and, thereby, improvement in thermal losses.

Ramadan *et al*. (2007) performed experimental investigation on a double-glass double-pass solar air heater with a limestone and gravel packed bed (DPSAHPB) above the heater absorber plate. Mass and porosity of the packed bed material and effects of mass flowrate of air were studied. packed bed material with low porosity and higher mass was recommended from the result for increasing the outlet temperature of air. It was found that the hydrothermal efficiency increases with increasing mass flow to a typical value of 0.05 kg/s, after which the increase in thermal efficiency becomes negligible. It is recommended to use a packed bed system with a mass flow rate of 0.05 kg/s or less to reduce the pressure in the entire system. **Ramani *et al*. (2010)** also performed theoretical and experimental analysis of double pass counter flow solar air heater with and without porous material for thermal performance improvement. Based on volumetric heat transfer coefficient mathematical model was developed and parameters effect on the thermal performance and pressure drop also discussed. The result revealed that, 20-25 % and 30-35 % higher thermal efficiency was found in double pass solar air collector with porous material compared to without porous material and single pass collector, respectively.

Reverse flow double-pass solar air heater with longitudinal fins at the bottom of absorber analyzed analytically and experimentally by **Pramanik *et al*. (2017)**. It is found that the instantaneous efficiency and air outlet temperature increased up to 69% and 94°C respectively. Theoretical analysis has been made as well for the present set up. The difference between the theoretical and experimental values lies within 1.23-9.75%. **Fudholi *et al*. (2014)** also conducted performance analysis of solar drying system consists of a finned double-pass solar collector, a blower, and a flatbed drying chamber. It took 33 h to dry red chili from 80 % to 10 %(wb) in 33 h. The SEC was 5.26 kW h/kg. The values of evaporative capacity and improvement potential was from 0.13 kg/s to 2.36 kg/s and 0 W to 135 W, respectively. The efficiencies of the solar collector, drying system, pick-up, and exergy were 28%, 13%, 45%, and 57% respectively.

Shamekhi *et al*. (2018) experimentally investigated an indirect mode, DPSD consisting of wire mesh as the packing substrate. Based on the results obtained, the maximum temperature difference between the air inlet and outlet of the solar heater is approximately 29 ℃, which occurs at a flow rate of Q = 0.006125 m^3/s. This difference between the collector outlet and the ambient decreases significantly with increasing volume flow. Whereas increasing the flow rate from 0.006125 m /s 3 to 0.01734 m /s 3 improved the collector thermal efficiency by ~20%; any further increase of flow rate (i.e. to 0.034378 m /s 3) had an adverse effect on the collector thermal efficiency.

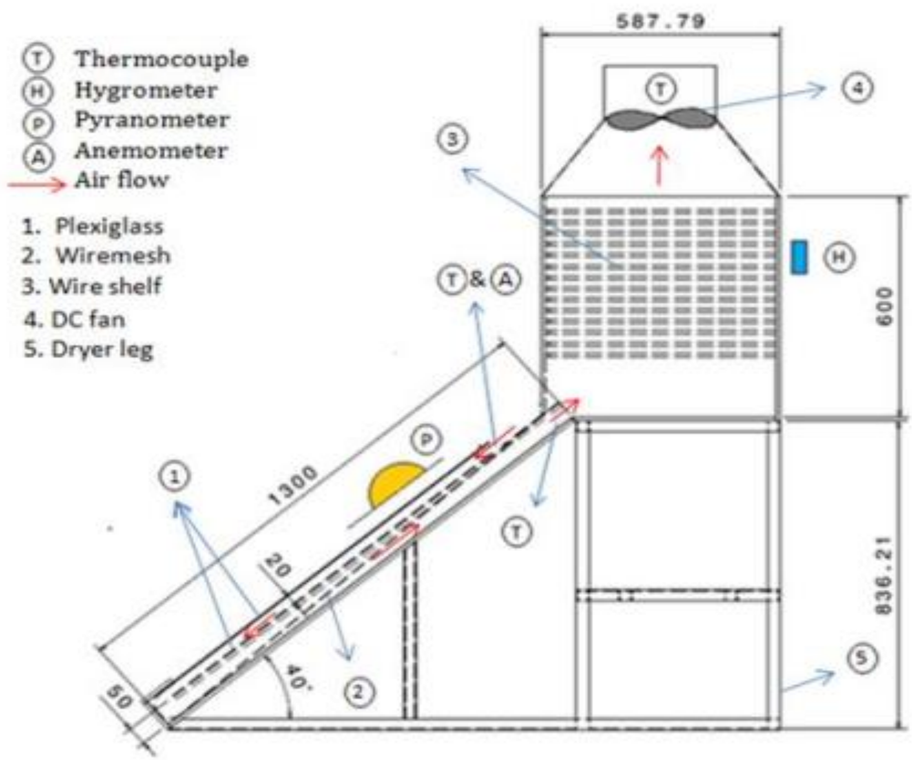

Figure 2.9 experimental setup of DPSD consisting of wire mesh as the packing substrate (Shamekhi *et al*., 2018)

2.5 Thermal Energy Storage

Energy storage is a key issue to be addressed to allow intermittent energy sources, typically renewable sources, to match energy supply with demand. There are numerous technologies for storing energy in various forms including mechanical, electrical, and thermal energy (Bal *et al*., 2010). Thermal Energy Storage (TES) is a technology which stores energy by heating, melting, or vaporizing a storage medium and the stored energy is used at a later time for various applications by cooling or solidifying the storage medium. Due to the fluctuating nature of the solar radiation throughout the day, a thermal energy storage system is required to be designed properly so as to achieve a continuous supply of heat (Gunjo, 2018). Thermal energy can be stored in well insulated fluids or solids as a change in internal energy of a material as sensible heat, latent heat and thermo-chemical or combination of these (Bal *et al*., 2010). The system stores heat energy when sufficient quantity is available and discharges when there is shortage. An overview of major technique of storage of solar thermal energy is shown in Fig. 2.10.

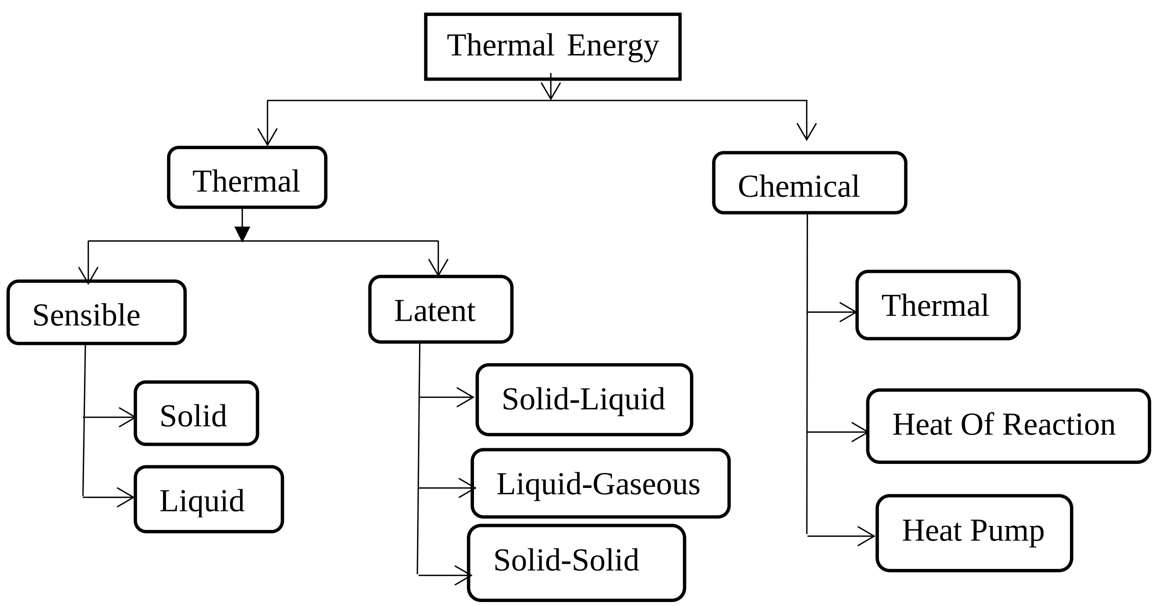

Figure 2.10 Different types of thermal storage of solar energy (Bal *et al*., 2010)

2.5.1 Sensible Heat Storage

In the sensible heat storage, thermal energy is accumulated by increasing the temperature of a liquid or solid using the heat capacity and changing the temperature of the material during the process of charging and discharging without undergoing phase change (Sonar, 2021). The specific heat of the material and temperature difference during heating decides the amount of heat storage (Solomon *et al*., 2020). Molten salts, oils and liquid metals, rocks etc. are used as sensible heat storage. However, water appears to be the best SHS liquid available because its high specific heat and inexpensiveness.

El-Sebaii *et al.* (2001) constructed and experimentally investigated natural convection indirect solar dryer using sand as a thermal storage material for drying different fruits (grapes, figs and apples) and vegetables (green peas, tomatoes and onions). The result showed that, equilibrium moisture content was reached after 72 h without storage and 60 h with storage material for seedless grapes which reduces the drying time by 12 h. Similarly, the performance of a natural convection solar tunnel dryer integrated with rock bed as a sensible heat storage material was tested by **Ayyapan and Mayilsamy (2012)** for drying copra. moisture content of copra was dropped from 52% (wb) to 7.1% (wb) in 54 and 60 h with and without storage, respectively. but it took 153 hours to reduce the content. but it took 153 h for open sun drying. The average thermal efficiency of the dryer was 15% and increased by 2% to 3% when using the storage material.

Chaouch *et al*. (2018) developed and investigated an indirect and direct forced convection solar dryer with pebble sensible heat storage medium. Pebble bed is placed in a plenum and cavity below the direct drying chamber and the solar collector, respectively. The sensible heat storage system enhanced the thermal efficiency of the drying chamber by 11.8 % and solar collector by 28 %. SHS maintained efficiency of solar collector for an hour after sun set. **Saravanakumar and Mayilsamy (2010)** developed and tested the thermal performance of a forced convection flat plate solar air heater with sensible heat storage material. A centrifugal blower was used to increase the outlet temperature of the collector and efficiency (10–20%). Among the sensible heat storages used, Gravel with iron scraps has achieved better efficiency. It was also observed that forced convection solar dryers are more suitable for drying high-quality products even in a cloudy climate. Similarly, the performance of an indirect forced convection solar drier integrated with different sensible heat storage maternal has been developed by **(Mohanraj and Chandrasekar, 2009)** and tested by drying chili. The heat storage unit is placed inside flat plate solar air heater. Moisture content of chili was reduced from 72.8% to 9.1% (wet basis) within 24h. the specific moisture extraction rate and average dryer efficiency was estimated to be 0.87 kg/kWh and 21%, respectively for a mass flow rate of 0.25 kg/s.

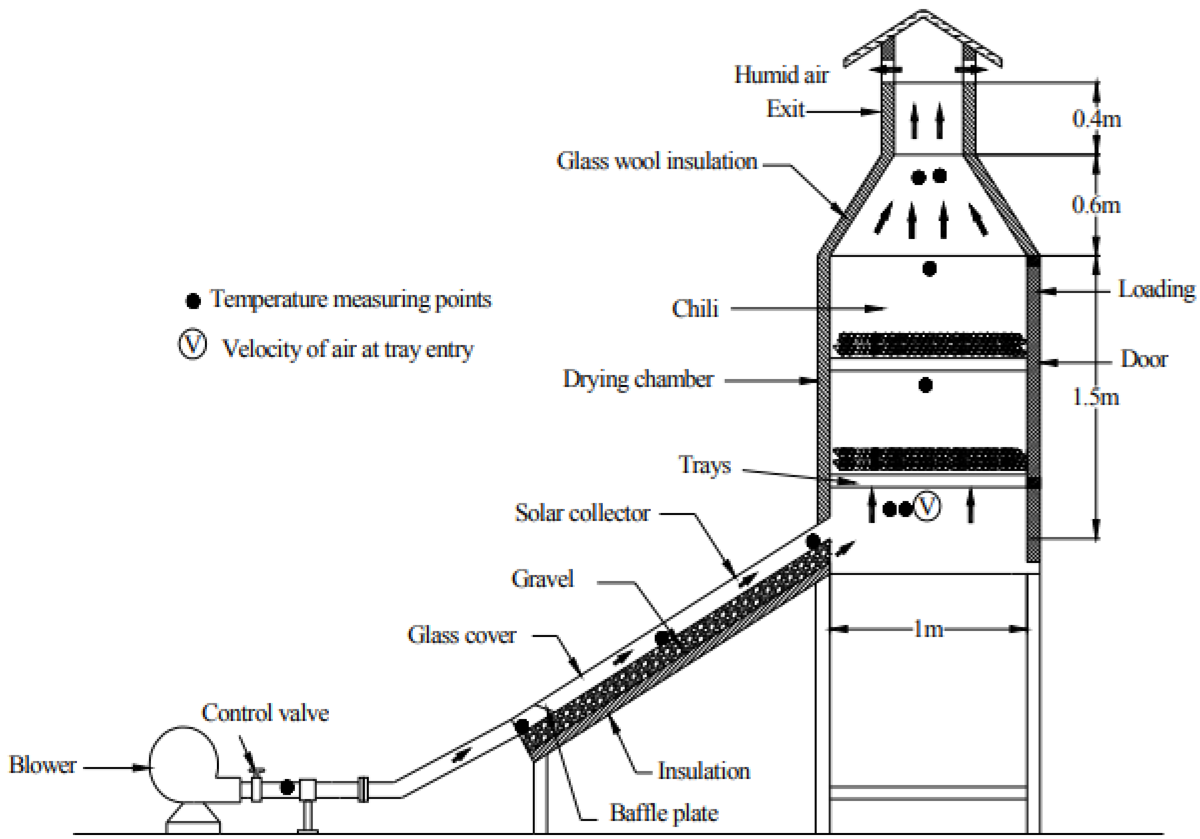

Figure 2.11 Schematic View of Experimental Setup (Mohanraj and Chandrasekar, 2009)

2.5.2 Latent Heat Storage

Latent heat storage (LHS) is the absorption or release of heat when a storage material undergoes a phase change from solid to liquid or from liquid to gaseous or vice versa at a more or less constant temperature. LHS also known as phase change materials and offers the possibility of storing higher amounts of energy per unit storage material mass compared to SHS systems.

Any latent heat energy storage system possesses at least the following three components (Bal *et al.*, 2010):

- A suitable PCM with its melting point in the desired temperature range.
- A suitable heat exchange surface.
- A suitable container compatible with the PCM

Remaining the temperature of medium more or less constant, storing more heat per unit volume, absorbing, or releasing heat while maintaining nearly constant temperature, and simultaneous charging and discharging are some of the advantages of LHS systems over SHS systems.

2.5.2.1 Classification of phase change materials

There are three types of phase change materials used in application: Organic, Inorganic and Eutectic. Organic materials are further described as paraffin and nonparaffin. Paraffins consist saturated hydrocarbon chains of CnH2n+2 and are known to be safe, reliable, predictable, less expensive, and non-corrosive. However, they also have low thermal conductivity. The non-paraffin organics are the most numerous of the phase change materials with highly varied properties. They include a wide range of organic materials such as fatty acids, esters, alcohols, and glycols (Fufa *et al*., 2019 and Soares, 2016).

Salt hydrates are inorganic PCMs that consist of salt and water in a crystal matrix when they solidify. They can have wide range of latent heat and phase change temperatures depending on the mixture. Other branch of inorganic PCMs are metallics, which includes the low melting metals and metal eutectics.

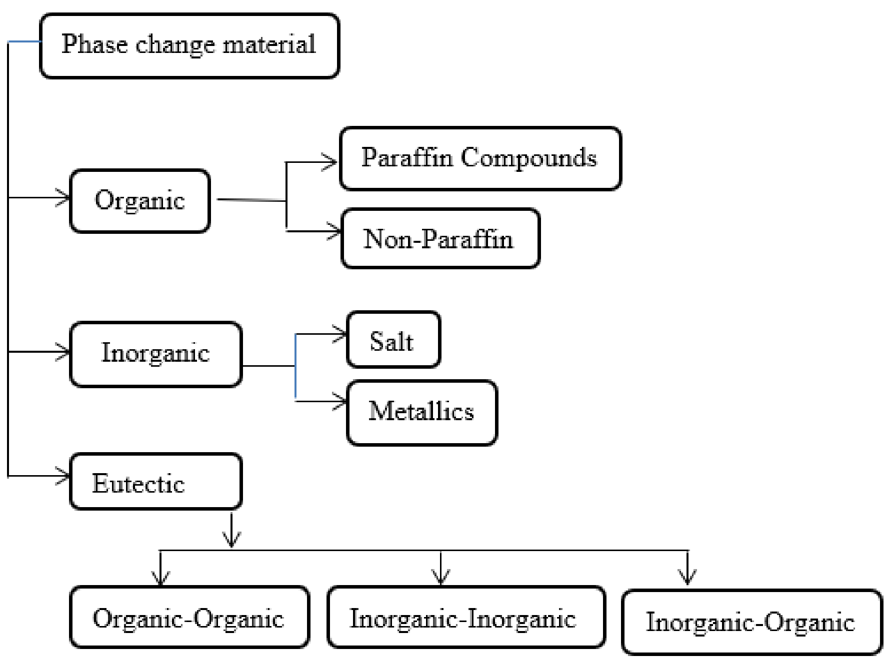

Figure 2.12 Classification of PCMs (Ali and Deshmukh, 2020)

A eutectic is a minimum-melting composition of two or more components, each of which melts and freezes congruently forming a mixture of the component crystals during crystallization (Tyagi and Buddhi, 2007). Eutectic PCMs are subdivided into organic-organic, organic-inorganic and inorganic-inorganic.

Devahastin and Pitaksuriyarat (2006) investigated the feasibility of using a latent heat storage (LHS) with paraffin wax as PCM. The result shows that, the drying time was 100 and 70min at air velocities of 1 and 2 m/s without the LHS and 180 and 165min with LHS. Energy extractable from the LHS was 1920 and 1386 kJ min/kg and the energy savings were 40% and 34% for inlet ambient air velocity of 1 and 2 m/s, respectively.

Shalaby and **Bek (2014)** experimentally investigated forced, indirect solar dryer (ISD) design using PCM. The ISD was tested under no load with and without PCM at a wide range of mass flow rates (0.0664–0.2182 kg/s). It is found that after using the PCM, the temperature of the drying air is higher than ambient temperature by 2.5–7.5 °C after sunset for 5 hours at least. In addition, the mass flow rates of 0.1204 and 0.0894 kg/s give the peak values of the drying temperature when the ISD is operated with and without PCM, respectively. The design successfully maintains the desired temperature for 7 consecutive hours every day and achieved the final MC within 12-18 h. Similarly, **El Khadraoui *et al*. (2017)** designed and experimentally investigated an indirect type forced convection solar dryer using Phase Change Material (PCM). The components of the dryer are solar air panel for a direct heating, solar energy accumulator (solar air collector with PCM) and drying chamber. The daily solar energy accumulator reached an energy and exergy efficiency of 33.9 % and 8.5 %, respectively. Using the solar energy accumulator enhanced the drying chamber temperature by 4-16 °C all the night and lowered the relative humidity of drying chamber by 17-34.5 % compared to ambient temperature.

Shalaby *et al*. (2014) studied previous work on solar dryers with PCM. It is concluded that, recent research focused on PCMs because of its higher TES density compared with SHS materials. It is inferred that carbon fibers, expanded graphite, graphite foam and high thermal conductive particles may improve the η_{th} of solar energy devices employing paraffin waxes. **Miró *et al*. (2016)** proposed a new methodology to select proper PCM for thermal storage application. It is concluded that, selection of a PCM must consider not only thermal properties but also health hazard and both cycling and thermal stability. Health hazard is related with the handling of the material, and both cycling and thermal stabilities with durability.

2.5.3 Thermo-chemical Energy Storage

Thermo-chemical systems rely on the energy absorbed and released in breaking and reforming molecular bonds in a completely reversible chemical reaction. In this case, the heat stored depends on the amount of storage material, the endothermic heat of reaction, and the extent of conversion (Bal *et al*., 2010). Amongst above thermal heat storage techniques, latent heat thermal energy storage is particularly attractive due to its ability to provide high-energy storage density per unit mass and per unit volume in a more or less isothermal process.

2.6 Literature Summary and Research Gap

Several studies have been examined on different types of solar dryers, and indirect solar dryers have been found to have higher efficiency in terms of drying rate and product quality than direct type of solar dryers. However, the efficiency and heat gain for most solar dryer is low. To overcome this problem, a double pass solar air heater provided with performance enhancement techniques such as using packed bed materials (PBMs), extended surfaces and corrugated absorbing surfaces has been investigated by several researchers. On the other hand, to minimize the gap between solar energy availability and operating time, various researchers have used both sensible and latent heat storage, and the later have improved the efficiency of the solar dryer better because it can store more heat. Paraffin wax is widely used because of its high heat storage capacity, low melting point, compatibility with all metal containers, and availability. It was observed that there is a little experimental study on the effects of baffles on DPSAH and also placing the PCM inside a solar air heater can cause heat loss.

Therefore, this study presents an experimental evaluation of solar dryer using an integrated baffled double pass solar air heater to enhance the efficiency of the solar air heater and a thermal energy storage inside the drying chamber to minimize the heat loss from the storge for a red chili drying application.

CHAPTER THREE

METHODOLOGY

3.1 Introduction

In this chapter, the methodology used to achieve the objectives of this thesis, data sources and collection techniques, and materials and equipment's used have been discussed. Estimation of solar radiation intensity by applying empirical formulas for Adama city using the weather data which was collected from Eastern and central Oromia metrological service center is presented.

3.2 Methodology

Theoretical and experimental analysis are approaches that were used as a methodology in this study. The theoretical approach uses governing equations for the analysis of the solar dryer components. For the experimental performance analysis, the prototype was constructed after sizing of each component and selecting the materials to be used. First double pass solar air heater was tested. Then, the double pass SAH is modified by inserting baffles as enhancement technique. The experimental result is validated with similar previous works. The overall methodology followed in this study is described using flow chart in Figure 3.1.

3.3 Data Collection

Both primary and secondary sources are used when collecting data. The primary sources of data are meteorological data of the test site obtained from nearby meteorological station and moisture content of the product to be dried (red chilli) which is evaluated using oven. The secondary source of data are data obtained from literature review of different books, journals and from websites.

3.4 Materials and Equipment's

Samples of chilli were obtained from Wenji Kuriftu, East Shewa Zone of Oromia Region, Ethiopia. About 0.1 kg of red chili were taken and dried in an oven at a temperature of 105 ± 1 ℃ for 24 hours to measure the moisture content. The initial and final masses of the red chili were recorded using an electronic balance and the average moisture content of the chilli was 81 %.

The main components of the dryer are a double pass flat plate solar collector, drying chamber with latent heat storage unit, and blower. Solar collector is a part where the solar radiation will be absorbed and collected. It has glazing material, which is top cover of the collector, absorber plate which absorb the solar radiation, base plate, and insulation to minimize heat loss. Drying chamber is a box where the product to be dried is placed and it contain latent heat storage unit and trays. Blower is used to increase the velocity (mass flow rate) of the air. Materials used for developing the experimental prototype are obtained by purchasing from local markets. Thermocouple thermometer and digital weight balance are used to measure temperature and weight of the product, respectively.

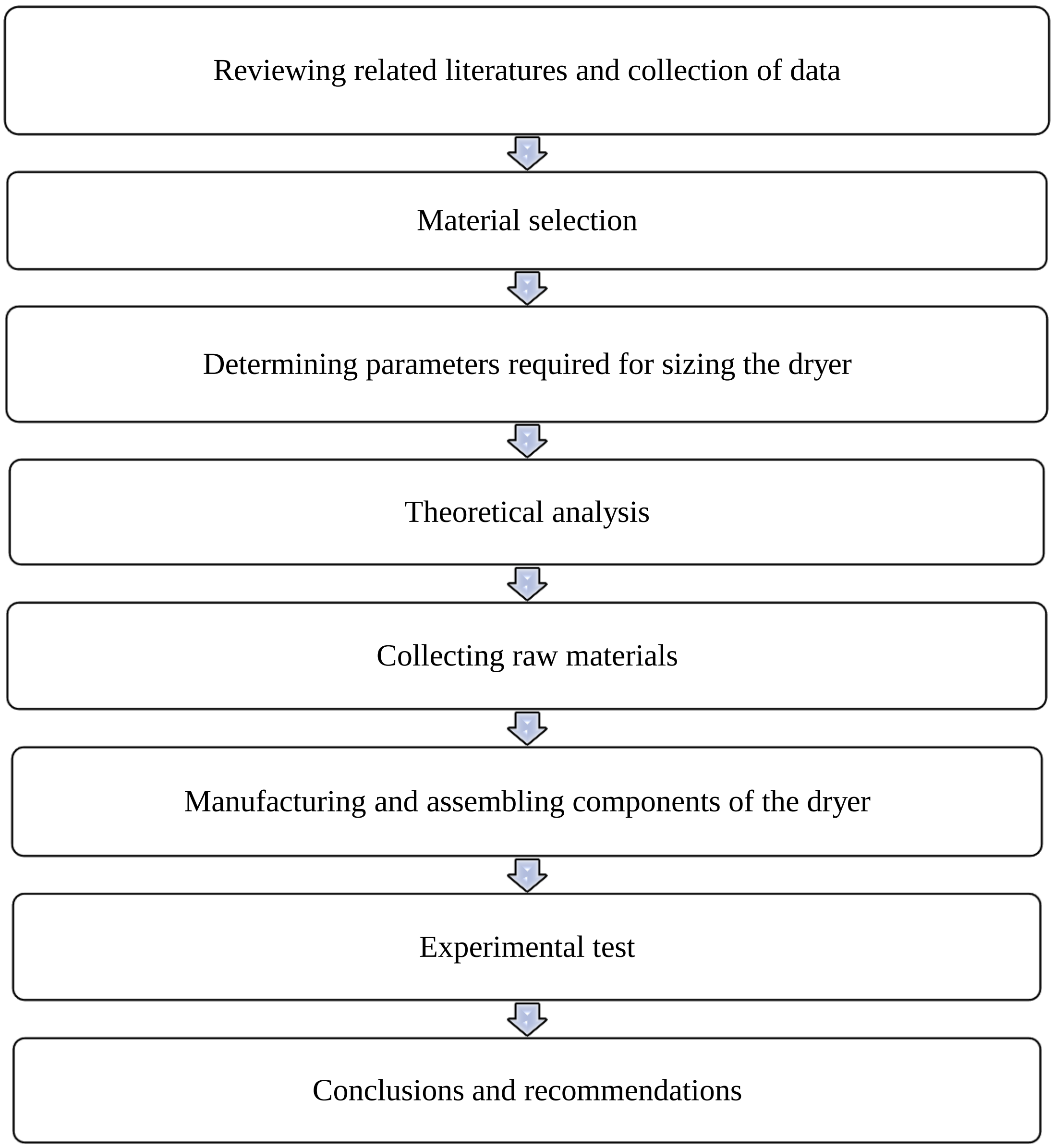

Figure 3.1 Methodology of the study

3.5 Solar Radiation Estimation

Solar radiation can be captured and turned into useful forms of energy, such as heat and electricity, using different technologies and solar air heater is one of them. To calculate the total amount of solar energy incident on solar collector, solar radiation intensity data is mandatory. Estimation of solar radiation intensity by applying empirical formulas using meteorological data is used to overcome the problem associated with solar radiation measuring instrument.

3.5.1 Basic Sun - Earth Angles

The geometric relationships between a plane of any particular orientation relative to the earth at any time (whether that plane is fixed or moving relative to the earth) and the incoming beam solar radiation, that is, the position of the sun relative to that plane, can be described in terms of several angles (Duffie and Beckman, 1980). Some of the angles are:

A. **Latitude (ϕ)**: the angular location north or south of the equator, north positive; $-90^\circ \leq \phi \leq 90^\circ$.

B. **Declination (δ)**: the angular position of the sun at solar noon (i.e., when the sun is on the local meridian) with respect to the plane of the equator, north positive; $-23.45^\circ \leq \delta \leq 23.45^\circ$.

$$\delta = 23.45 \sin\left(\frac{360(284 + n)}{365}\right) \tag{3.1}$$

Where, n is day of the year which is counted starting from January 1.

C. **Slope or tilt angle (β)**: the angle between the plane of the surface in question and the horizontal; $0^\circ \leq \beta \leq 180^\circ$. ($\beta > 90^\circ$ means that the surface has a downward-facing component.)

D. **Surface azimuth angle (γ)**: the deviation of the projection on a horizontal plane of the normal to the surface from the local meridian, with zero due south, east negative, and west positive; $-180^\circ \leq \gamma \leq 180^\circ$.

E. **Hour angle (ω)**: the angular displacement of the sun east or west of the local meridian due to rotation of the earth on its axis at 15° per hour; morning negative, afternoon positive.

$$\omega = [solar\ time - 12{:}00](hr) \times 15° \tag{3.2}$$

F. **Angle of incidence (θ)**: the angle between the beam radiation on a surface and the normal to that surface.

$$\cos\theta = \left\{\begin{matrix} \sin\delta\sin\phi\cos\beta - \sin\delta\cos\phi\sin\beta\cos\gamma + \cos\delta\cos\phi\cos\beta\cos\omega \\ + \cos\delta\sin\phi\sin\beta\cos\gamma\cos\omega + \cos\delta\sin\beta\sin\gamma\sin\omega \end{matrix}\right\} \tag{3.3}$$

And

$$\cos\theta = \cos\theta_z\cos\beta + \sin\theta_z\sin\beta\cos(\gamma_s - \gamma) \tag{3.4}$$

Additional angles are defined that describe the position of the sun in the sky:

G. **Zenith angle (θz)**: the angle between the vertical and the line to the sun, that is, the angle of incidence of beam radiation on a horizontal surface.

$$\cos\theta_z = \cos\phi\cos\delta\cos\omega + \sin\phi\sin\delta \tag{3.5}$$

H. **Solar altitude angle (α_s)**: the angle between the horizontal and the line to the sun, that is, the complement of the zenith angle.

I. **Solar azimuth angle (γ_s)**: the angular displacement from south of the projection of beam radiation on the horizontal plane. Displacements east of south are negative and west of south are positive.

$$\gamma_s = sign(\omega)\left|\cos^{-1}\left(\frac{\cos\theta_z\sin\phi - \sin\delta}{\sin\theta_z\cos\phi}\right)\right| \tag{3.6}$$

3.5.2 Solar Radiation Data

Six years data from 2015 up to 2019 of Adama (latitude=8.54° north of the equator, longitude =39.27° E and Elevation = 1712 m above sea level) was collected from Eastern and central Oromia meteorological service center. The collected data includes duration of sunshine hours, maximum and minimum temperature, relative humidity, and wind speed. Figure 3.2 and 3.3 shows monthly average daily sunshine hours and monthly average maximum and minimum temperatures of Adama.

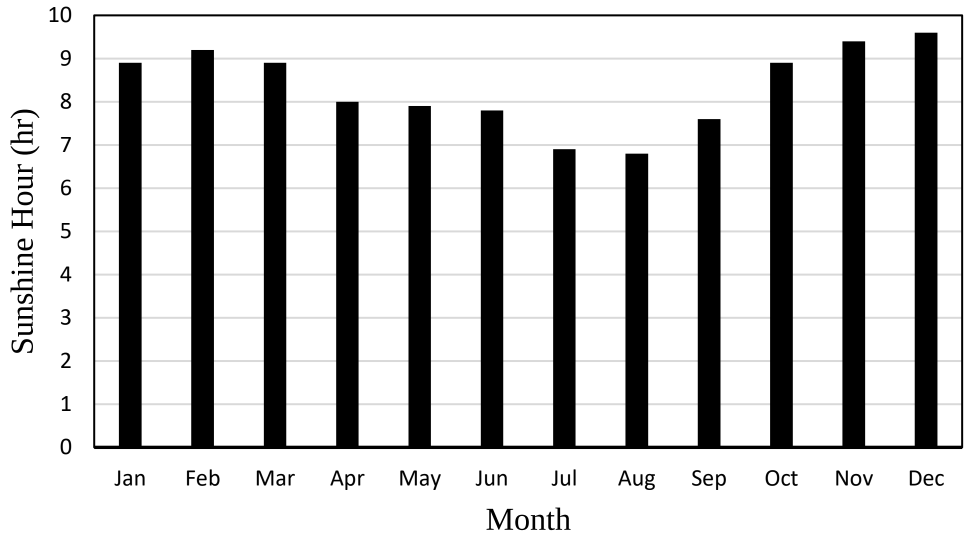

Figure 3.2 Monthly average daily sunshine hour of Adama

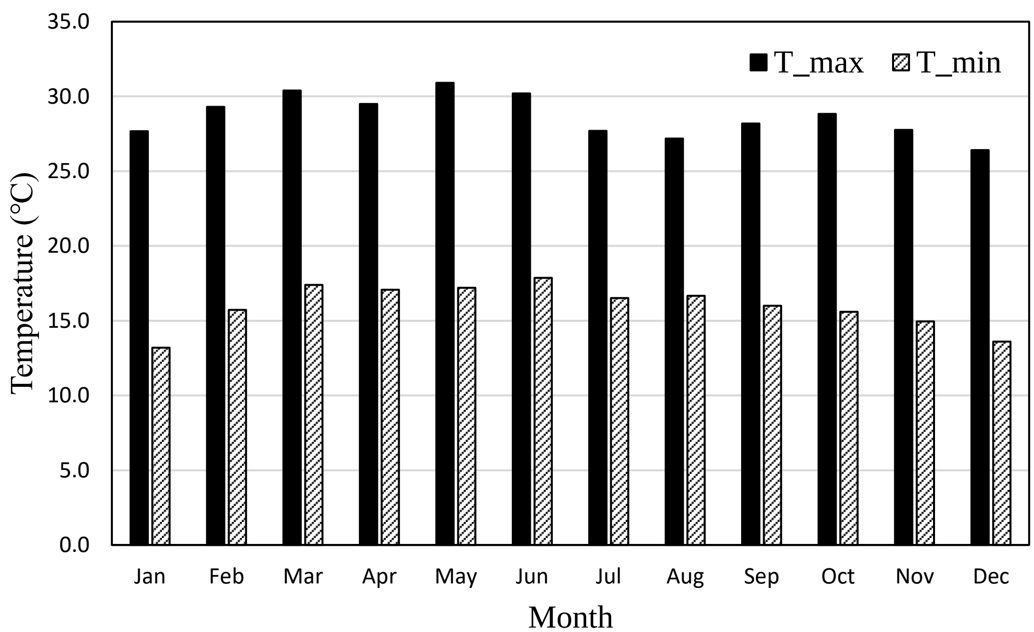

Figure 3.3 Monthly average maximum and minimum temperatures of Adama.

3.5.3 Extraterrestrial Radiation

Due to elliptical orbit of the Earth's motion around the Sun, the Sun–Earth distance is not fixed but rather varies around the year, and the maximum variation is up to 1.7 %. For the n^{th} day of the year, the solar intensity on a plane perpendicular to the direction of solar radiation is given by (Tiwari and Tiwari, 2016):

$$I_{ext} = I_{sc}[1.0 + 0.033\cos(360n/365)] \tag{3.7}$$

Where, I_{sc} is the solar constant defined as the radiant solar (energy) flux received in the extraterrestrial region on a plane of unit area kept perpendicular to the solar radiation at the mean Sun–Earth distance. The value of solar constant is 1367 W/m^2.

The solar radiation (I_0) incident on a horizontal plane in the extraterrestrial region (outside the atmosphere) in W/m^2 can be obtained as follows:

$$I_{\mathrm{o}} = I_{ext} \times \cos\theta_z \tag{3.8}$$

Or

$$I_o = I_{sc}[1.0 + 0.033\cos(360n/365)][\cos\phi\cos\delta\cos\omega + \sin\phi\sin\delta] \tag{3.9}$$

The daily extraterrestrial solar radiation on a horizontal surface (H_o) in kw/m^2day can be determined by integrating Eqn. (9) during the period from sunrise to sunset and one gets:

$$H_o = \frac{24}{1000 \times \pi} I_{sc}\left[1.0 + 0.033\cos\left(\frac{360n}{365}\right)\right]\left(\cos\phi\cos\delta\sin w_s + \frac{2\pi w_s}{360}\sin\delta\sin\phi\right) \tag{3.10}$$

Where, n is mean day of the month; w_s is sun set hour angle. $w_s = \cos^{-1}(-\tan\phi\tan\delta)$

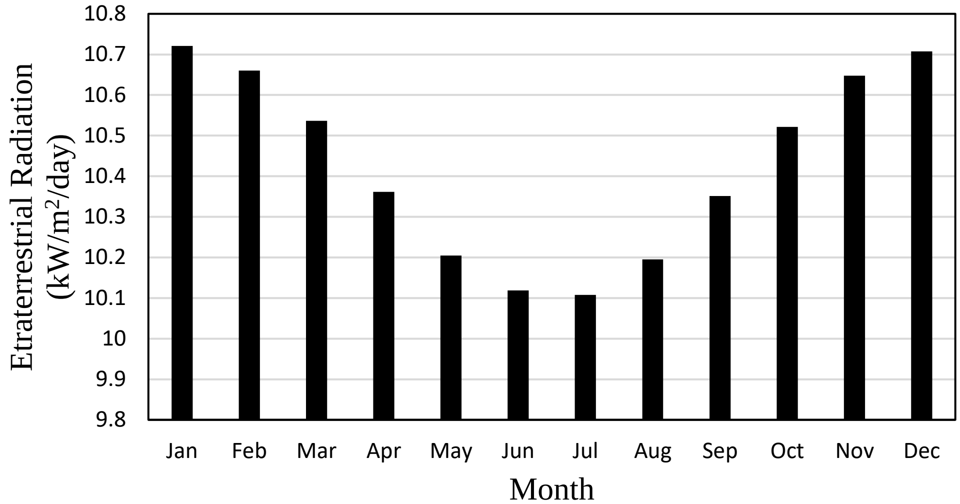

Figure 3.4 Monthly average daily extraterrestrial radiation on a horizontal surface

3.5.4 Estimation of Monthly Average Daily Global Radiations on a Horizontal Surface

The first correlation proposed for estimating the monthly average daily global radiation is based on the method of Angstrom (1924). The original Angstrom-type regression equation-related monthly average daily radiation to clear day radiation in a given location and average fraction of possible sunshine hours and expressed as follow (Muzathik *et al*, 2011):

$$\frac{\bar{H}}{\bar{H}_o} = a + b\left(\frac{\bar{n}_s}{\bar{N}_s}\right) \tag{3.11}$$

Where: $\bar{H}$ is monthly average daily global solar radiation on horizontal surface.

$\bar{H}_o$ is monthly average daily extraterrestrial solar radiation on a horizontal surface.

$\bar{n}_s$ is monthly average daily hours of bright sunshine.

$\bar{N}_s$ is monthly average of the maximum possible daily hours of bright sunshine.

$$\bar{N}_s = \left(\frac{2}{15}\right) w_s \tag{3.12}$$

a and b are empirical constants (regression parameters) and can be determined from:

$$a = -0.110 + 0.235 \cos\phi + 0.323\left(\frac{\bar{n}_s}{\bar{N}_s}\right) \tag{3.13}$$

$$b = 1.449 - 0.533 \cos \phi - 0.694 \left(\frac{\bar{n}_s}{\bar{N}_s}\right) \tag{3.14}$$

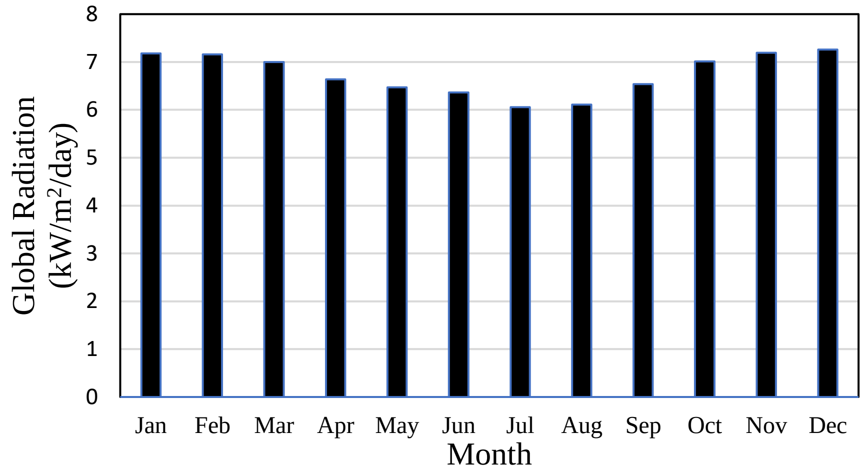

Figure 3.5 Monthly average daily global radiation on a horizontal surface

3.5.5 Estimation of Monthly Average Daily Diffuse and Beam Radiations

The monthly average daily diffuse radiation on a horizontal surface ($\bar{H}_d$) in kw/$m^2 day$ can be determined from the monthly average daily global radiation on a horizontal surface and the number of bright sunshine hours (Tiwari and Tiwari, 2016).

$$\frac{\bar{H}_d}{\bar{H}} = 0.931 - 0.814 \left(\frac{\bar{n}_s}{\bar{N}_s}\right) \tag{3.15}$$

The monthly average daily beam radiation ($\bar{H}_b$) on a horizontal surface is the difference between the monthly average daily global and diffuse radiations.

$$\bar{H}_b = \bar{H} - \bar{H}_d \tag{3.16}$$

The monthly average daily global, diffuse and beam radiation on a horizontal surface of Adama city averaged for five years of climatic condition is indicated in Figure 3.6.

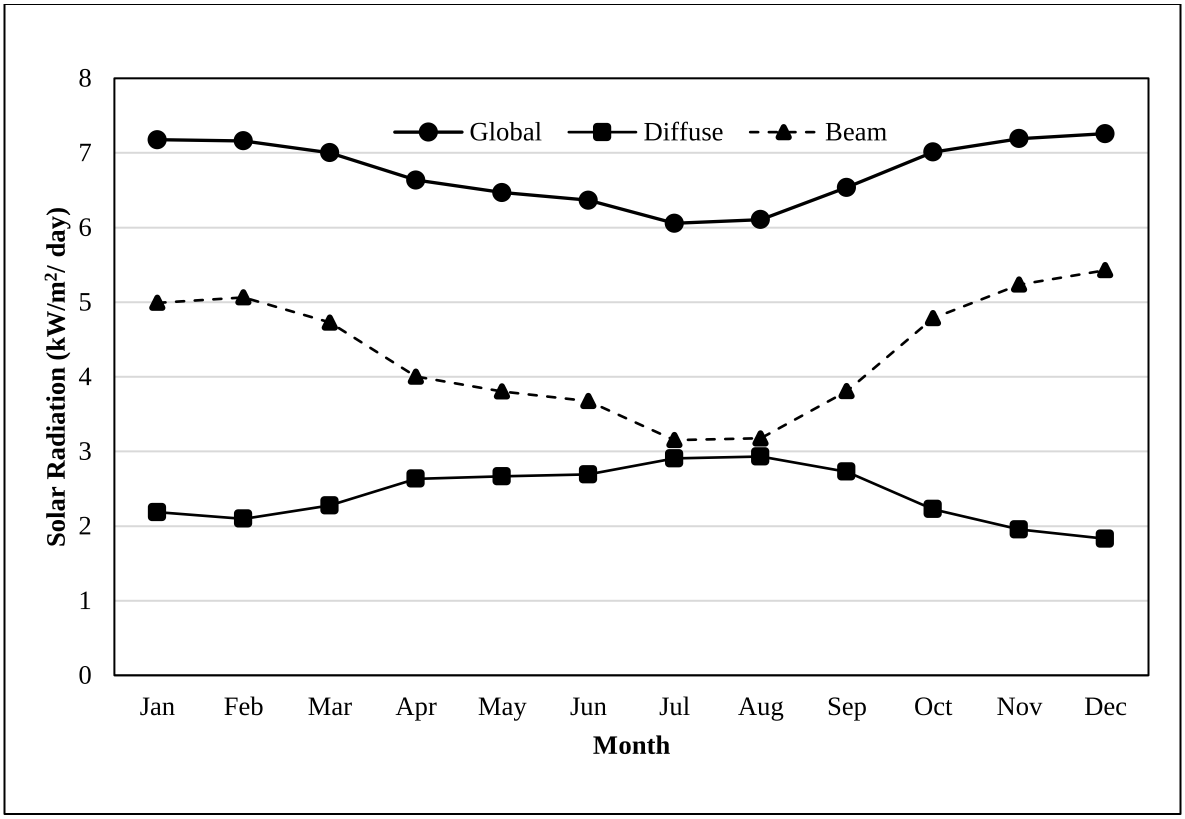

Figure 3.6 Monthly average daily global, diffuse and beam radiation on a horizontal surface

3.5.6 Estimation of Monthly Average Hourly Global Radiation on a Horizontal Surface

The monthly average hourly global radiation on a horizontal surface ($\bar{I}$) in W/m^2 can be determined from the monthly average daily global radiation on a horizontal surface (Duffie and Beckman, 1980).

$$\frac{\bar{I}}{\bar{H}} = \frac{\pi}{24}(a + b\cos\bar{w})\frac{\cos\bar{w} - \cos\bar{w}_s}{\sin\bar{w}_s - \frac{\pi}{180}\bar{w}_s\cos\bar{w}_s} \tag{3.17}$$

Where:

$$a = 0.409 + 0.5016\sin(\bar{w}_s - 60) \tag{3.18}$$

$$b = 0.6609 - 0.4767\sin(\bar{w}_s - 60) \tag{3.19}$$

Hourly variation of global radiation at each representative day of month for each of 24 hours in an hour interval is presented in Figure 3.7.

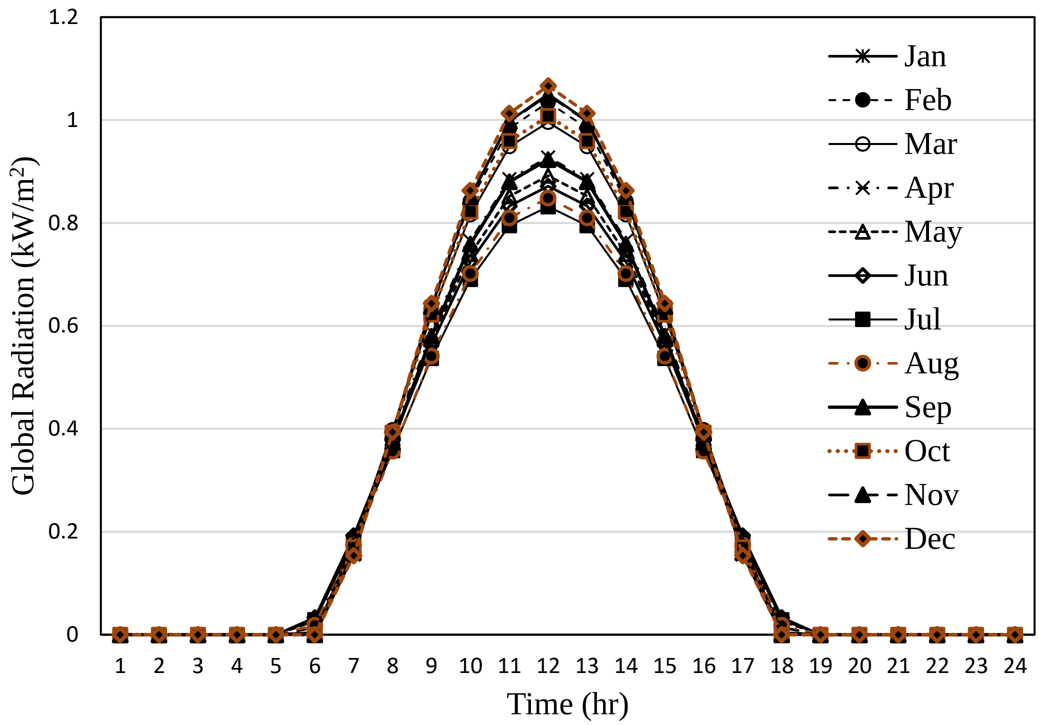

Figure 3.7 Monthly average hourly global solar radiation on a horizontal surface

As the graph shows global radiation intensity is detected from 6AM up to 18PM of the day (maximum at solar noon and minimum at sunset and sunrise).

3.5.7 Estimation of Monthly Average Hourly Diffuse and Beam Radiations on a Horizontal Surface

The monthly average hourly diffuse radiation on a horizontal surface ($\bar{I}_d$) in W/m^2 can be calculated from the knowledge of monthly average daily diffuse radiation on a horizontal surface (Duffie and Beckman, 1980).

$$\frac{\bar{I}_d}{\bar{H}_d} = \frac{\pi}{24} \frac{\cos \bar{w} - \cos \bar{w}_s}{\sin \bar{w}_s - \frac{\pi}{180} \bar{w}_s \cos \bar{w}_s} \tag{3.20}$$

Hourly variation of diffuse radiation at each representative day of month for each of 24 hours in an hour interval is presented in Figure 3.8.

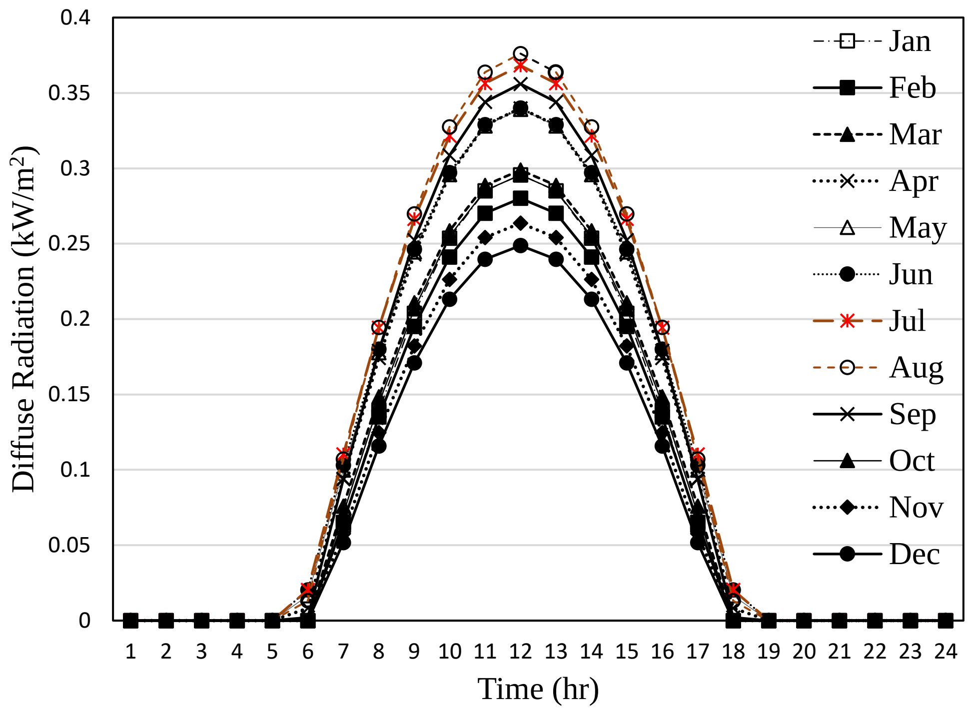

Figure 3.8 Monthly average hourly diffuse solar radiation on a horizontal surface

The monthly average hourly beam radiation on a horizontal surface ($\bar{I}_b$) is the difference between the monthly average hourly global and diffuse radiations.

$$\bar{I}_b = \bar{I} - \bar{I}_d \tag{3.21}$$

Hourly variation of beam radiation at each representative day of month for each of 24 hours in an hour interval is presented in Figure 3.9.

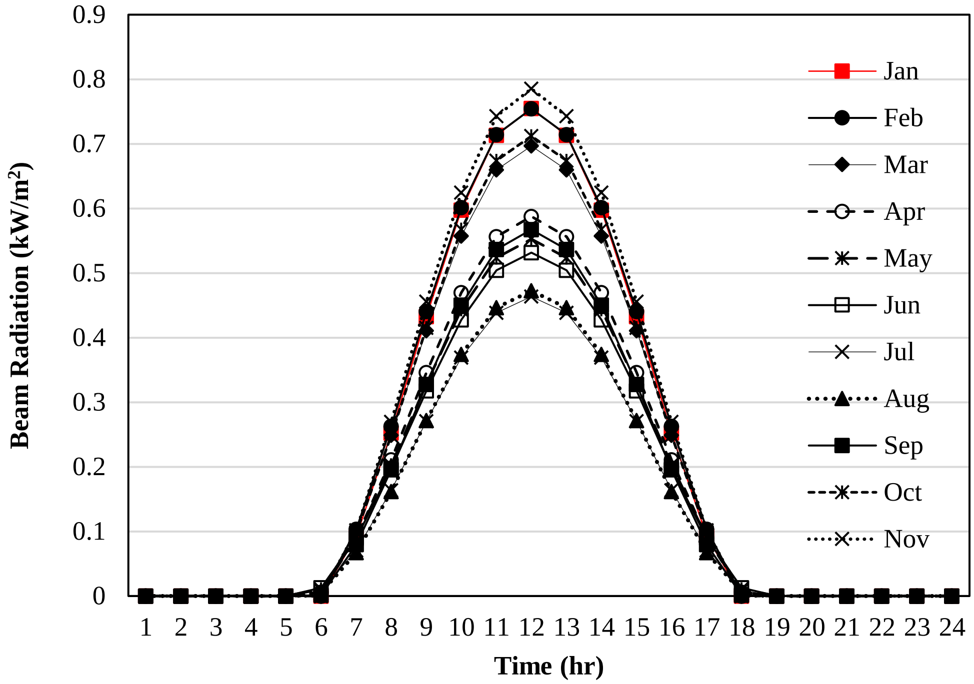

Figure 3.9 Monthly average hourly beam solar radiation on a horizontal surface

3.5.8 Estimation of Total Incident Solar Radiation on a Tilted Surface

The incident solar radiation on an inclined (tilted) surface is the sum of the beam, diffuse and reflected solar radiation from various surfaces (from a horizontal surface and surfaces surrounding it). Therefore, the total incident solar radiation on a surface tilted at an angle β can be expressed in terms of the global, beam, diffuse and the total reflected radiation to the tilted surface (Duffie and Beckman, 1980) and shown in Figure 3.10 for Adama.

$$I_T = I_b R_b + I_d\left(\frac{1+\cos\beta}{2}\right) + (I_b + I_d)\rho\left(\frac{1-\cos\beta}{2}\right) \tag{3.22}$$

Where: I_T is total hourly irradiance on a tilted surface (W/m^2).

I_b and I_d are hourly beam and diffuse irradiance (W/m^2), respectively.

R_b is the beam radiation factor which can be defined as the ratio of the incident beam radiation on a tilted surface to that on a horizontal surface.

$$R_b = \frac{\cos\theta}{\cos\theta_z} \tag{3.23}$$

β is surface slope angle.

ρ is reflectivity of ground and its value is 0.2 for ordinary ground (Tiwari and Tiwari, 2016).

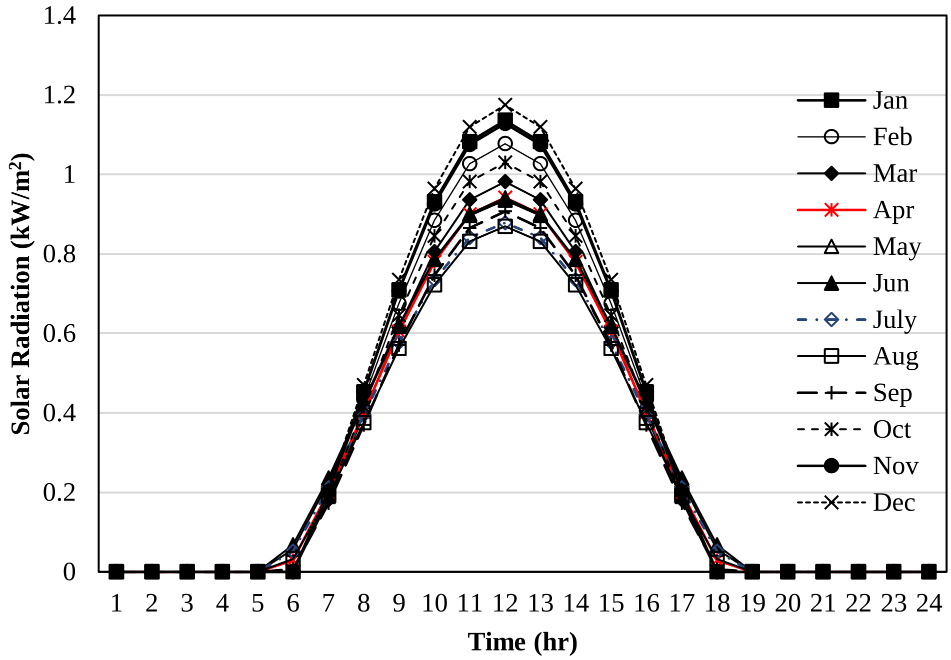

Figure 3.10 Monthly average hourly total incident solar radiation on a tilted surface

The amount of total solar radiation incident on a flat plate collector is a function of collector tilt angle. It is generally known that for a collector installed in the northern hemisphere, the optimum collector orientation is south facing ($\gamma = 0$) and the optimum tilt depends upon the latitude of the site and the day of the year. (Tiwari and Tiwari, 2016 and Ahmad and Tiwari, 2009) suggested optimum tilt angle is, β = latitude + 15°.

3.5.9 Estimation of Hourly Variation of Atmospheric Temperature

Hourly variation of atmospheric temperature was estimated from the daily maximum and minimum temperatures. A sin-exponential model proposed by Parton and Logan (1981) was used and it describes the diurnal cycle by a sine function during daytime and a decreasing exponential function during nighttime. The model assumes maximum temperature will occur sometime during the daylight hours before sunset and the minimum temperature will occur during the early morning hours. The mathematical description for the daytime and nighttime, respectively were expressed:

For daylight hours

$$T(H) = (T_{max} - T_{min}) \sin\left(\frac{\pi m}{Y + 2a}\right) + T_{min} \quad (24)$$

For night-time hours

$$T(H) = (T_{sunset} - T_{min}) \exp\left(-\frac{bn}{Z}\right) + T_{min} \quad (25)$$

Where:

T(H) is the temperature at any hour of the day or night period determined from m and n.

Y and Z are the length of the day and the night in h, respectively.

a is lag coefficient for TMAX= 1.80 h and b is night-time temperature coefficient = 2.20.

T_{sunset} is temperature at sunset (°C).

m is the number of hours after the T_{min} occurs until sunset and n is the number of hours after sunset until the time of the T_{min}.

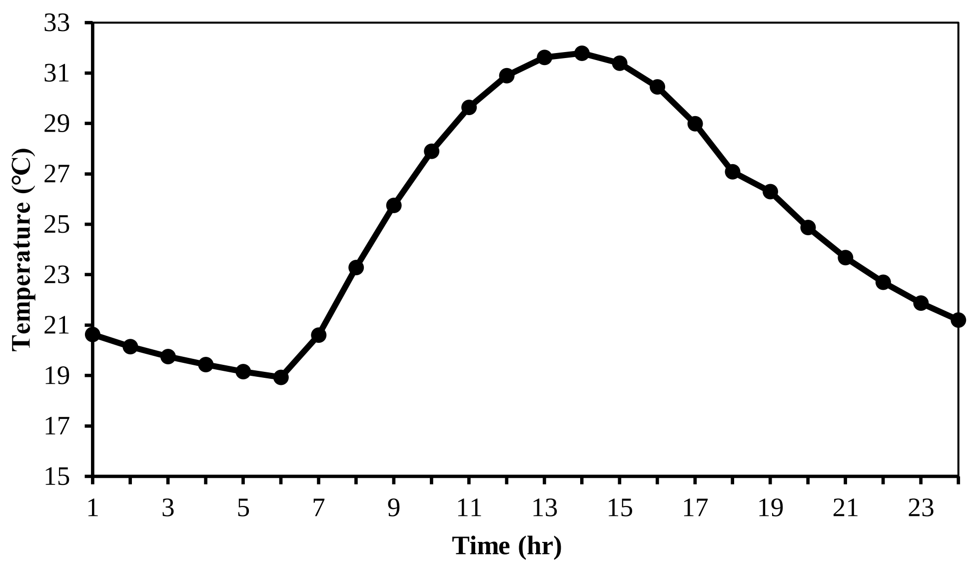

Figure 3.11 Average variation of ambient temperature of Adama.

CHAPTER FOUR

THEORETICAL ANALYSIS OF INDIRECT SOLAR DRYER

4.1 Introduction

This chapter presents the theoretical analysis of indirect solar air dryer which has double pass solar air heater with baffle and latent heat storage inside drying chamber. The analysis includes overall design of the dryer which is sizing of the components of the dryer (flat plate solar air collector, drying chamber, and latent heat storage). Selection of material for solar air heater is presented in detail. Energy and exergy analysis of the solar dryer components are also discussed.

4.2 Design of the Solar Air Dryer

The main design specifications for the dryer includes the moisture to be removed from the product, quantity of energy and mass of air required for the drying process, the mass flow rate and volumetric air flow, the output temperature of the dryer, and sizing of the components of the dryer.

4.2.1 Design of Components of the Dryer

Before calculating and designing the solar dryer component values specification of initial parameters (assumptions) are mandatory based on the collected data.

Initial parameters

The specification is important for overall design of the dryer. The initial parameters are listed below in Table 4.1.

Table 4.1 Specifications for the design of the dryer

Parameter	**Values and assumptions**
Initial moisture content	81 %
Final moisture content	10 % (Sahar *et al*., 2015)
Sample weight	5 kg
Average solar radiation	0.744 kW/m^2
Average ambient temperature	28 ℃
Average relative humidity	57 %
Desired drying temperature	55 ℃ (Kaleemullah and Kailappan, 2005; Castillo-Téllez *et al*., 2017)

1. **Angle of tilt (β) of solar collector**

Angle of tilt (β) of solar collectors is given by (Thakuria, 2018):

$$\beta = \phi + 15° \tag{4.1}$$

Where, ϕ is latitude of the location where solar air dryer tested

2. **Amount of Moisture to be Removed from the Product, kg (m_w)**

The amount of moisture to be removed from the product, m_w, can be determined by the following equation (Musembi *et al*., 2016):

$$m_w = m_p \left(\frac{m_i - m_f}{100 - m_f} \right) \tag{4.2}$$

Where; m_w is the amount of moisture to be removed from the product, m_p is initial mass of product to be dried, m_i is the initial moisture content in % wet basis and m_f is the final moisture content % wet basis. The amount of moisture to be removed from the product will be:

$$m_w = 3.94 \text{ kg}$$

3. **Quantity of heat energy required for evaporating moisture from product, Q_r**

The quantity of heat required to evaporate moisture from the product to be dried is given by the following equation (Musembi *et al*., 2016):

$$Q_r = m_w * h_{fg} \tag{4.3}$$

Where; Q_r is the amount of energy required for the drying process, kJ; m_w is mass of water vapour to be evaporated, kg; h_{fg} is latent heat of vaporization of water, kJ/kg.

The latent heat of vaporization was calculated using equation given by (Youcef-Ali *et al*., 2002)

$$h_{fg} = 4.186 * (597 - 0.56 T_p) \tag{4.4}$$

Where; T_p is maximum allowable temperature of the dried product in °C.

Thus, h_{fg} = 4.186*(597-0.56*55) = 2370.1 kJ/kg and from Eqn. (4.3) the amount of energy required to evaporate 3.94 kg of moisture is:

$$Q_r = 9.34 \text{ MJ}$$

4. Volumetric air flow and Mass flow rate

The total volume of air (V_a) required for removing the moisture from the product is evaluated from the equation given by (Forson *et al*., 2007):

$$V_a = \frac{m_w h_{fg} R_a T_a}{C_{pa} P_a (T_0 - T_f)} \tag{4.5}$$

where, T_f = temperature of air leaving the drying bed obtained from the following relationship.

$$T_f = T_a + 0.25(T_0 - T_a) \tag{4.6}$$

R_a = gas constant, kJ/kg. K; T_0 = temperature of air at the collector outlet, °C; P_a = partial pressure of dry air in the atmosphere, N/m^2 C_p = specific heat capacity of air, kJ/kg.K.

The mass flow rate of air needed to effect the drying is given by (Abubakar *et al*., 2018)

$$\dot{m}_a = \dot{V}_a \rho_a \tag{4.7}$$

Where,

$$\dot{V}_a = \frac{V_a}{t_d} \tag{4.8}$$

$\dot{V}_a$ = volume flow rate of the drying air, m^3/s and t_d = drying time per day, hrs.

Substituting the values of m_w = 3.94 kg, h_{fg}=2370.1 kJ/kg, R_a = 0.287 kJ/kg.K, T_0 = 55 °C, T_a = 28 °C, C_{pa} = 1.005 kJ/kg.K, P_a = 101.325 kN/m^2, ρ_a = 1.2 kg/m^3 and t_d = 7 hr into Eqn. (6.5-6.8) gives T_f = 34.75 °C, V_a = 391.4 m^3, $\dot{V}_a$ = 0.0155 m^3/s and $\dot{m}_a$ = 0.0186 kg/s.

4.2.1.1 Sizing of solar air heater

In this thesis, a double pass solar air heater (DPSAH) was selected for drying application. The concept of double pass arrangement reduces the top heat loss coefficient considerably which, improves the thermal efficiency with a little additional expenditure over the conventional air collectors (Ramani *et al*., 2010). In a DPSAH, the air first passes through the upper channel in the double pass collector between the top glass cover and the absorber plate and then recirculated in opposite direction through the lower channel between the absorber plate and back plate as shown in Figure 4.1.

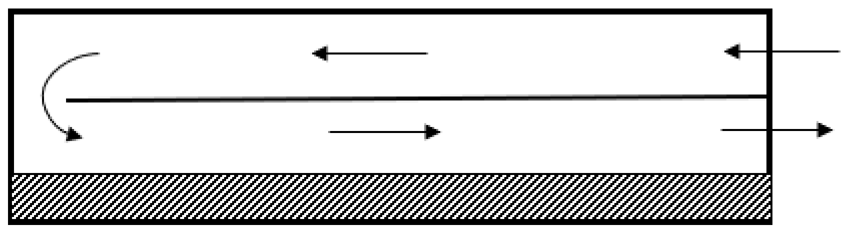

Figure 4.1 Schematic of double pass SAH

The area of the collector is where the solar radiation will be converted to heat energy and in the design of flat plate solar air heater it depends on the heat gain by the working fluid and solar radiation incident on it. When the area of the collector is larger the more solar energy will be absorbed, and the more heat will be produced. It can be calculated from energy balance as follow.

Heat received by the collector (Q_c): the total collected solar energy falling on the collector can be obtained from equation 4.9 (Musembi *et al*., 2016).

$$Q_c = I_t A_c \tag{4.9}$$

Useful heat collected by the collector (Q_u): It is an energy that comes from the dryer collector, and it will be calculated as shown in the Equation 4.10 as follow (Montero *et al*., 2010).

$$Q_u = \dot{m}_a c_{pa}(T_0 - T_a) \tag{4.10}$$

The efficiency of solar collector (η_c) is defined as the ratio of the useful energy gain to the incident solar energy and expressed as (Al-Juamily *et al*., 2007 and Montero *et al*., 2010):

$$\eta_c = \frac{Q_u}{Q_c} = \frac{\dot{m}_a c_{pa}(T_0 - T_a)}{I_t A_c} \tag{4.11}$$

By rearranging equation (4.11) area of the collector will become:

$$A_c = \frac{\dot{m}_a c_{pa}(T_0 - T_a)}{I_t \eta_c} \tag{4.12}$$

Where, η_c is collector efficiency and its value being 30 to 50% (Sodha *et al*., 1987), in %. Substituting each value in equation (4.12) yields:

$$A_c = 1.94\ m^2$$

Taking approximate value, the collector size = 2 m^2

The absorber surface area is approximately equal to the surface area of collector receiving solar insolation. Therefore, the absorber surface area becomes:

$$A_{ab} = A_c = L_c W_c \tag{4.13}$$

Where, L_c, W_c = length and width of the solar collector, respectively. Then either the length or the width of the collector will be assumed and calculated.

$$L_c = \frac{A_c}{W_c} \tag{4.14}$$

Assuming the width of the collector 1 m and the length will be: L_c = 2.0 m.

4.2.1.1.1 Enhancement of double pass solar air heaters with baffles

To obtain effective thermal efficiency from a flat plate solar collector, heat must be efficiently transferred from the absorbing plate to the flowing air. The heat transfer rate of a solar collector is an important parameter that affects the efficiency of the collector (Aldabbagh *et al*., 2010). Various modification has been recommended by different researchers to enhance the heat transfer rate in solar collector such as incorporating fins, baffles, and back bed inside the solar air heater.

Baffles provide an additional heat transfer surface area and promote air turbulence in the collector. The main concept of integrating baffles inside collector is to reduce dead zones and increase heat transfer area. The study conducted by (Romdhane, 2007) recommended that for a collector with a size of 2 m × 1 m, the number of baffles should be 6 to 12 which occupies 60% - 80% of the collector width. Therefore, six baffles which occupies 60 % of the collector width were placed between the base plate and the absorber plate.

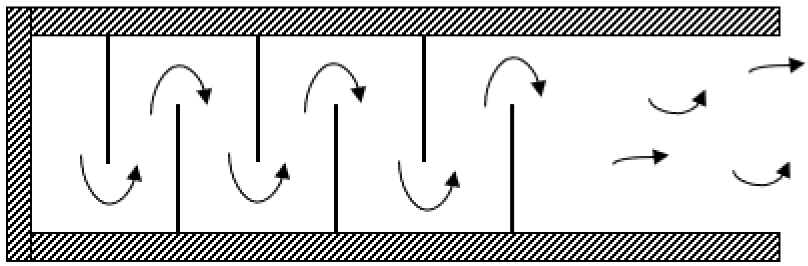

Figure 4.2 Schematic top view of collector with baffles.

4.2.1.1.2 Material selection for SAH

A. Absorber plate

The main element of a flat-plate solar collector is the absorber plate. The function of absorber plate is to absorb the maximum possible amount of solar irradiance, transfer this heat into the working fluid, and lose a minimum amount of heat back to the surroundings. Thermal conductivity, absorptivity, corrosion resistance, durability, availability, and cost are some of the factors to be considered while selecting absorber plate. Steel sheet metal was selected due to its availability and cost and painted black for better absorptivity.

B. Glazing

Glazing is the top cover of a solar collector and it used to minimize convective and radiant heat loss from absorber, to transmit the incident solar radiation to the absorber plate with minimum loss, and to protect the absorber plate from outside environment. Other important characteristics of glazing materials are reflection (r), absorption (α), and transmission (τ). To attain maximum efficiency, reflection and absorption should be as low as possible, whilst transmission should be as high as possible. Thus, factors for consideration in selecting the glazing materials include strength of material, durability, no degradability when exposed to UV light, and low costs. The use of 4 mm glass thick improves the performance of air solar collector by 7.6% compared to 3, 5, and 6 mm glass thicknesses (Alghoul *et al*., 2005 and Bakari *et al*., 2014). In the present work, plain glass was selected as the glazing material of solar air heater. Glass is selected due to its advantage in terms of its high transmittance of the incoming radiation, its life span compared with plastic, and availability in local market compared to other glazing materials. lazing materials.

Table 4.2 Summary of material and property specification of solar air heater

Description	**Specification**
Collector type	Double pass flat plate collector
Collector area	2.0 m^2
Glazing • Material • Dimension • Thickness • Transmissivity	 Transparent glass 2.0 m x 1.0 m 4 mm 0.90
Absorber plate • Material • Dimension • Thickness • Thermal conductivity • Absorptivity	 Black painted steel sheet metal 1.9 m x 1.0 m 1 mm 66 W/m.K 0.85
Base plate • Material • Dimension • Thickness	 Galvanized iron sheet 2 m x 1 m 0.8 mm
Baffle • Material • Dimension • Thickness	 Steel sheet metal 0.6 m x 0.04 m 1 mm
Gap between absorber plate and glass cover	40 mm
Gap between base plate and absorber plate	40 mm
Insulation • Material • Thickness • Thermal conductivity	 Polyurethane foam 25 mm 0.0285 W/m.K

C. Insulation

To reduce the conduction and convection losses through the back and sides of the flat plate SAH, an insulation should be used. Selection of insulating material should and selected based on initial cost, thermal conductivity, and durability. A wide range of insulating materials are available such as polyurethane form, expanded polystyrene, fiber glass, and plywood. Polyurethane foam and plywood were selected due to their availability in local market and low cost for the back and sides of the collector, respectively.

D. Frame and support

Square pipe steel and angle iron were selected and used to construct the frame and support of the solar collector to withstand its weight. It provides the rigidity and desired inclination to the solar radiations.

4.2.1.2 Sizing of drying chamber

The effective drying bed area, A_{db} is obtained from first principles by relating the solid density of the wet material to its mass and the corresponding volume as (Forson *et al*., 2007):

$$A_{db} = \frac{m_p}{\rho_b h_l \xi} \tag{4.15}$$

Where m_p is the mass of the crop to be dried, ρ_b is the bulk density of the crop on wet basis, h_l is product thickness, and ξ is the crop porosity.

The total volume can be related to bulk density as (Abubakar *et al*., 2018):

$$V_T = \frac{m_p}{\rho_b} \tag{4.16}$$

The true density, bulk density and porosity are 900 kg/m^3, 410 kg/m^3 and 53.74% for chilli pepper, respectively (Ilori *et al*., 2018). Substituting the values of m_p = 5 kg, ρ_b = 410 kg/m^3 , ζ = 53.74 % and h_l = 10 mm into Eqn. (4.15) and (4.16) yields, A_{db} = 2.30 m^2 and V_T = 0.0122 m^3.

Considering the number of trays as 3 and the width of the collector (W_c) equal to the width of the drying chamber (W_{dc}). The area of tray, A_t and length of tray, L_t can be obtained from the following equation:

$$A_t = \frac{A_{db}}{n} \tag{4.17}$$

And

$$L_t = \frac{A_t}{W_t} \tag{4.18}$$

Where, n = number of trays; the value of area of tray, A_t and length of tray, L_t will become 0.767 m^2 and 0.767 m, respectively.

4.2.1.3 Design of thermal energy storage

Thermal energy storage is developed for solar drying system to maintain approximately uniform drying temperature and to continue the drying process for a few additional hours when solar radiation is not available. The design includes selection of a storage material and sizing of heat storage unit.

4.2.1.3.1 Selection of storage material

Phase change material (PCM) is selected due to the following advantages (Bal *et al*., 2010):

- In LHS systems the temperature of the medium remains more or less constant since it undergoes a phase transformation.
- PCMs absorb and emit heat while maintaining a nearly constant temperature.
- They store 5–14 times more heat per unit volume than sensible storage materials such as water, masonry, or rock.
- Thermal storage capacity per unit mass and unit volume for small temperature differences is high.
- Thermal gradients during charging and discharging are small.
- Simultaneous charging and discharging are possible with appropriate selection of heat exchanger.

The main criteria for selecting PCMs for drying operation is their melting temperature. PCMs with melting temperature between 38°C and 65°C are recommended for solar energy storage for dehydrating agricultural based products (Regin *et al*., 2008). For the present case, in addition to the melting temperature range, availability in the local market and cost was considered while selecting the PCM. Thus, paraffin wax of having average melting temperature in the range of 58–60 ℃ has been chosen as the energy storage material since it is safe and easily available in the local market. Table 4.3 shows the physical property of paraffin wax.

Table 4.3 Thermo-physical properties of selected paraffin wax (Sukontasukkul *et al*., 2019)

Property	**Value**
Melting point (℃)	58-60
Heat of fusion (kJ/kg)	189
Thermal conductivity (W/m℃)	0.21
Specific heat (J/kg℃)	2284
Density (kg/m^3)	910

4.2.1.3.2 Sizing of PCM storage

The PCM storage unit is located at the inner bottom of the drying compartment to reduce the heat losses and for construction simplicity. No insulation is provided for the PCM storage since it is placed inside the dryer chamber. Heat is transferred from the hot air, which comes from the collector outlet to the paraffin wax during the charging process and the reverse during discharging process for off-sunshine hours.

The melting time of the enclosed PCM is major parameters to select shape and size of the container. Rectangular geometry is the general encapsulation method as it is possible to achieve more surface area per unit volume of PCM container (Raj and Velraj, 2010). They numerically investigated the thermal performances of rectangular and cylindrical containers. The melting time for the two containers was compared, and their outcomes conveyed that a rectangular container involves half of the melting time as that of a cylindrical one of the same volume and heat transfer area. Square geometry is preferred over rectangular. In this geometry uniform strains are experienced at all faces during transformation of PCM. Hence, a square geometry is selected for this research.

The quantity of heat needed to be stored in the thermal energy storage system can be estimated by assuming the storage will store the heat for 2 off-sunshine hours per day as follow:

$$Q = \dot{m}_a c_{pa} (T_d - T_a) t \tag{4.19}$$

The amount of PCM required was determined from the relationship (Gunjo, 2018)

$$Q = m_{pcm}\left[c_{pcm}(T_m - T_i) + L_{pcm}\right] \tag{4.20}$$

The volume of the PCM can be calculated from,

$$V_{pcm} = \frac{m_{pcm}}{\rho_{pcm}} \tag{4.21}$$

Where, m_{pcm} and ρ_{pcm} are mass and density of PCM material, respectively. Substituting each value on the above equations yield Q = 3516.7 kJ, m_{pcm} = 13 kg and V_{pcm} = 0.0142 m^3.

Based on the calculated volume, the size of the PCM container is determined. The specifications of the PCM container are presented in Table 4.4.

Table 4.4 Specification of PCM container

PCM container's parameters	**Specification**
Material	Aluminum
Shape	Square
Size	0.40 m x 0.40 m x 0.044 m
Number of containers	2

4.3 Energy and Exergy Analysis

The energy and exergy analysis of the drying system was performed based on the general mass and energy conservation equations. The data obtained from the experiments were used to perform the energy and exergy analyses. The basic data requirements are the temperature of the air streams at different locations, the mass flow rate of air, the energy inflows and outflows of the drying system, and the mass of moisture removed from the product.

4.3.1 Energy Analysis

The energy analysis of the drying system was performed based on the general mass and energy conservation equations by employing first law of thermodynamics for main components of the dryer. During the energy analysis, the flow in the drying system was assumed to be steady. The general mass and energy conservation equations for steady flow are explained, as given in equations (4.22) and (4.23), respectively (Cengel *et al.*, 2011).

$$\sum \dot{m}_{ia} = \sum \dot{m}_{0a} \tag{4.22}$$

$$\dot{Q} - \dot{W} = \sum \dot{m}_{oa}\left(h_{oa} + \frac{{V_{oa}}^2}{2} + Z_{oa}\text{g}\right) - \sum \dot{m}_{ia}\left(h_{ia} + \frac{{V_{ia}}^2}{2} + Z_{ia}\text{g}\right) \tag{4.23}$$

Where, $\dot{Q}$ and $\dot{W}$ are heat and work transfer rates, respectively in W; $\dot{m}_{oa}$ and $\dot{m}_{ia}$ are outlet and inlet mass flow rates of air in kg/s, respectively; h_{oa} and h_{ia} are outlet and inlet enthalpies of air in kJ//kg, respectively; V_{oa} and V_{ia} are inlet and outlet velocities of air in m/s, respectively; Z_{oa} and Z_{ia} are inlet and outlet heights from the reference plane in m, respectively; g is acceleration due to gravity in m/s^2.

In this drying system, mass flow rate is assumed uniform from inlet to outlet and any change in it is negligible.

4.3.1.1 Energy analysis of solar air heater

In the dryer, the effects of the kinetic and potential energies were neglected since the inlet and outlet of the solar air heaters were located at the same height from the ground and the change in velocity between the inlet and the exit was negligible. Therefore, the equations of mass and energy conservation for the SAH can be expressed by equations (4.24) and (4.25), respectively.

$$\dot{m}_{ia} = \dot{m}_{oa} = \dot{m}_a \tag{4.24}$$

$$\dot{Q}_{in} - \dot{Q}_{ls} = \dot{m}_a(h_{oa} - h_{ia}) \tag{4.25}$$

Where, $\dot{Q}_{ls}$ is the rate of heat loss in the solar air heater in W; $\dot{Q}_{in}$ is the rate of heat input to the SAH in W, and illustrated by equation (4.26) as follow:

$$\dot{Q}_{in} = \alpha_a \tau_g I_{rad} A_c \tag{4.26}$$

Where, α_a and τ_g are absorptivity of the absorber plate and transmissivity of the glass cover, respectively.

The right-hand term of Eq. (4.25) is known as the useful heat gained by SAH, and it can be obtained by measuring the inlet and outlet temperature of the air heaters and the mass flowrate of air. It can be written as (Rabha and Muthukumar, 2017 and Rabha *et al*., 2017):

$$\dot{Q}_{uc} = \dot{m}_a c_{pa}(T_{oc} - T_{ic}) \tag{4.27}$$

The rate of heat loss from the solar air heater can be determined as:

$$\dot{Q}_{ls} = \dot{Q}_{in} - \dot{Q}_{uc} = \alpha_a \tau_g I_{rad} A_c - \dot{m}_a c_{pa}(T_{oc} - T_{ic}) \tag{4.28}$$

The instantaneous energy efficiency of the SAH is defined as the ratio of the useful heat gained to the solar radiation incident on the absorber surface (Bahrehmand *et al.*, 2015). Therefore, for the SAH, it is presented by equation (4.29) as:

$$\eta_{SAH} = \frac{\dot{m}_a c_{pa}(T_{oc} - T_{ic})}{\alpha_a \tau_g I_{rad} A_c} \tag{4.29}$$

4.3.1.2 Energy analysis of energy storage

The energy balance of TES is done based on the first law of thermodynamics with following assumptions (Lakshmi *et al.*, 2021).

- Thermo-physical properties of the air are considered as constant.
- Amount of paraffin wax is constant during charging, storing, and discharging.
- Charging, storing, and discharging of the wax are finite.

The instantaneous heat input to the storage during the charging process is expressed by (Dincer and Rosen, 2011):

$$\dot{Q}_{ch} = \dot{m}_a c_{pa}\left(T_{i,es} - T_{o,es}\right) \tag{4.30}$$

Then, net heat input to the storage during the charging period is given by Eq. (4.31)

$$Q_{ch} = \int_0^t \dot{Q}_{ch} dt \tag{4.31}$$

Similarly, the instantaneous heat and the net heat recovered from the storage during the discharging period are given by Eqs. (4.32) and (4.33), respectively.

$$\dot{Q}_{dich} = \dot{m}_a c_{pa}\left(T_{o,es} - T_{i,es}\right) \tag{4.32}$$

$$Q_{dich} = \int_0^t \dot{Q}_{dich} dt \tag{4.33}$$

The overall energy efficiency of the storage or the percentage of the energy recovered is defined as the ratio of the net heat recovered to the net heat input. It is expressed by the following equation.

$$\eta_{es} = \frac{Q_{dich}}{Q_{ch}} \tag{4.34}$$

4.3.1.3 Energy analysis of drying chamber

During the dehumidification process at the drying chamber, the heat used can be estimated by employing the following equation (Akbulut and Durmuş, 2010):

$$\dot{Q}_{dc} = \dot{m}_a c_{pa}\left(T_{i,dc} - T_{o,dc}\right) \tag{4.35}$$

Where, $T_{i,dc}$ and $T_{o,dc}$ are inlet and outlet temperatures of the drying chamber in °C, respectively.

During the drying process, the energy utilization ratio of the drying chamber (EUR) was calculated using the following equation (Akbulut and Durmuş, 2010):

$$EUR = \frac{\dot{m}_a c_{pa}\left(T_{i,dc} - T_{o,dc}\right)}{\dot{m}_a c_{pa}\left(T_{o,SAH} - T_{i,SAH}\right)} \tag{4.36}$$

4.3.2 Exergy Analysis

The exergy uses the conservation of the mass and the energy principles together with the second law of thermodynamics for the design and analysis of the energy systems (Kocaa *et al*., 2008). The exergy is defined as the amount of maximum work, which can be produced by a system or a flow of matter or energy as it comes to equilibrium with a reference environment (El Khadraoui *et al*., 2017)

Exergy analysis is performed for each component of the drying system and the following assumptions are made during the analysis.

- The flow is assumed to be steady.
- The effects of the kinetic and the potential energy are neglected.
- The effect of moisture content on the heat capacity of the air is neglected.
- The exergy loss in the product is neglected.
- The change in the pressure between the inlet and out is neglected.

Therefore, the rate form exergy equation for the steady flow system with one inlet and exit and considering the above assumptions can be expressed as follows (Rabha *et al.*, 2017):

$$\dot{E}x = \dot{m}_a c_{pa}\left[(T - T_{amb}) - T_{amb}\ln\left(\frac{T}{T_{amb}}\right)\right] \tag{4.37}$$

4.3.2.1 Exergy analysis of the solar air heater

Under steady state condition, the equation of exergy balance takes the following form (Jafarkazemi and Ahmadifard, 2013)

$$\sum \dot{E}x_{in} - \sum \dot{E}x_{out} = \sum \dot{E}x_{dest} \tag{4.38}$$

Where, $\dot{E}x_{in}$, $\dot{E}x_{out}$ and $\dot{E}x_{dest}$ are the inlet, outlet, and destructed exergy rate, respectively.

The inlet exergy to the collector consists of the exergy of absorbed heat from sun ($\dot{E}x_{rad}$) and the exergy of inlet fluid ($\dot{E}x_{in,f}$). A major part of inlet exergy to the system is that solar radiation which is absorbed by the absorption plates and obtained using the expression (Yadav and Kaushal, 2014)

$$\dot{E}x_{rad} = \left[1 - \frac{T_{amb}}{T_s}\right]\dot{Q}_{in} \tag{4.39}$$

Where, T_s is the apparent sun temperature as exergy source which is approximately 3/4 of the blackbody temperature of the sun. It is assumed to be 4500 K in this analysis.

And the exergy of inlet fluid ($\dot{E}x_{in,f}$) and outlet fluid ($\dot{E}x_{out,f}$) expressed as:

$$\dot{E}x_{in,f} = \dot{m}_a c_{pa}\left[\left(T_{i,SAH} - T_{amb}\right) - T_{amb}\ln\left(\frac{T_{i,SAH}}{T_{amb}}\right)\right] \tag{4.40}$$

$$\dot{E}x_{out,f} = \dot{m}_a c_{pa}\left[\left(T_{o,SAH} - T_{amb}\right) - T_{amb}\ln\left(\frac{T_{o,SAH}}{T_{amb}}\right)\right] \tag{4.41}$$

Obviously, the difference between these two components ($\dot{E}x_{in,f}$ and $\dot{E}x_{out,f}$) represents the amount of exergy loss in the collector and expressed as

$$\dot{E}x_{out,f} - \dot{E}x_{in,f} = \dot{m}_a c_{pa}\left[\left(T_{o,SAH} - T_{i,SAH}\right) - T_{amb}\ln\left(\frac{T_{o,SAH}}{T_{i,SAH}}\right)\right] \tag{4.42}$$

The exergy destruction in the solar air heater is given by Eq. (4.43) (Esen, 2008):

$$\dot{E}x_{dest} = \left(1 - \frac{T_{amb}}{T_s}\right)\dot{Q}_{in} - \dot{m}_a c_{pa}\left[\left(T_{o,SAH} - T_{i,SAH}\right) - T_{amb}\ln\left(\frac{T_{o,SAH}}{T_{i,SAH}}\right)\right] \tag{4.43}$$

The exergy efficiency of the solar air heater is expressed as follows (Akpinar and Koçyiğit, 2010)

$$\eta_{Ex,SAH} = 1 - \frac{\dot{E}x_{dest}}{\dot{E}x_{i,SAH}} \tag{4.44}$$

Or

$$\eta_{Ex,SAH} = \frac{\dot{E}x_{re,air}}{\dot{E}x_{i,SAH}} = \frac{\dot{m}_a c_{pa}\left[\left(T_{o,SAH} - T_{i,SAH}\right) - T_{amb}\ln\left(\frac{T_{o,SAH}}{T_{i,SAH}}\right)\right]}{\left(1 - \frac{T_{amb}}{T_s}\right)\dot{Q}_{in}} \tag{4.45}$$

4.3.2.2 Exergy analysis of energy storage

During charging and discharging process, the instantaneous exergy input to the energy storage and exergy recovered from the storage, respectively, are expressed as (Dincer and Rosen, 2011):

$$\dot{E}x_{ch} = \dot{m}_a c_{pa}\left[\left(T_{i,es} - T_{o,es}\right) - T_{amb}\ln\left(\frac{T_{i,es}}{T_{o,es}}\right)\right] \tag{4.46}$$

$$\dot{E}x_{dich} = \dot{m}_a c_{pa}\left[\left(T_{o,es} - T_{i,es}\right) - T_{amb}\ln\left(\frac{T_{o,es}}{T_{i,es}}\right)\right] \tag{4.47}$$

The net exergy input and exergy recovered during the charging and discharging periods, respectively, are calculated as:

$$Ex_{ch} = \int_0^t \dot{E}x_{ch}dt \tag{4.48}$$

$$Ex_{dich} = \int_0^t \dot{E}x_{dich}dt \tag{4.49}$$

The exergy efficiency of the energy storage system is defined as the ratio of the net exergy recovered from the energy storage during the discharging period to the net exergy input to the storage during the charging period (Koca *et al*., 2008).

$$\eta_{Ex,es} = \frac{Ex_{dich}}{Ex_{ch}} \tag{4.50}$$

4.3.2.3 Exergy analysis of drying chamber

The exergy inflow and outflow of the drying chamber are estimated by equations (4.51) and (4.52), respectively (Fudholi *et al*., 2014).

$$\dot{E}x_{i,dc} = \dot{m}_a c_{pa}\left[\left(T_{i,dc} - T_{amb}\right) - T_{amb}\ln\left(\frac{T_{i,dc}}{T_{amb}}\right)\right] \tag{4.51}$$

$$\dot{E}x_{o,dc} = \dot{m}_a c_{pa}\left[\left(T_{o,dc} - T_{amb}\right) - T_{amb}\ln\left(\frac{T_{o,dc}}{T_{amb}}\right)\right] \tag{4.52}$$

During the solar drying process, the exergy losses are determined as:

$$\dot{E}x_{loss} = \dot{E}x_{i,dc} - \dot{E}x_{o,dc} \tag{4.53}$$

The exergy efficiency of the drying cabinet is the ratio of the exergy outflow to the exergy inflow of the drying cabinet (Aghbashlo *et al*., 2013). It is expressed as:

$$\eta_{Ex,dc} = \frac{\dot{E}x_{o,dc}}{\dot{E}x_{i,dc}} \tag{4.54}$$

4.4 Performance Parameters of the Overall Drying System

The specific energy consumption (SEC) of the drying system is defined as the ratio of the total energy input to the drying system to the amount of moisture evaporated from the dried product and it is computed as (Fudholi *et al*., 2014):

$$SEC = \frac{P_t}{m_w} \tag{4.55}$$

The energy inputs to this drying system are the solar radiation incident on solar air heaters surface and the electrical energy consumed by the blower. Therefore, the total energy input is computed by the following equation.

$$P_t = [(I_{rad}A_c) + P_{bl}]t_d \tag{4.56}$$

The mass of the moisture 'm_w' evaporated from the product while reducing the moisture content from the initial value of m_i to the final value of m_f was obtained by Eq. (4.57) as follow:

$$m_w = m_p\left(\frac{m_i - m_f}{100 - m_f}\right) \tag{4.57}$$

The theoretical thermal efficiency, the ratio of the actual temperature drops to the maximum possible temperature drop of the drying air in the drying chamber was evaluated by the following equation (Rabha *et al*., 2017).

$$\eta_{dc} = \frac{T_{i,dc} - T_{o,dc}}{T_{i,dc} - T_{amb}} \tag{4.58}$$

The overall thermal efficiency of the drying system is calculated by Eq. (4.59). It is defined as the ratio of the energy required to evaporate the moisture from the product to the total energy input into the drying system.

$$\eta_{ds} = \frac{m_w h_{fg}}{P_t} \tag{4.59}$$

CHAPTER FIVE

EXPERIMENTAL SETUP AND PROCEDURE

5.1 Introduction

This chapter presents the conceptual model, working principle, manufacturing process, experimental setup and procedure followed while testing the prototype of an indirect forced convection solar dryer. The conceptual model of the system was developed using CATIA V5R20. The working principle of the system is explained in detail. Manufacturing process of each component for preparing the prototype is presented with descriptive photos. Finally, the measuring and testing devices used are presented.

5.2 Conceptual Model

The schematic diagram of indirect forced convection (active) solar dryer drawn using CATIA V5R20. The system consists of a flat plate double pass solar collector with baffle, drying chamber, thermal storage unit inside drying chamber, blower, frame, and support. The conceptual design of the dryer is shown in Figure 5.1.

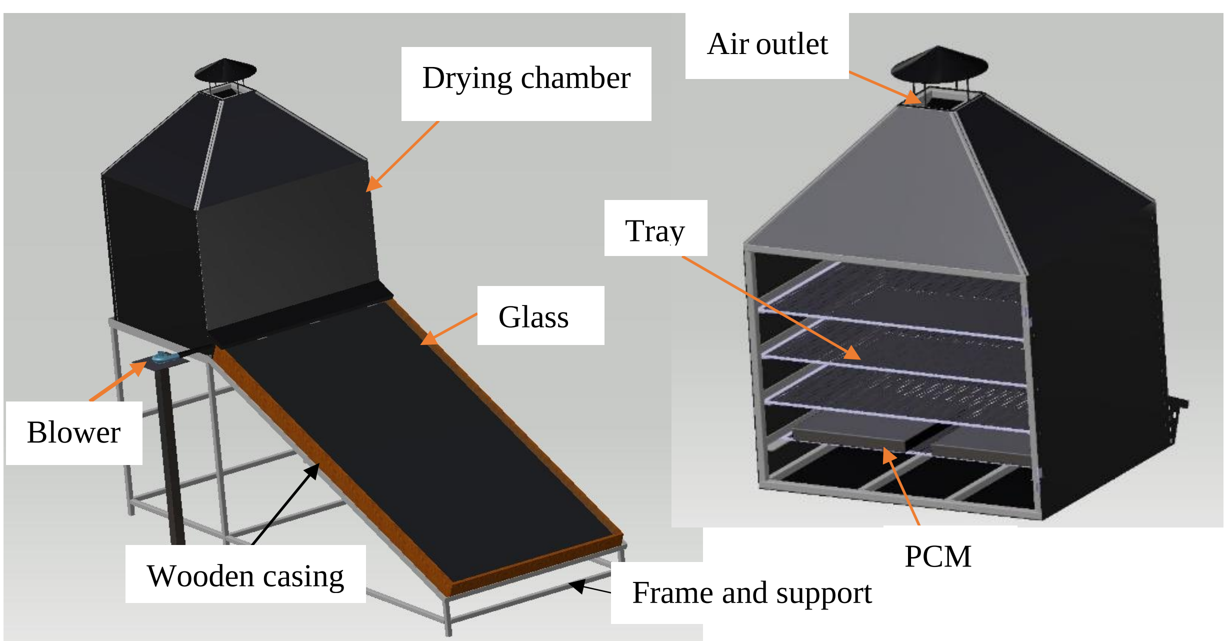

Figure 5.1 Conceptual schematic of indirect solar dryer

5.3 Working Principle

The developed indirect type solar dying system consists of a flat plate solar collector with baffle, drying chamber, thermal storage unit inside drying chamber and a blower as illustrated in Figure 5.2. In this system, a double pass flat plate solar collector will absorb sun's radiant energy and transfer it to the heat transfer fluid, which is air in this case. The drying chamber receives heated air exiting from the solar air heater, having temperature sufficiently higher than the ambient air. The drying chamber houses latent heat storage container, which is filled by paraffin wax, at the bottom and three drying trays. During charging, when the temperature of the air leaving the solar air heater is higher than the temperature of the PCM, heat will be transferred from the air to the PCM. Considering that during the discharge period, when the temperature of the air leaving the solar air heater is lower than the PCM, the stored heat will be released from the PCM, causing the air temperature to rise. Then, the air passes through three drying trays to dry the product and ventilates to the atmosphere through air outlet after removing the moisture from the surface of the products. A blower system which helps in accelerating the heated air from solar collector to the drying chamber is integrated as an active mode.

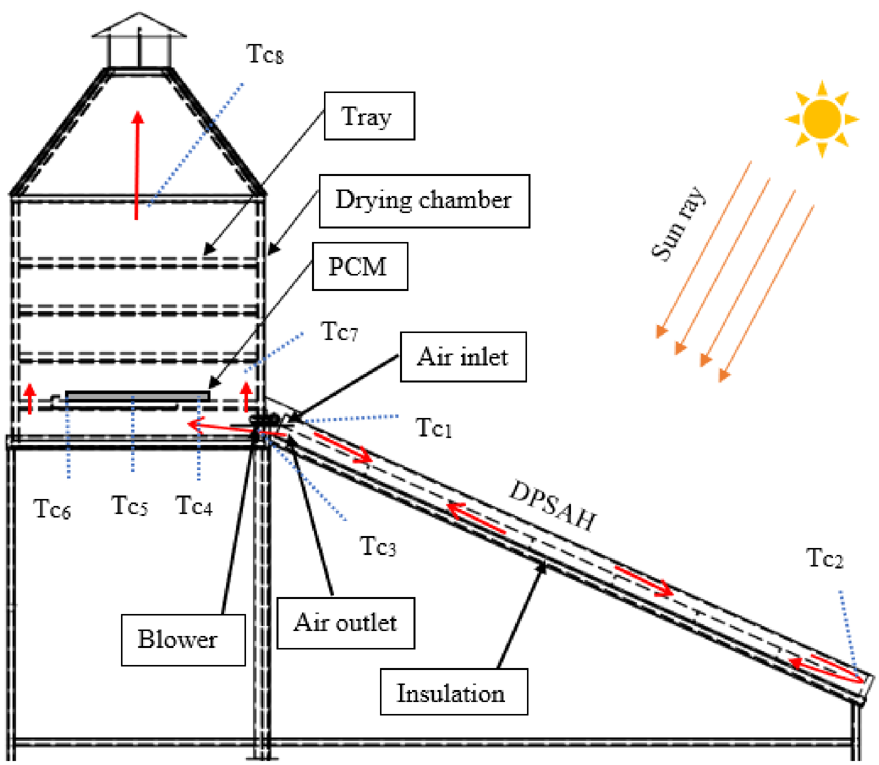

Figure 5.2 Schematic layout of the solar dryer (Tc-Thermocouple).

5.4 Manufacturing Process

The components of the dryer are the solar air heater, drying chamber, and latent heat storage. Each step used to construct components of the dryer and its assembly is shown, described, and discussed in this section as follow.

5.4.1 Construction of the Flat Plate Solar Air Heater

The collector is the main part of the dryer that collect the useful energy (solar energy) that comes from the sun and transfer the heat to the air that comes from the ambient air and passes through it. A rectangular box, having size 2.04 m x 1.04 m x 0.10 m (length x width x height) was constructed from plywood of thickness 0.02 m as demonstrated in Figures 5.3. Additionally, the solar air heater contains base plate, absorber plate, insulation, and glass cover. The base plate is 2 m × 1 m galvanized iron sheet with 0.8 mm thickness. A 20 mm thick foam is placed below the base plate and above plywood as insulation.

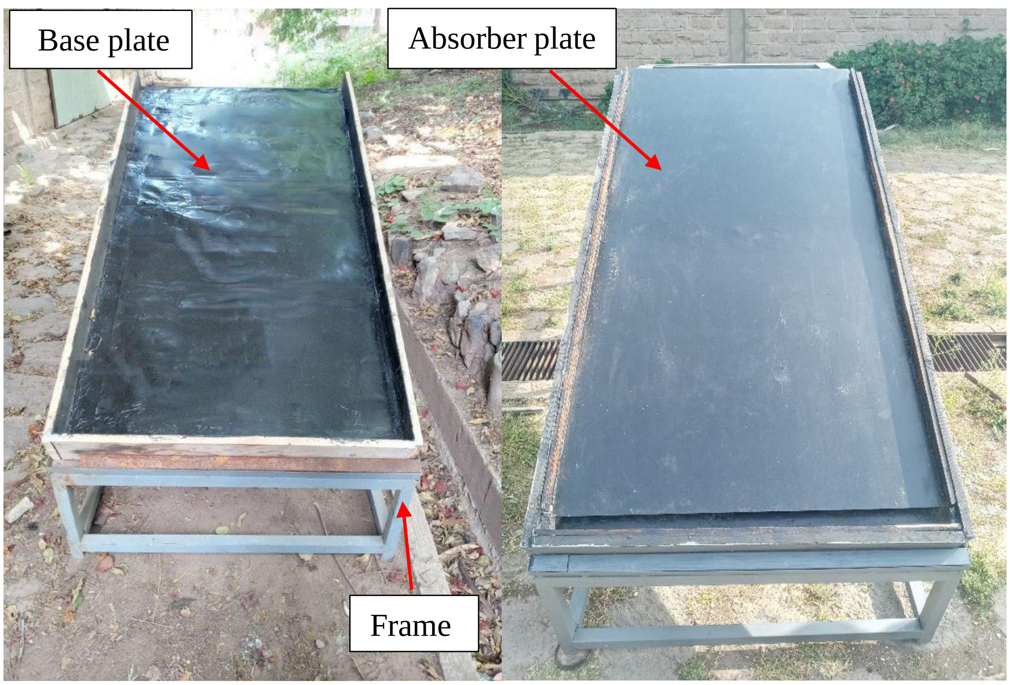

Figure 5.3 Manufacturing of double pass solar collector

Black painted steel sheet of 1.9 m × 1 m and 1.0 mm thick is used as absorber plate and placed at a gap of 40 mm from the bottom plate. Six baffles with width of 0.60 m from left and right side of casing and height of 0.04 m are placed in between the base plate and absorber plate having equal space, which is 250 mm, with one another for the second test. This arrangement of baffles was placed to guide the flow of air stream in to zigzag so that it could absorb additional energy. Key objective of providing baffles in such system was to deliver more contact area to get more heat for additional heat transfer.

a b

Figure 5.4 (a) Placement of baffles into base plate and (b) pictorial view of SAH

The glazing is a 2.0 m × 1.0 m and 4 mm thick plain glass and placed at a gap of 40 mm from the absorber plate. The collector is mounted facing south tilted at an angle of 24° as shown in Figure 5.4 (b).

5.4.2 Construction of the Drying Chamber

The drying chamber is where the drying product will be placed and heated by the hot air that comes from the collector. Its structure was fabricated from steel bar and angle iron whereas its body is constructed with plywood to avoid heat losses which was locally available. The size of the drying chamber was made as per the design standards, having dimensions of 0.80 m x 1.00 m x 0.80 m (length x width x height) as demonstrated in Figure 5.5. A trapezoidal shaped cover is placed at the top of the chamber to remove hot air that have the moisture on it and comes from the chamber to the outside environment. The chamber has a door at one side (backside) which is used for loading and unloading.

Figure 5.5 Manufacturing process of drying chamber

As discussed in the previous chapter this dryer has three trays used to carry the drying product. The trays are made of wired mashed (Figure 5.6) with very tiny holes used to transfer heat throughout the dryer. They have a dimension of 0.76 m x 0.96 m. The gap between the trays is 0.15 m from one another. Each tray was kept on an angle iron fixed to inner side of walls of the chamber.

Figure 5.6 Pictorial view of drying chamber and loaded tray

5.4.3 Construction of Latent Heat Storage Container

Thermal energy storage is done by using phase change material (PCM) as latent heat storage. A square shape PCM container were fabricated from aluminum sheet for better heat transfer as shown in Figure 5.7 (b). The size of the container is 0.40 m x 0.40 m x 0.044 m (length x width x height). The container is filled with 13 kg paraffin wax to store the excess heat of the daytime. The paraffin wax modules were first crushed into smaller pieces and melted using electric stove and finally poured into the container through the PCM filling hole as presented in Figure 5.7 (c).

Figure 5.7 (a) Placement of PCM container inside drying chamber, (b) PCM container, (c) filling process

5.4.4 Construction of Supporter Structure

The supporting structure were prepared using welding process to hold the wooden casing of the collector and drying chamber. It provides the rigidity and desired inclination to the solar radiations. The collector is mounted on a 2.08 m × 1.04 m frame constructed from square metal pipe and angle iron at an angle equal with the collector tilt angle of 24° as shown in Figure 5.3 (a). The drying chamber is placed on a 1.04m× 0.804m×1.04m frame constructed from square metal pipe and angle iron as shown in Figure 5.7 (a). The whole supporting structure is painted varnish to improve its life as it always remains in the open environment.

5.5 Experimental Setup

An indirect solar dryer in forced convection mode with PCM inside the drying chamber was designed, developed, and installed at Adama Science and Technology University, Adama, Ethiopia facing south and tilted at an angle of 24°. Photograph of the complete experimental setup of the integrated solar thermal system used for the present investigation is shown in Figure 5.8.

Figure 5.8 Experimental setup of the dryer

The experimental setup consists of four foremost parts which are double pass solar air collector with baffle, blower, drying chamber and LHS unit inside drying chamber as presented in Figure 5.8. The heat source for the installed dryer is obtained from the solar air collector using air as heat transfer fluid which is derived into the collector with the help of blower connected at the inlet of the collector. A blower system provides atmospheric air into the solar air collector and helps in accelerating the heated air from solar collector to the drying chamber. To get variable flow rate in the system the speed of the blower is controlled using speed controller of the blower. Paraffin wax in the form of PCM was placed in the square containers inside the drying chamber bottom for thermal storage system. Three drying trays of same size are employed above the PCM containers in three rows in the drying chamber as demonstrated in Figure 5.7 (a).

5.6 Experimental Procedure

The experimental study was carried out for two different conditions:

i. Solar air heater without baffles
ii. Solar air heater with baffles

The first experiment is done on double pass solar air heater without baffles. Two thermocouples were placed at the inlet and outlet of the solar air heater and another thermocouple is placed in between the outlet of the first fluid pass and the inlet of the second fluid pass to measure the temperature of the air and to evaluate its performance. The second experiment was conducted to investigate the effect of baffles on the performance of solar collector while 5 kg of red chilli is loaded to dry. In this experiment baffles are placed between the base plate and the absorber plate and PCM container was placed inside drying chamber. Three thermocouples were placed inside the thermal energy storage container at different locations to measure the temperature of the PCM which determines whether the PCM is completely melted or not. Another two thermocouples are placed after PCM container and at the outlet of drying chamber as shown in Figure 5.2.

Open-air drying was also carried out while testing the solar dryer in order to compare the drying time and product quality with the drying time and product quality dried in the solar dryer. Samples of the product were weighed using a digital weighing machine in a three-hour interval to determine the moisture loss from the red chilli. In each experiment, the inlet and outlet temperature of the solar air heater, drying chamber, and temperature of air after it passes the thermal energy storage was recorded every 30 minutes interval.

5.7 Measuring Instruments

The temperature during the experiments were measured using well calibrated K-type thermocouple thermometer, based on the procedure described in APPENDIX A, at different locations of the dryer. Thermocouple wires were fixed at different locations of the prototype to measure temperature at the collector and drying chamber. The thermocouples can read values between 0 to 800 °C with an error of ±2.

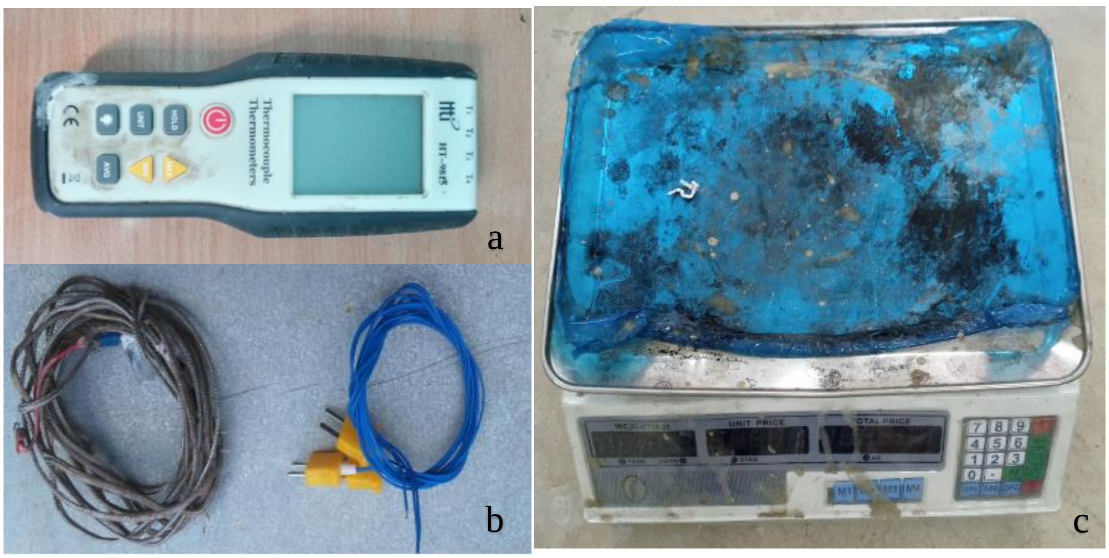

Figure 5.9 Measuring instruments (a) Thermocouple thermometer, (b) Thermocouple wire, (c) Digital weight balance

Digital weight balance with a ±0.5 g accuracy is used to measure the weight of the samples. Fig.5.9 shows the photograph of thermometer and thermocouple wires used for temperature measurement and digital weight balance.

CHAPTER SIX

RESULT AND DISCUSSION

6.1 Introduction

In this chapter, the experimental results obtained from the designed indirect solar dryer is presented. Performance of each component of the dryer and essential points that arise from the results are discussed in detail. Finally, the economic analysis of the solar dryer is presented.

6.2 Solar Radiation and Ambient Aemperature

The drying experiment was performed for five consecutive days (23-27 June 2021), starting from 9:00 h to 18:00 h. The variation in ambient temperature during testing period and the estimated monthly average hourly incident solar radiation on a tilted surface of June are shown in Figure 6.1. The ambient air temperature was in the range of 23℃ and 34 ℃ with an average of 28.9 ℃.

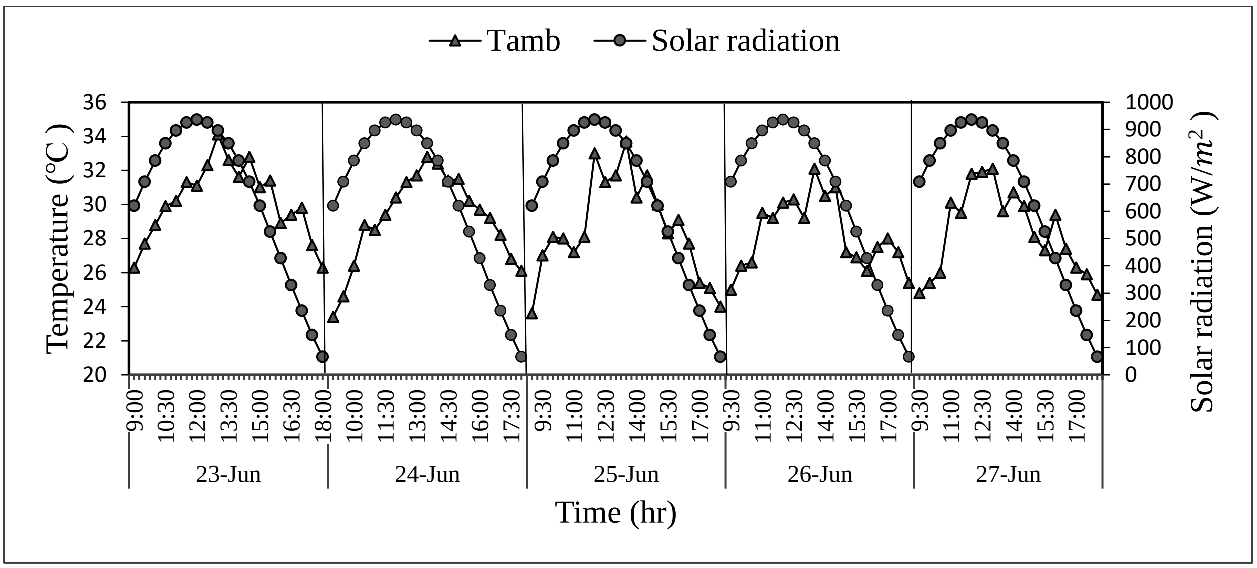

Figure 6.1 Variation of ambient temperature with time and estimated solar radiation of Adama in June.

6.3 Experimental Results of the Solar Air Heater

To investigate the performance of the double pass flat plate solar air heater, inlet (ambient) and outlet temperature of the collector were recorded in a 30 min interval. The various results obtained are presented and discussed in the following sub sections.

6.3.1 SAH Outlet Temperature Variation

Figure 6.2 exhibit the inlet and outlet temperature variations of the solar air heater with time for five consecutive days (23-27 June 2021). As the Figure illustrates, the outlet temperature of the solar air heater varied from 33.9 ℃ to 70.9 ℃ at mass flowrate of 0.018 kg/s. The outlet temperature of the solar air heater increases with increase in solar radiation intensity. The maximum outlet air temperature of the SAH was 70.9 ℃ recorded in the last day of the experiment at 13:00 h and the minimum was 33.9 ℃ recorded in the third day of the experiment at 9:00 h. A slight fluctuation was recorded in the second, third and fourth day of the experiment due to cloud cover at peak hour.

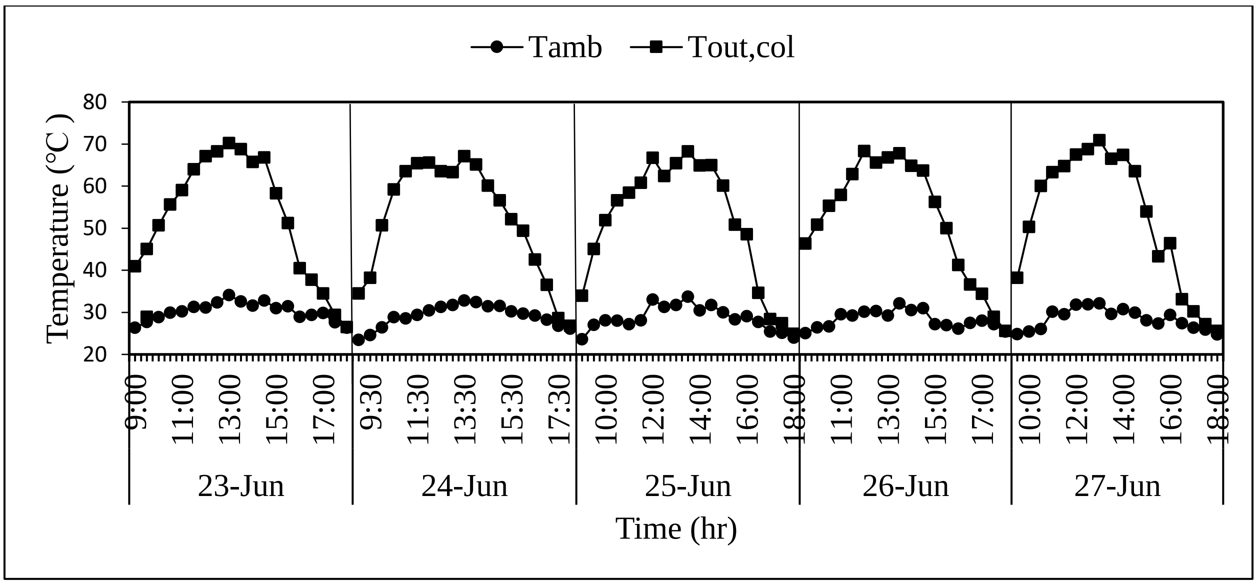

Figure 6.2 Variation of inlet and outlet temperatures of the SAH with time.

6.3.2 Useful Heat Gain and Thermal Efficiency of the SAH

The variation of average useful heat gain of the solar air heater with respect to time is illustrated in Figure 6.3. The instantaneous useful heat gain of the air is evaluated from measured inlet and outlet temperature of air at a flowrate of 0.018 kg/s. It is observed that the instantaneous useful heat gain increases with the increase in the intensity of incident solar radiation until 13:00 h and decreases when the intensity decrease. This is because useful heat gain is strongly influenced by the incident solar radiation into the collector. During the solar drying process, the average useful energy gained for the consecutive days from the collector ranged from 10.5 W to 646.9 W.

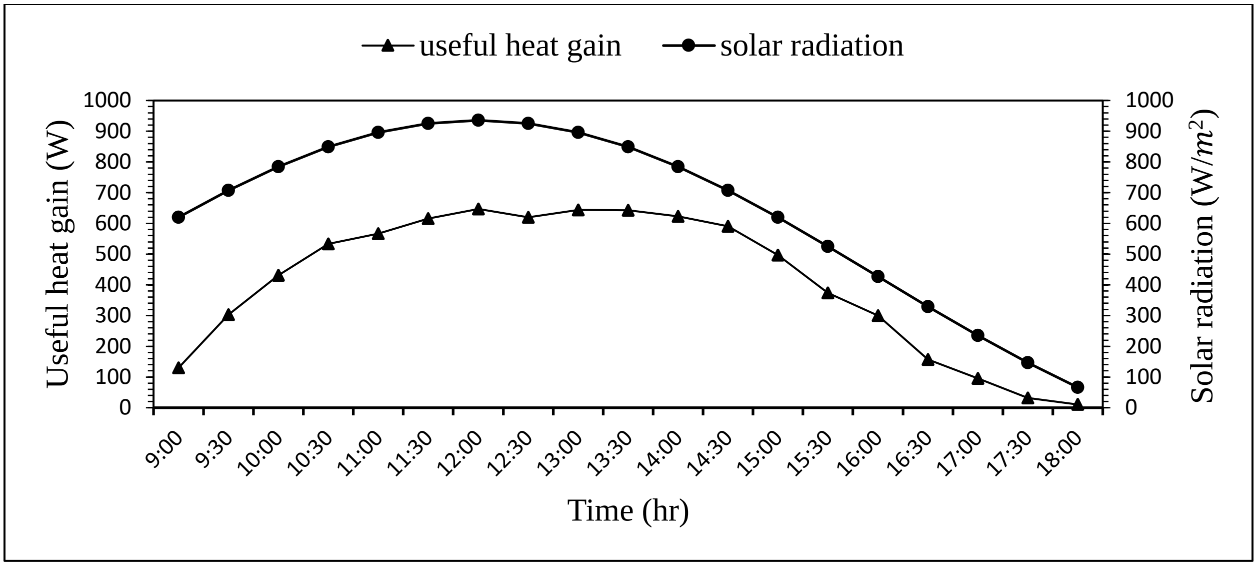

Figure 6.3 variation of average useful heat gain of five days with time.

The variation of thermal efficiency of the solar air heater with baffle as a function of time for five consecutive days are shown in Figure 6.4. The average thermal efficiencies of the SAH from day 1 to day 5 were found as 33.12 %, 35.58 %, 34.24 %, 35.94 % and 34.86, respectively. The graph showed that the instantaneous thermal efficiency increases rapidly during the time interval between 9:00 and 11.30 a.m. after that, further increase is at a slower rate relative to the previous one until noon and reaches its peak from 14:00 -15:00 h, and then it starts decreasing.

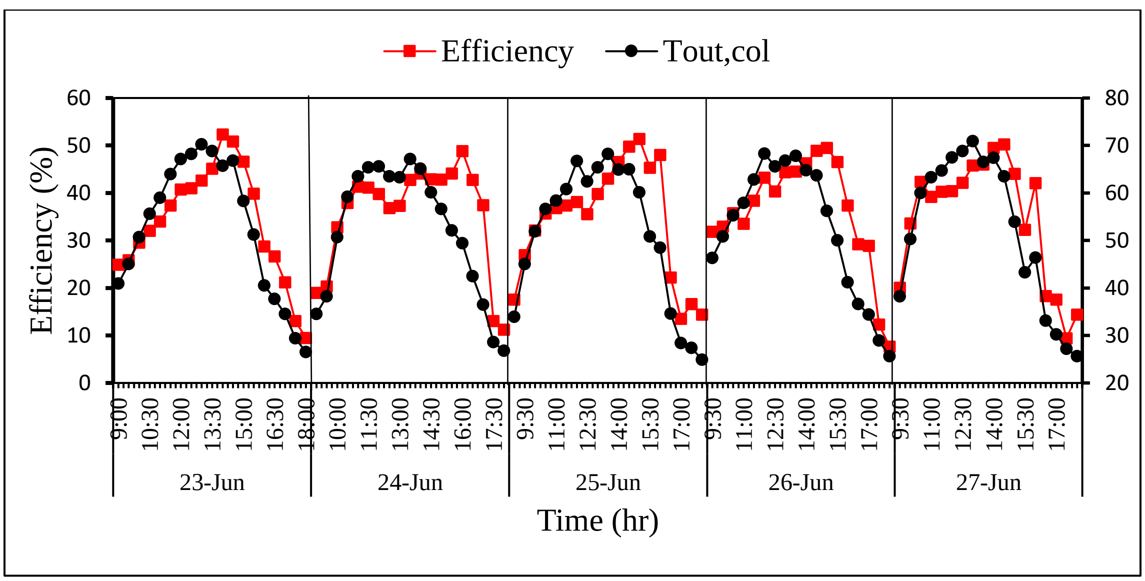

Figure 6.4 Variation in thermal efficiency of SAH for five consecutive days.

The pattern of efficiency is related with change in temperature of air in the collector and solar radiation intensity. The efficiency of the collector ranged from 9.4 % to 52.3 % with an average value of 34.8 % at a drying air flow rate of 0.018 kg/s.

6.3.3 Exergy Efficiency of the SAH

Exergy efficiency is a true measure of the performance of solar air heater which indicate the amount of heat converted into useful work. The variation of the exergy efficiency of the SAH with time for five consecutive days are depicted in Figure 6.5. The exergy efficiency is highly dependent on the outlet temperature of the collector and increases when it increases. The maximum exergy efficiency was found on the first day of the experiment which is 2.35 % at 14:30 h and the minimum is 0.012 % found at 18:00 h. The average exergy efficiency of the solar air heater was 1.58 %.

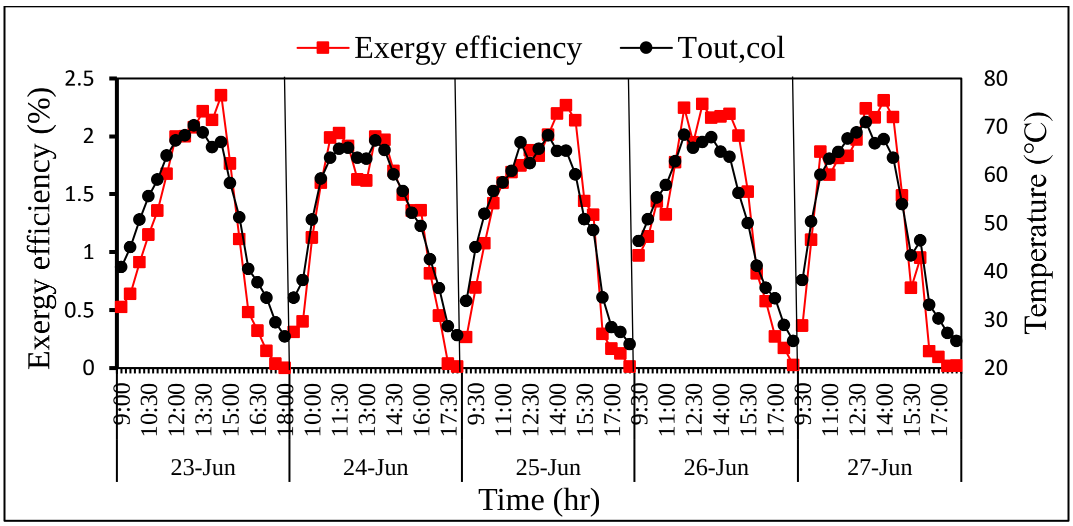

Figure 6.5 Change in exergy efficiency of the SAH with time.

6.4 Comparison of Various Performance Parameters for SAH with and without Baffles

In this sub section, effect of adding baffles on the performance of double pass SAH is investigated and discussed. Inlet and outlet temperature of the collector were recorded in 30 minutes interval for three consecutive days (16-18 June 2021) for SAH without baffles and after integrating baffles into the collector for five consecutive days (23-27 June, 2021) during the drying process.

6.4.1 Comparison of Change in Temperature of Air for SAH with and without Baffles

Figure 6.6 shows the effects of adding baffles on change in air temperature of the double pass solar air heater. The maximum change in air temperature of the SAH was 35.8 ℃ and 29.3 for with and without baffles, respectively. It is also observed that, the change in air temperature of SAH with baffles is 2.2 to 8.6 ℃ higher than that of without baffles from 10:00 to 16:00 h with an average increment of 6 ℃. This temperature increment is obtained due to more heat transfer area created by the integrated baffles in between absorber and base plate.

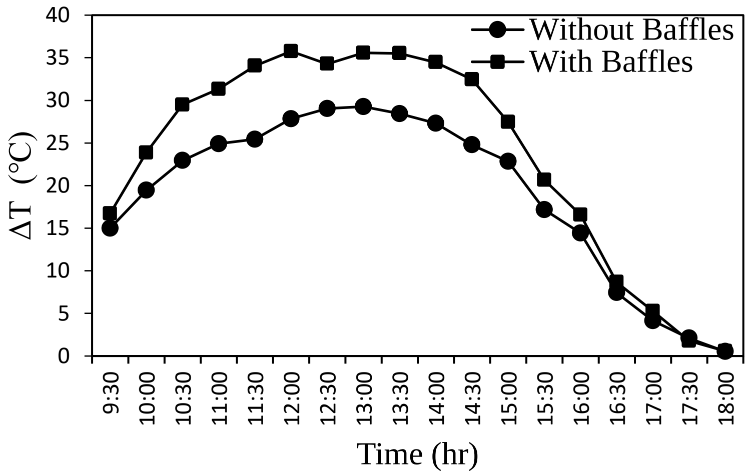

Figure 6.6 Variation of change in air temperature of SAH with and without baffles.

6.4.2 Comparison of Energy Efficiency of SAH with and without Baffles

Figure 6.7 illustrates the effect of adding baffles in the thermal efficiency of doble pass SAH.

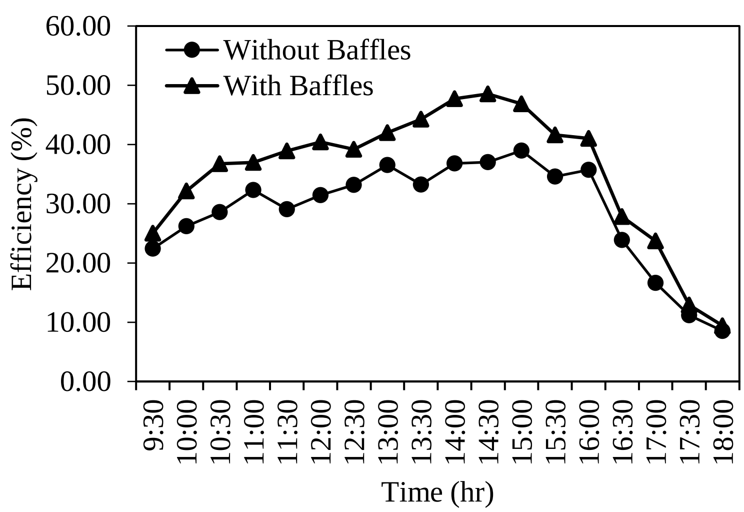

Figure 6.7 Effect of baffles on collector thermal efficiency.

Average thermal efficiency of the SAH with and without baffles were found to be 34.8 and 28.9 %, respectively. It is clearly observed that, the thermal efficiency of the double pass SAH with baffles is 3 to 11.5% higher than that of without baffles with an average value of 7%.

6.4.3 Comparison of Exergy Efficiency of SAH with and without Baffles

Figure 6.8 shows the increment in exergy efficiency of the solar collector because of baffles addition. For both cases the exergy efficiency is dependent on the intensity of solar radiation falling on the collector and maximum exergy efficiency of 2.29 % at 14:00 h and 1.68 % at 13:30 were achieved for SAH with and without baffles, respectively. It is observed that, the addition of baffles enhances the exergy efficiency of the double pass solar air heater and an average exergy value of 1.57 % and 1.04 % were found during the experimental investigation of SAH with and without baffles, respectively

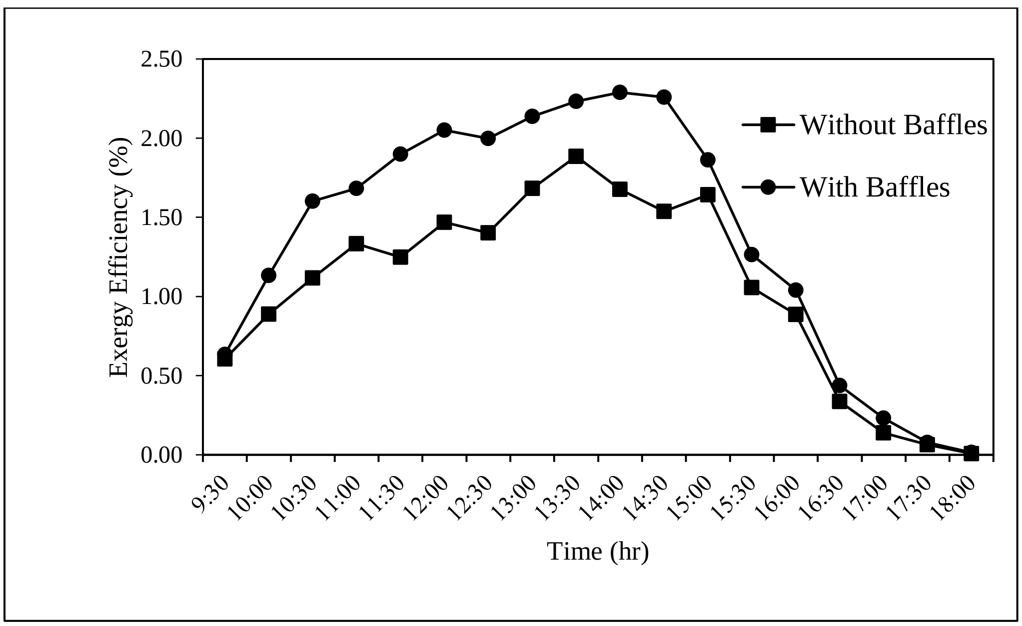

Figure 6.8 Effect of baffles on collector exergy efficiency.

6.5 Effects of Mass Flowrate on Change in Temperature and Thermal Efficiency of SAH

The change in air temperature of solar air heater is highly affected by mass flow rate. The variation of change in temperature of solar air heater for three different mass flowrates is illustrated in Figure 6.9 below. It is observed that, the change in air temperature of SAH has inverse relation with the mass flowrate. This is because the temperature of absorber plate in the SAH increases as less amount of air passes into it and vice versa. The maximum change in air temperature of solar air heater for mass flowrate of 0.0186 kg/s, 0.037 kg/s and 0.056 kg/s were 35.8 ℃, 26.7 ℃ and 21.2 ℃, respectively.

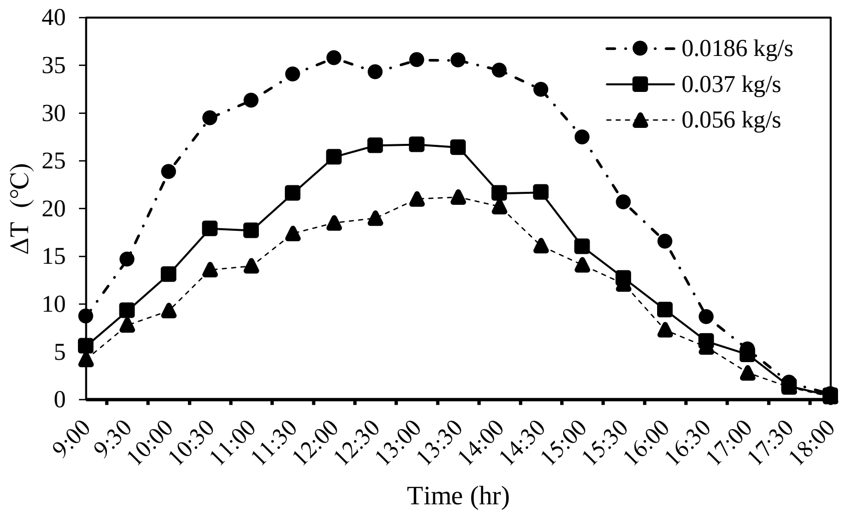

Figure 6.9 Effect of mass flowrate on change in temperature of double pass SAH with baffles.

The variation of thermal efficiency of the solar air heater with time for three different mass flowrate values, which are 0.0186 kg/s, 0.037 kg/s and 0.056 kg/s, is presented in Figure 6.10. It is clearly observed that the thermal efficiency of the SAH increases with an increased mass flow rate, this is due to the increase in useful heat gain for nearly similar heat input.

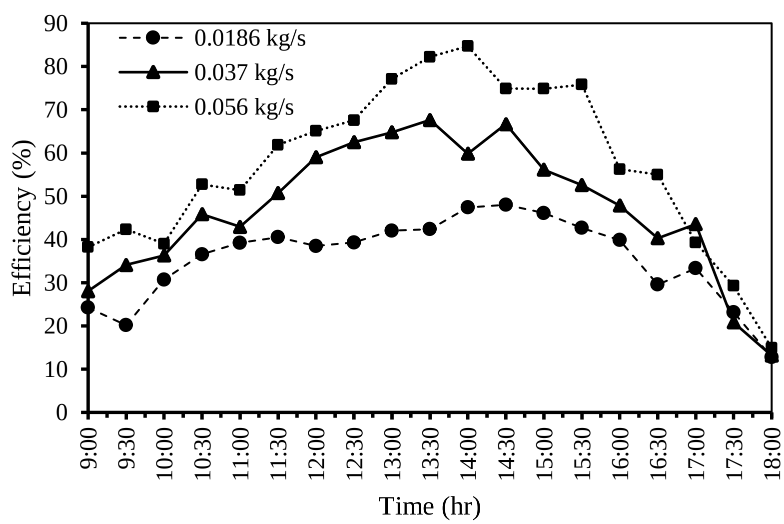

Figure 6.10 Effect of mass flowrate on energy efficiency of double pass SAH with baffles.

The thermal efficiency takes maximum values at solar noon for each mass flowrate and decreases sharply toward sunset. The average thermal efficiency of the solar air heater for each mass flowrate is showed in Figure 6.11.

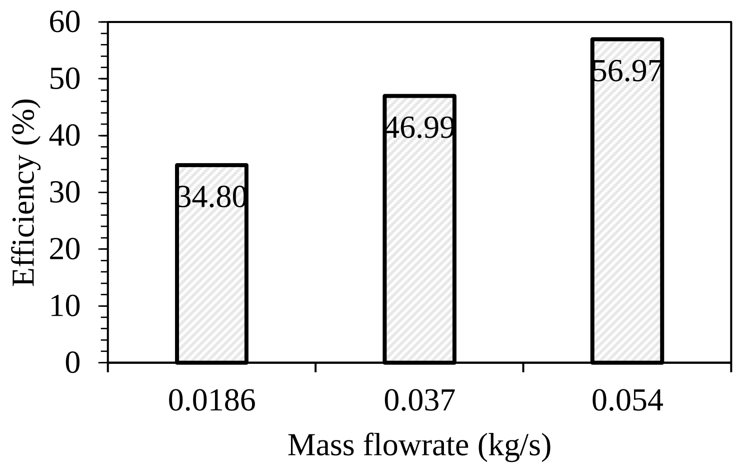

Figure 6.11 Average thermal efficiency of SAH for different mass flowrate.

6.6 Experimental Results of Dryer (Drying Chamber)

To investigate the performance of the dryer, 5 kg of fresh red chilli was loaded in the drying chamber. The experiment was conducted for five consecutive days (23-27 June, 2021) and measurements of inlet and outlet temperature of the chamber was recorded an interval of 30 minute. The dried chilli was distributed equally in to three trays and the weights of the chilli in each tray were measured till the experiment was stopped to evaluate moisture loss from the product.

6.6.1 Variation of Inlet Air Temperature of the Drying Chamber before and after PCM

The variation in inlet temperature of drying chamber and after it passes PCM storage with time for five consecutive days are depicted in Figure 6.12. It was observed that, the temperature of air before it passes the storage, which is the outlet temperature of the collector, varied with the solar radiation intensity. Thus, it increased with time and reached the maximum value between 12:00 h and 14:00 h. Afterward it started decreasing and became almost equal to the ambient temperature after 16:30 h due to very low solar radiation intensity. However, the air temperature after it passes the PCM storage, which is drying temperature, remained higher than the ambient temperature by 6–9 °C until the experiment was stopped at 18:00 h.

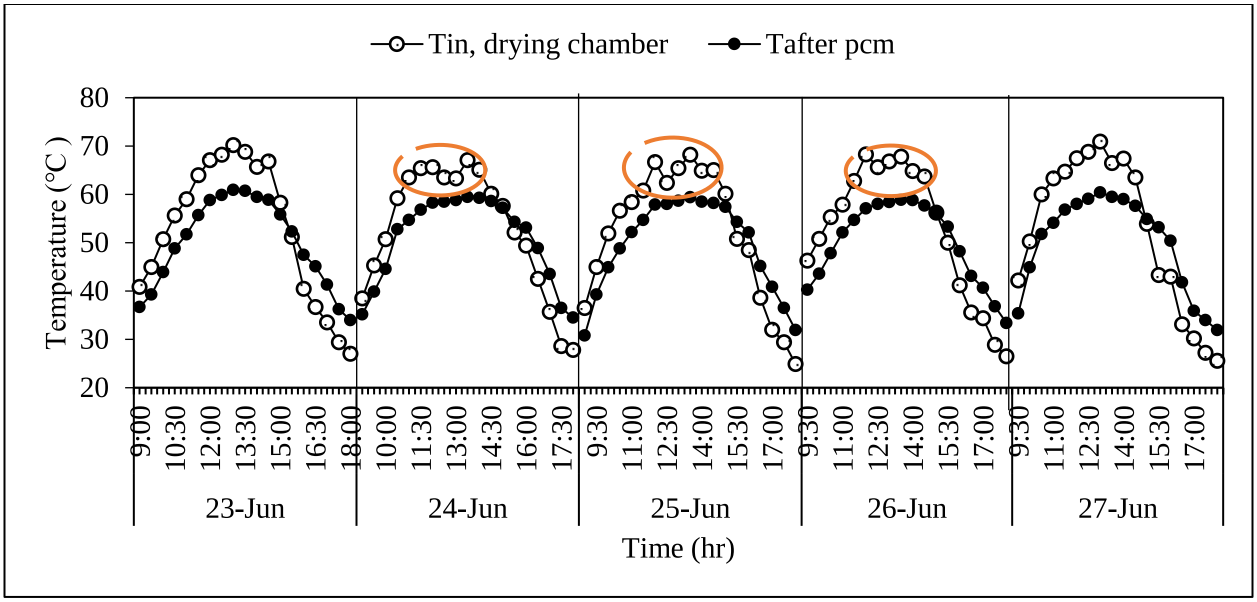

Figure 6.12 Effect of PCM on inlet air temperature of the drying chamber.

The inlet temperature of air in to chamber before it passes the storage varied from 27 ℃ to 70.9 ℃ with an average value of 52.4 ℃ whereas after it passes the PCM storage its value varied between 30.8 ℃ and 60.9 ℃ with an average value of 49.8 ℃. It was observed that the outlet air temperature of the SAH (inlet air temperature of drying chamber) fluctuated in most of the days, especially in the second, third and fourth day of the experiment, because of solar radiation intensity fluctuation between 12:00 h and 14:00 h as shown in Figure 6.13 which is harmful for the product quality. However, presence of PCM storage in the chamber diminished the fluctuation in the air temperature and supplied air at near constant temperature to the product (Trays).

6.6.2 Variation of Paraffin Wax Temperature at Different Locations

The temperature variation of paraffin wax at different locations of the rectangular storage during the charging and discharging process is shown Figure 6.13. To get information about the melting and solidifying behavior of the paraffin wax, three thermocouples were inserted inside the box in the nearest side (Tc_4), at the center (Tc_5) and farthest side (Tc_6) from the inlet of drying chamber as illustrated in Figure 5.2. As expected, it was observed that the temperature of the wax for the nearest side of the storage increased and decreased first during the charging and discharging processes, respectively. The wax temperature was increased when the inlet air temperature of the drying chamber increased and decreased when it became lower than the wax temperature.

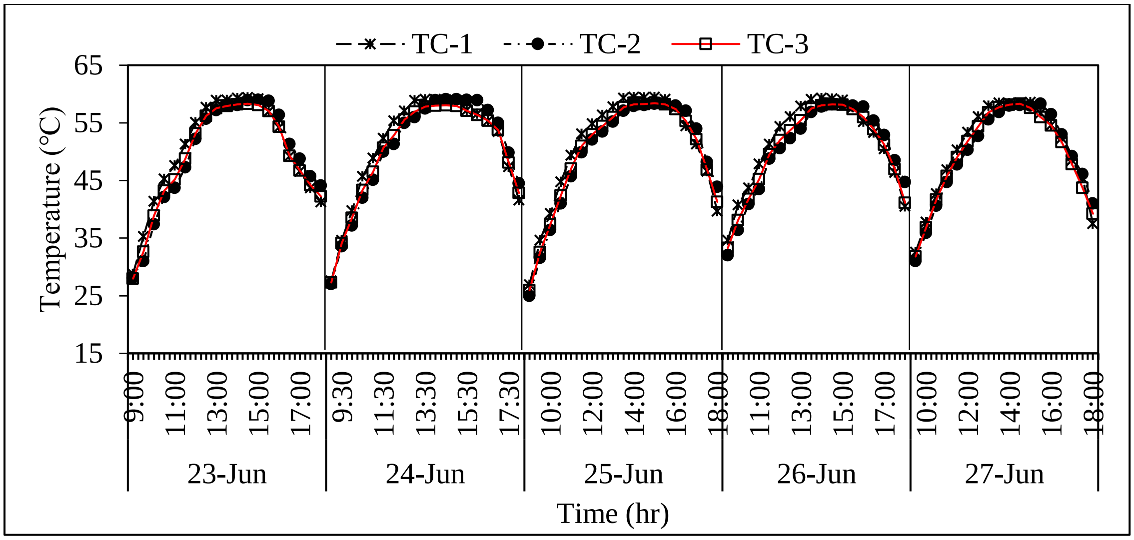

Figure 6.13 Variation in the wax temperature at different locations.

6.6.3 Variation of Inlet and Outlet Temperature of the Chamber

Figure 6.14 presents the variation in the temperature of drying air before first tray and outlet of the drying chamber for four consecutive days. The inlet temperature of the drying chamber before first tray was varied between 34.5 ℃ and 61 ℃ with an average value of 52.4 ℃ whereas the outlet temperature of air from the drying chamber varied between 30.8 ℃ and 52.2 ℃ with an average value of 42.4 ℃. It is observed that, the outlet air temperature from the drying chamber increased with increment in the number of days. This was due to the less moisture content of the chilli toward the end of the drying process. As a result, the highest and lowest outlet air temperature found in the last and first day of the experiment, respectively.

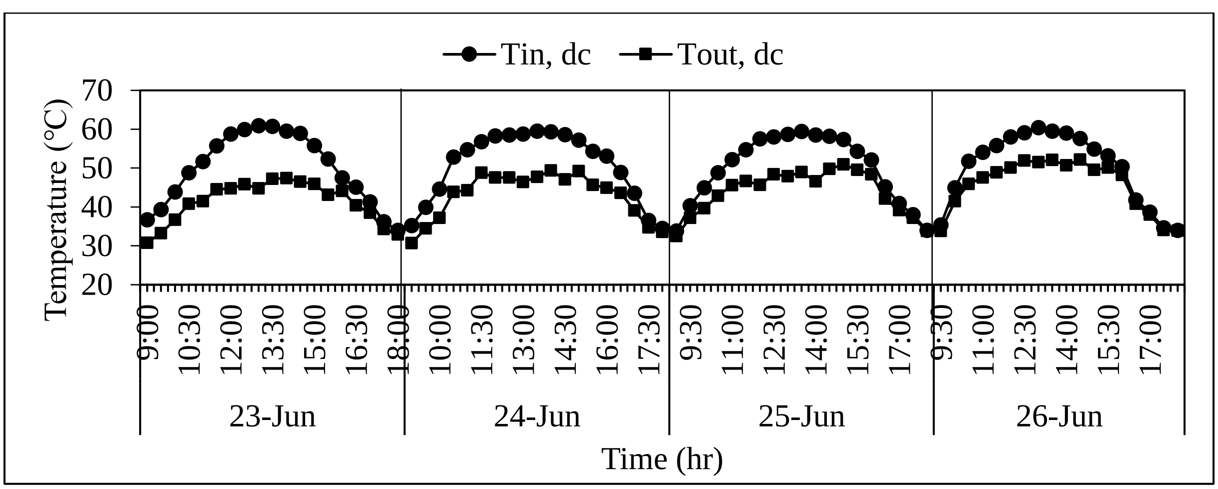

Figure 6.14 Variation of Inlet and outlet temperature of the chamber with time.

6.6.4 Heat Used by the Drying Chamber

The variation of heat used by the drying chamber for the purpose of drying red chilli for four consecutive days with time is presented in Figure 6.15.

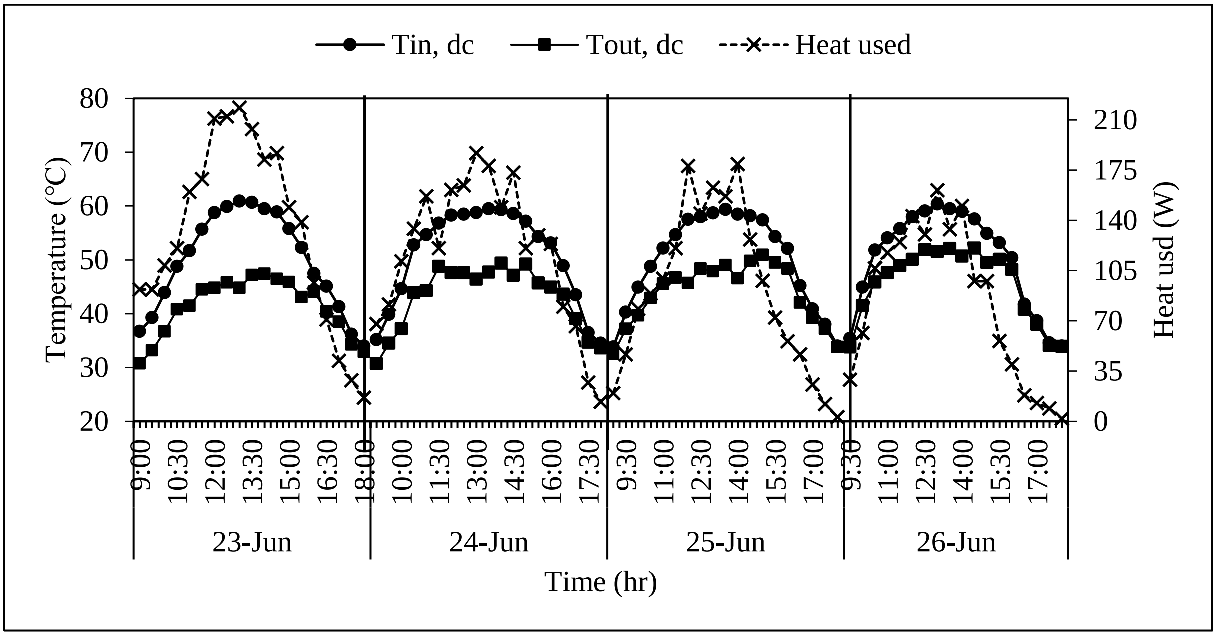

Figure 6.15 Variation of heat used by the drying chamber with time.

It is observed that, the heat used in the drying chamber increased as the inlet air temperature of the chamber increase. In addition to that, the heat used during the drying processes is higher in the first day of the experiment and decreases as the number of days increase. This was due to the less amount of moisture to be removed from the product toward the end of the drying process. The maximum heat used in the drying chamber found to be 218 W.

6.6.5 Thermal Efficiency of the Drying Chamber

The variation in thermal efficiency of the drying chamber with respect to time for four consecutive days are depicted in Figure 6.16. The thermal efficiency of the drying chamber found to be varied between 5.3% and 60.7% with an average value of 31.1%. It was noticed that, the energy efficiency decreases when the number of drying increases unlike outlet temperature of the drying chamber. This was due to the decrement in moisture content to be removed from the product toward the end of the experiment. It is also observed that, not only toward the end of the experiment, energy efficiency of the dryer of the drying chamber decreased for last hour of daily experiment due to decrease in inlet temperature of the drying chamber because of low solar radiation intensity.

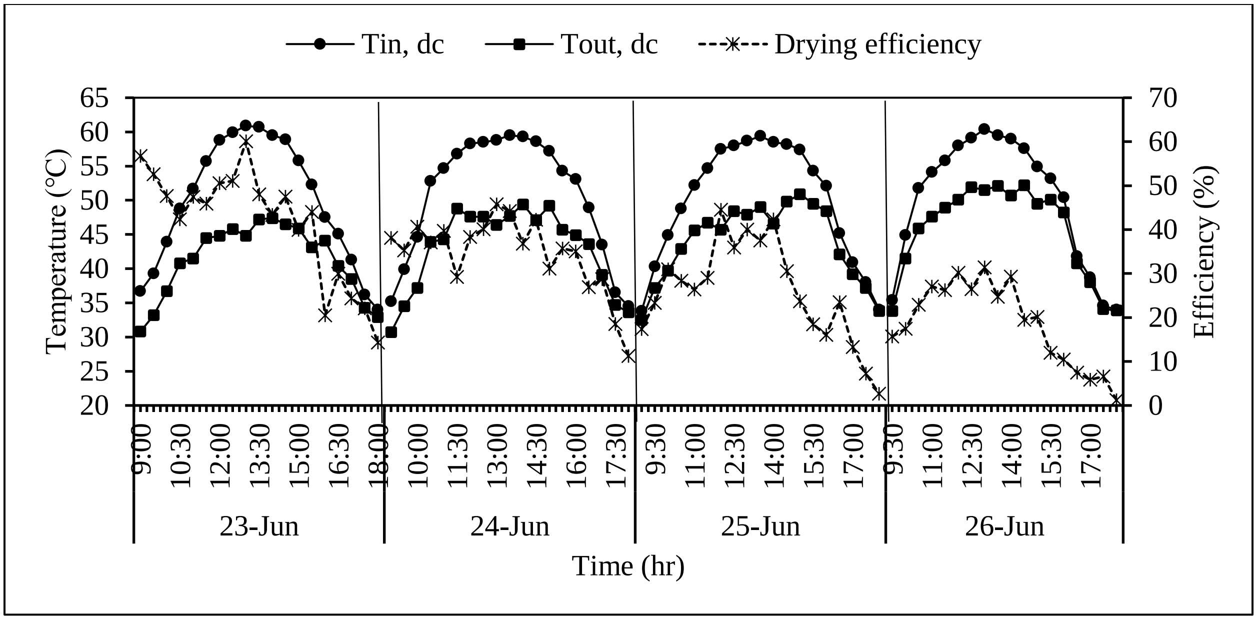

Figure 6.16 Variation in thermal efficiency of the drying chamber with time.

6.6.6 Exergy Inflow, Outflow, and Exergy Efficiency of the Drying Chamber

Variation of exergy inflow, exergy outflow and exergy efficiency of the drying chamber as a function of time are presented in Figure 6.17. The exergy inflow of the drying chamber varied in the range of 1.4 W to 20.9 W with an average value of 11.4 W and it is highly dependent on the inlet air temperature of the chamber whereas the exergy outflow of the chamber is a function of outlet air temperature of the chamber and varied between 0.5 W and 12.4 W with average value of 5.2 W. As a result, it was observed that the rate of decrement in the former is very high compared to the later one toward the end of the day since the inlet air temperature of the drying chamber is very low and the outlet air temperature did not decrease in the same manner. The exergy efficiency increased with advancing drying days. Thus, the highest exergy efficiency was observed in the last days of the drying process. This was due to the presence of low moisture content of the product (chilli) towards the end of the drying process. As expected, the exergy efficiency also increased for the last hour of drying time of the day due to decrease in exergy inflow. The exergy efficiency of the drying chamber was ranged from 16.5 % to 97.6 % with an average value of 50.7 %. Similar types of results were reported by Fudholi *et al*. (2014), Akpinar and Koçyiğit (2010), Akbulut and Durmuş (2010) and Rabha and Muthukumar (2017) for drying red chilli (43-97%), mint (34.7–87.7%), mulberry (44.4.-93.3%) and red chilli (24.3-98.9%) in the solar dryer, respectively.

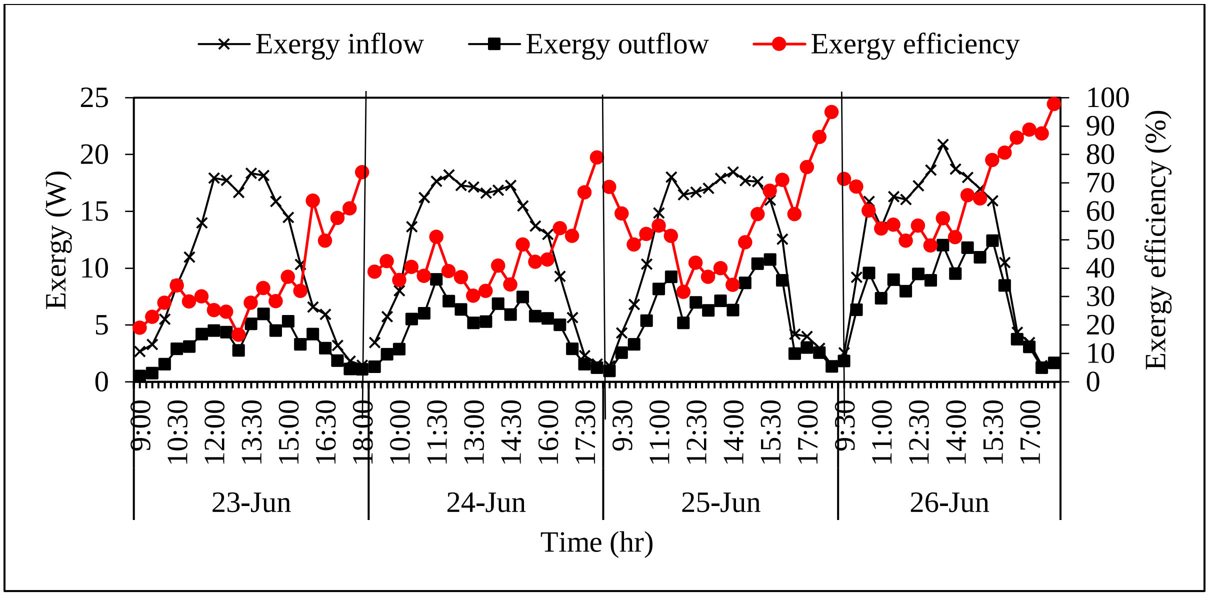

Figure 6.17 Variation in exergy inflow and outflow, and exergy efficiency of the drying chamber

6.7 Moisture Removed from the Sample

The variation in moisture of content of the dried red chilli with drying time for solar and open sun drying is presented in Figure 6.18. The moisture content of the red chilli was determined by measuring its weight and calculating the weight loss within three hours interval. The moisture content of the red chilli sample was reduced from the initial value of 81 % (w.b.) to the final value of 11.7 % (w.b.) in 29 h (four days) in the solar dryer drying and 14.32 % in 56 h in the open sun drying.

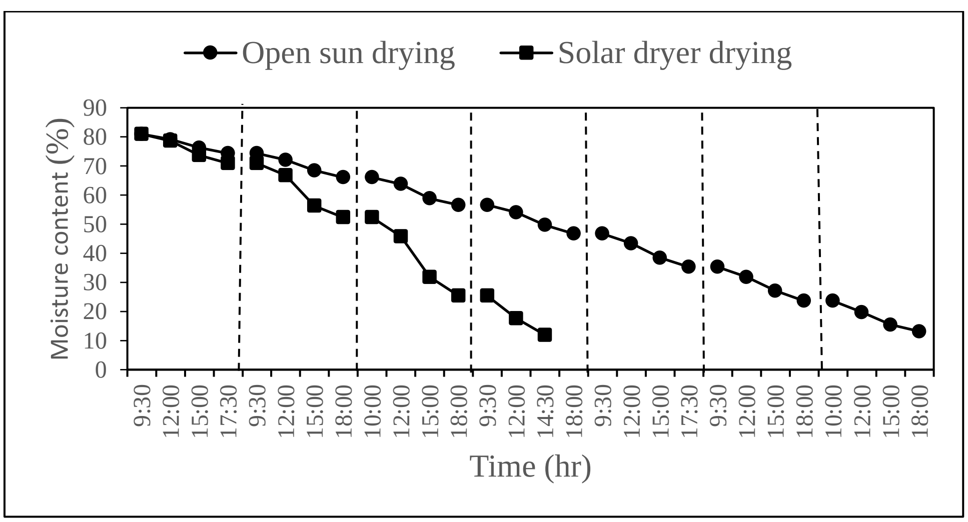

Figure 6.18 Moisture content (w.b.) variation with drying time for red chilli.

Figure 6.19 Red chilli samples (a) before drying, (b) after solar drying and (c) after sun drying

It is clearly observed that, the highest moisture removal was achieved during the first day of the drying process and the moisture removal rate decreased toward the end of drying process. This was happened due to reduction in moisture to be removed toward the end. The sun drying sample took 93.1% longer drying time in comparison with the sample dried in the developed solar dryer. Figure 6.19 (a) shows the photograph of the fresh red chilli taken before drying, and Figure 6.19 (b) and (c) shows after drying in the solar dryer and open sun, respectively. It is also observed that the colour of red chilli dried in the solar dryer is better than that of dried in open sun.

The change in the drying rates with the drying time is shown in Figure 6.20. It is observed that the drying rate of the red chilli dried in the solar dryer is faster than that of open sun drying, and it decreases continuously as the number of drying days advanced. The maximum drying rate was visible during the peak sunshine hour of the day when the solar radiation intensity and the drying air temperature were maximum. The drying rate of the red chilli dried in the solar dryer was faster than the open sun drying till the first 24 h of the drying period, and afterwards, the drying rate became low due to low moisture content compared to the dried chilli in the open sun drying.

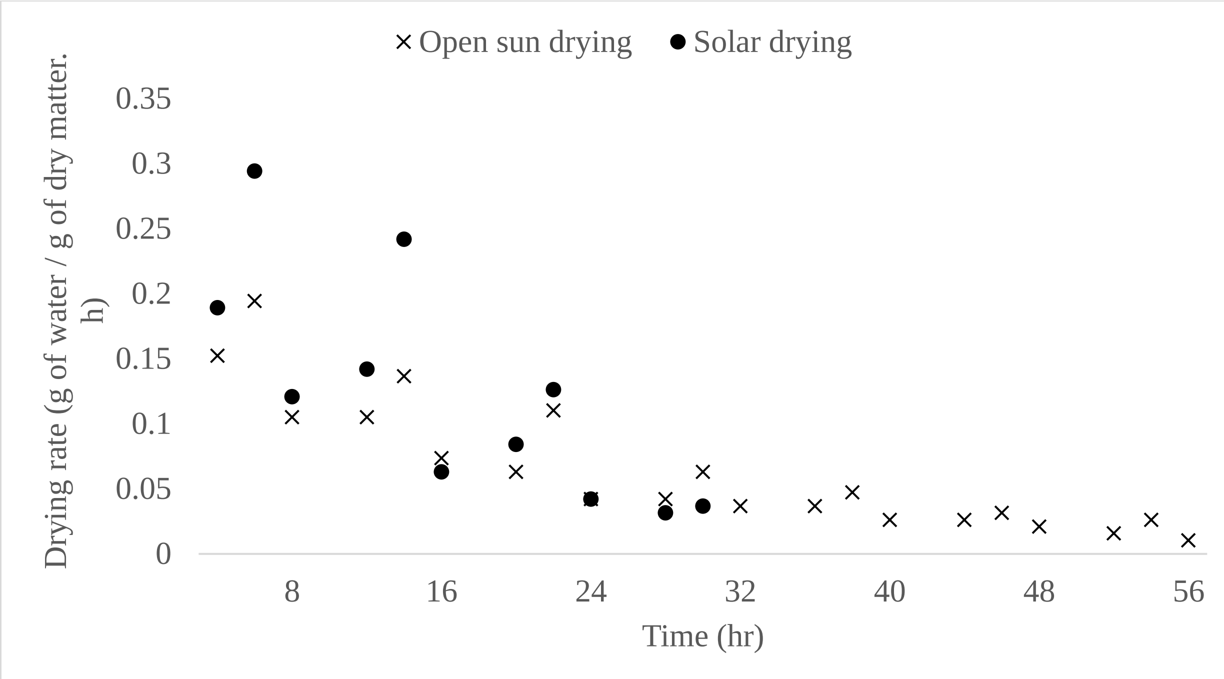

Figure 6.20 Drying rate of red chilli as a function of drying time.

The mass of evaporated moisture from 5 kg of red chilli while reducing the moisture content from an initial value of 81 % to 11.7 % in wet basis was 3.94 kg. The average intensity of the solar radiation incident on the surface of the solar collector was estimated to be 501.17 W/m^2 and the total area of the solar collector was 2 m^2. The power consumed by the blower was 50 W, and the dryer was operated daily for 8 h. The latent heat evaporation of water was calculated using equation (4.4) at an average drying air temperature of 55 °C and found to be 2.371 MJ/kg. The heat required to evaporate 3.94 kg of moisture was 9.342 MJ which is found using equation (4.3).

The total energy input to the drying system during the entire drying period was 106.7 MJ which is determined from equation (4.56). The specific energy consumption of the dryer was found to be 7.52 kWh per kg of moisture which is found by applying equation (4.55) and close to the value (6.8 kWh/kg) reported by Rabha and Muthukumar (2017) for drying red chilli. The electrical energy consumption of blower per kg of moisture removal was 0.56 kWh which was only 7.4 % of the total specific energy consumption. Thus, 92.6 % of the total energy used for drying the product in the newly developed dryer was harvested from the free and eco - friendly solar energy. The overall efficiency of the drying system is determined using Eqn. (4.59) and found to be 8.75

%. Almost similar results were reported by César *et al*. (2020), Ayyapan *et al*. (2012) and Rabha and Muthukumar (2017), for drying copra, tomato, and red chilli, respectively.

6.8 Economic Analysis

Economic analysis generally considers fixed cost, drying cost, and payback period. In economics, fixed costs are expenses that are not dependent on the level of products. Fixed cost (FC) comprised of costs of all components, including solar air heater, PCM storage unit, drying chamber with trays, insulation, blower, and manufacturing cost. Table 6.1 presents construction cost of the solar air dryer with component price.

Table 6.1 cost of components of the solar air dryer

No.	Components	Cost (Et. birr)
1	Glass	1500
2	Absorber plate steel sheet metal	1200
3	Wood and plywood	1150
4	Aluminum PCM container	750
5	PCM (paraffin wax)	1600
6	Drying chamber with trays	950
7	Blower	1800
8	Supporting structure	600
9	Manufacturing cost	1500
	Total	11,050

The annualized cost of the dryer (C_{ad}) can be calculated as (Elkhadraoui *et al*., 2015):

$$C_{ad} = C_{ac} + C_m - SV_a + C_{ec} \tag{6.1}$$

Where, C_{ac} is annual capital cost, C_m is maintenance cost, SV_a is annual salvage value and C_{ec} is annual electricity cost for running the blower.

A. Annual capital cost

The annual capital cost and salvage value are calculated using eqn (6.2) and (6.3), respectively:

$$C_{ac} = C_{ccd} F_c \tag{6.2}$$

And

$$SV_a = SV F_s \tag{6.3}$$

Where, C_{ccd} is capital cost of the dryer, F_c is capital recovery factor, SV is the salvage value of the dryer taken as 10 % of the capital cost of the dryer and F_s is the salvage fund factor.

The capital recovery factor and the salvage fund factor are given by equation (6.4) and (6.5), respectively as follow:

$$F_c = \frac{i(1+i)^n}{(1+i)^n - 1} \tag{6.4}$$

And,

$$F_s = \frac{i}{(1+i)^n - 1} \tag{6.5}$$

Where, i is the interest rate assumed to be 11 % and n is the life period assumed to be 10 years.

B. Annual electric cost of blower

The annual running cost of electricity for the dryer consumed by the blower is given by:

$$C_{ec} = P_{bl} \times t_y \times C_{ue} \tag{6.6}$$

Where, P_{bl} is the power consumed by the blower, t_y is the number of hours the blower run each year and C_{ue} the unit charge for electricity.

The cost of drying per kilogram of dried product (C_d) is then calculated by (Elkhadraoui *et al.*, 2015):

$$C_d = \frac{C_{ad}}{M_y} \tag{6.7}$$

Where, M_y is the amount of dried product removed from the solar dryer per year and defined as:

$$M_y = \frac{m_{p,b} n_{d,y}}{n_{d,b}} \tag{6.8}$$

Where, $m_{p,b}$ is the mass of the product dried per batch, $n_{d,y}$ is the number of days of operation of the dryer per year and $n_{d,b}$ is the number of days of operation of the dryer per batch.

And the cost of fresh product per kilogram of the dried product ($C_{fp,d}$) is evaluated using equation (9) as:

$$C_{fp,d} = C_{fp}\left(\frac{m_{fp}}{m_{p,b}}\right) \tag{6.9}$$

Where, C_{fp} is the cost of fresh product per kg and m_{fp} is mass of fresh product loaded in the solar dryer per batch in kg.

Therefore, the cost of 1 kg of dried product (C_{dc}) for the solar air dryer is the summation of the cost of fresh product per kilogram of the dried product ($C_{fp,d}$) and the cost of drying per kilogram of dried product (C_d). Mathematically,

$$C_{dc} = C_{fp,d} + C_d \tag{6.10}$$

The saving per kilogram of dried product (S_{kg}) in the base year due to use of the solar dryer is calculated using:

$$S_{kg} = S_p - C_{dc} \tag{6.11}$$

Where, S_p is selling price of dried product.

Then, the saving per batch (S_b) and the saving per day (S_d) in the base year are evaluated using equation (6.12) and (6.13), respectively.

$$S_b = S_{kg}\, m_{p,b} \tag{6.12}$$

$$S_d = \frac{S_b}{n_{d,b}} \tag{6.13}$$

For the life of the system, the annual savings (S_j) for drying the typical product in the j^{th} year is obtained as (Elkhadraoui *et al*., 2015):

$$S_j = S_d n_{d,y}(1 + d)^{j-1} \tag{6.14}$$

Payback period (PP)

Payback period is the investment cost per average annual net income. The returns indicate recovered invested capital of the system. It is computed as (Elkhadraoui *et al*., 2015):

$$pp = \frac{\ln\left[1 - \frac{C_{ccd}}{S_j}(i - d)\right]}{\ln\left(\frac{1 + d}{1 + i}\right)} \tag{6.15}$$

Where, d is depreciation and can be calculated by subtracting salvage value from capital cost and divide this amount by its life span (in year) and found to be 9 %.

Table 6.2 Economic analysis result of the solar dryer

No.	Particulars	Cost
1	Capital cost (ET. Birr)	11050
2	Annual capital cost (ET. Birr)	1802
3	Maintenance cost (ET. Birr)	180.2
4	Salvage value (ET. Birr)	1105
5	Annual salvage value (ET. Birr)	69.5
6	Annual electric cost (ET. Birr)	428
7	Annual cost of the dryer (ET. Birr)	2340.7
8	Number of operation days of the dryer per batch (days)	4
9	Number of operation days of the dryer per year (days)	240
10	Quantity of product dried per batch (kg)	0.95
11	Quantity of product dried per year (kg)	57
12	Cost of drying per kilogram of dried product (ET. Birr)	41
13	Cost of 1 kg of dried product (ET. Birr)	251.5
14	Saving per kilogram of dried product (ET. Birr)	48.5
15	Saving per batch (ET. Birr)	46
16	Saving per day (ET. Birr)	11.5
17	Annual savings (ET. Birr)	5994.4
18	Payback period (years) Annual savings (ET. Birr)	2.04

Using the above equations, the economic analysis of the solar dryer is presented in Table 6.2. The capital cost of the dryer is 11050 (ET. Birr) and the annual saving due to the use of the dryer and the payback period are 5994.4 (ET. Birr) and 2.04 years, respectively.

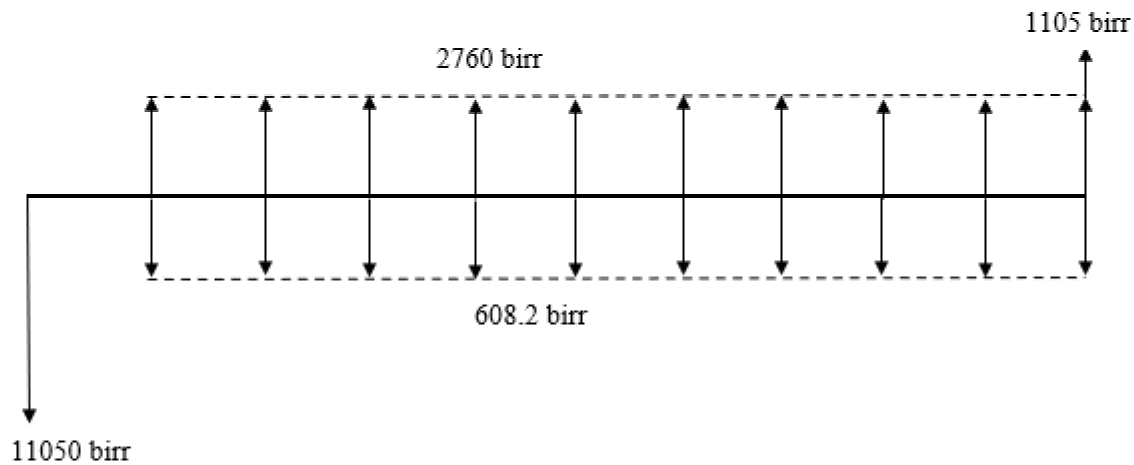

Figure 6.21 Cash flow diagram

CHAPTER SEVEN

CONCLUSIONS AND RECOMMENDATIONS

7.1 Conclusions

In this study experimental investigation and performance evaluation of a forced convection indirect solar dryer using enhanced double pass solar air heater and integrated phase change material inside drying chamber for drying of red chilli has been caried out. The components of the drying system were sized based on requirements to dry 5 kg of red chilli and constructed from locally available materials. Experimentation was conducted in three phases. In the first phase, experiment was conducted to examine double pass solar air heater without baffles. In the second phase, drying of red chilli was conducted using enhanced solar air heater (solar air heater with baffles) and integrated phase change material inside drying chamber. During this experiment, open air drying was also caried out to examine and compare drying time and product quality with the solar drying. In the third phase, effects of mass flowrate on the performance of double pass solar air heater were investigated experimentally. Data were recorded for calculation purpose which include measurement of temperature and weighting of dried sample and the energy and exergy analysis were conducted to evaluate the performance of the components of the dryer and overall drying system. Lastly, economic analysis of the drying system has been conducted. The following conclusions are drawn from the experimental investigation of the drying system:

- The change in air temperature of the SAH with baffles was 2.2 to 8.6 ℃ higher than that of SAH without baffles with an average increment of 6 ℃ and the thermal efficiency of the double pass SAH with baffles was 3 to 11.5 % higher than that of without baffles with an average value of 7 %.
- The addition of baffles enhances the exergy efficiency of the double pass solar air heater from an average exergy value of 1.04 % to 1.57 % and for both cases the exergy efficiency is dependent on the intensity of solar radiation falling on the collector.
- The change in air temperature of solar air heater is highly affected by mass flow rate and decreases when the mass flowrate increases. Unlike change in air temperature, the thermal efficiency of the SAH increases with an increase mass flow rate. Maximum change in air temperature of 35.8 ℃, 26.7 ℃ and 21.2 ℃ and an average thermal efficiency of 34.80 %,

46.99 %, and 56.97 % were obtained for mass flowrate of 0.0186 kg/s, 0.037 kg/s and 0.056 kg/s.

- Addition of PCM storage in the drying chamber reduced the fluctuation in the air temperature and supplied air at near constant temperature to the product (Trays).
- The average thermal efficiency of the drying chamber was 31.1 %. The average exergy inflow, outflow, and exergy efficiency of the drying chamber were 11.4 W, 5.2 W, and 50.7 %, respectively.
- Drying of red chillli took 29 h and 56 h to reduce the moisture content from an initial value of 81 % (w.b.) to the final value of 11.7 % (w.b.) and 14.32 % in the solar dryer and open sun drying, respectively. The solar dryer reduced the drying time by 48.2 % and better quality was achieved. The overall efficiency of the drying system was 8.75 %.
- The specific energy consumption was 7.52 kWh per kilogram of moisture and the electrical energy consumption of the blower was 0.56 kWh per kilogram of moisture which was 7.4% of the total energy consumption and the remaining 92.6% energy was harvested from solar energy.

7.2 Recommendations

An experimental study on the performance of indirect solar dryer using double pass solar air heater with baffle and thermal energy storage inside the drying chamber for red chilli drying application has been carried out in this research. It provides a solution to reduce drying time and post-harvest losses. However, there is still a sufficient scope to improve the system performance and some of future scopes to study are

- In this study, the dryer was designed for 5 kg of red chilli. Thus, the dryer can be investigated further for large scale application.
- Since solar radiation is not available throughout the whole year, integrating other renewable energy mechanisms like biomass to support the solar drying system can be studied.
- Integrating photovoltaic source for the blower to improve the efficiency of the dryer and minimize its cost can be investigated.

REFERENCES

Abubakar, S., Umaru, S., Anafi, F. O., Abubakar, A. S., & Kulla, D. M. (2018). Design and performance evaluation of a mixed-mode solar crop dryer. *FUOYE J. Eng. Technol*, *3*, 22-26.

Aghbashlo, M., Mobli, H., Rafiee, S., & Madadlou, A. (2013). A review on exergy analysis of drying processes and systems. *Renewable and Sustainable Energy Reviews*, *22*, 1-22.

Akarslan, F. (2012). Solar-energy drying systems. *Modeling and Optimization of Renewable Energy Systems*, 1-20.

Akbulut, A., & Durmuş, A. (2010). Energy and exergy analyses of thin layer drying of mulberry in a forced solar dryer. *Energy*, *35*(4), 1754-1763.

Akpinar, E. K., & Koçyiğit, F. (2010). Energy and exergy analysis of a new flat-plate solar air heater having different obstacles on absorber plates. *Applied energy*, *87*(11), 3438-3450.

Alam, T., & Kim, M. H. (2017). Performance improvement of double-pass solar air heater–A state of art of review. *Renewable and Sustainable Energy Reviews*, *79*, 779-793.

Aldabbagh, L. B. Y., Egelioglu, F., & İlkan, M. (2010). Single and double pass solar air heaters with wire mesh as packing bed. *Energy*, *35*(9), 3783-3787.

Alghoul, M. A., Sulaiman, M. Y., Azmi, B. Z., & Wahab, M. A. (2005). Review of materials for solar thermal collectors. *Anti-Corrosion methods and materials*.

Ali, S., & Deshmukh, S. P. (2020). An overview: Applications of thermal energy storage using phase change materials. *Materials Today: Proceedings*, *26*, 1231-1237.

Al-Juamily, K. E., Khalifa, A. J. N., & Yassen, T. A. (2007). Testing of the performance of a fruit and vegetable solar drying system in Iraq. *Desalination*, *209*(1-3), 163-170.

Amer, B. M., Gottschalk, K., & Hossain, M. A. (2018). Integrated hybrid solar drying system and its drying kinetics of chamomile. *Renewable Energy*, *121*, 539-547.

Asl, J. H., Behbahani, L., & Azizi, A. (2017). Evaluation and comparing of natural and forced solar dryer for mint drying in Khuzestan province. *Journal of Agricultural Machinery*, *7*(1).

Ayyappan, S., & Mayilsamy, K. (2012). Solar tunnel drier with thermal storage for drying of copra. International journal of energy technology and policy, 8(1), 3-13.

Bahrehmand, D., Ameri, M., & Gholampour, M. (2015). Energy and exergy analysis of different solar air collector systems with forced convection. *Renewable Energy*, *83*, 1119-1130.

Bakari, R. (2018). Heat transfer optimization in air flat plate solar collectors integrated with baffles. *Journal of Power and Energy Engineering*, *6*(01), 70.

Bakari, R., Minja, R. J., & Njau, K. N. (2014). Effect of glass thickness on performance of flat plate solar collectors for fruits drying. *Journal of energy*, *2014*.

Bal, L. M., Satya, S., & Naik, S. N. (2010). Solar dryer with thermal energy storage systems for drying agricultural food products: A review. *Renewable and Sustainable Energy Reviews*, *14*(8), 2298-2314.

Baniasadi, E., Ranjbar, S., & Boostanipour, O. (2017). Experimental investigation of the performance of a mixed-mode solar dryer with thermal energy storage. *Renewable Energy*, *112*, 143-150.

Banout, J., Ehl, P., Havlik, J., Lojka, B., Polesny, Z., & Verner, V. (2011). Design and performance evaluation of a Double-pass solar drier for drying of red chilli (Capsicum annum L.). *Solar energy*, *85*(3), 506-515.

Bekele, A., Mishra, M., & Dutta, S. (2014). Performance characteristics of solar air heater with surface mounted obstacles. *Energy conversion and management*, *85*, 603-611.

Bhardwaj, A. K., Chauhan, R., Kumar, R., Sethi, M., & Rana, A. (2017). Experimental investigation of an indirect solar dryer integrated with phase change material for drying valeriana jatamansi (medicinal herb). *Case studies in thermal engineering*, *10*, 302-314.

Bolaji, B. O., & Olalusi, A. P. (2008). Performance evaluation of a mixed-mode solar dryer.

Bradford, K. J., Dahal, P., Van Asbrouck, J., Kunusoth, K., Bello, P., Thompson, J., & Wu, F. (2020). The dry chain: Reducing postharvest losses and improving food safety in humid climates. *Food Industry Wastes*, 375-389.

Castillo-Téllez, M., Pilatowsky-Figueroa, I., López-Vidaña, E. C., Sarracino-Martínez, O., & Hernández-Galvez, G. (2017). Dehydration of the red chilli (Capsicum annuum L., costeño) using an indirect-type forced convection solar dryer. *Applied Thermal Engineering*, *114*, 1137-1144.

Cengel, Y. A., Boles, M. A., & Kanoglu, M. (2011). *Thermodynamics: an engineering approach* (Vol. 5, p. 445). New York: McGraw-hill.

César, L. V. E., Lilia, C. M. A., Octavio, G. V., Isaac, P. F., & Rogelio, B. O. (2020). Thermal performance of a passive, mixed-type solar dryer for tomato slices (Solanum lycopersicum). *Renewable Energy*, *147*, 845-855.

Chamoli, S., Chauhan, R., Thakur, N. S., & Saini, J. S. (2012). A review of the performance of double pass solar air heater. *Renewable and Sustainable Energy Reviews*, *16*(1), 481-492.

Chaouch, W. B., Khellaf, A., Mediani, A., Slimani, M. E. A., Loumani, A., & Hamid, A. (2018). Experimental investigation of an active direct and indirect solar dryer with sensible heat storage for camel meat drying in Saharan environment. *Solar Energy*, *174*, 328-341.

Das, M., & Akpinar, E. K. (2020). Determination of thermal and drying performances of the solar air dryer with solar tracking system: Apple drying test. *Case Studies in Thermal Engineering*, *21*, 100731.

Devahastin, S., & Pitaksuriyarat, S. (2006). Use of latent heat storage to conserve energy during drying and its effect on drying kinetics of a food product. *Applied thermal engineering*, *26*(14-15), 1705-1713.

Dincer, I., & Rosen, M. A. (2011). *Thermal energy storage systems and applications*. John Wiley & Sons.

Duffie, J. A., & Beckman, W. A. (1980). Solar engineering of thermal processes (p. 16591). New York: Wiley.

Eke, A. B., & Arinze, E. A. (2011). Natural convection mud type solar dryers for rural farmers. *Nigerian Journal of Technological Development*, *8*(2), 92-108.

El Khadraoui, A., Bouadila, S., Kooli, S., Farhat, A., & Guizani, A. (2017). Thermal behavior of indirect solar dryer: Nocturnal usage of solar air collector with PCM. *Journal of cleaner production*, *148*, 37-48.

ELkhadraoui, A., Kooli, S., Hamdi, I., & Farhat, A. (2015). Experimental investigation and economic evaluation of a new mixed-mode solar greenhouse dryer for drying of red pepper and grape. *Renewable energy*, *77*, 1-8.

El-Khawajah, M. F., Aldabbagh, L. B. Y., & Egelioglu, F. (2011). The effect of using transverse fins on a double pass flow solar air heater using wire mesh as an absorber. *Solar energy*, *85*(7), 1479-1487.

El-Sebaii, A. A., Aboul-Enein, S., Ramadan, M. R. I., & El-Gohary, H. G. (2002). Experimental investigation of an indirect type natural convection solar dryer. *Energy conversion and management*, *43*(16), 2251-2266.

Esen, H. (2008). Experimental energy and exergy analysis of a double-flow solar air heater having different obstacles on absorber plates. *Building and Environment*, *43*(6), 1046-1054.

Forson, F. K., Nazha, M. A. A., Akuffo, F. O., & Rajakaruna, H. (2007). Design of mixed-mode natural convection solar crop dryers: Application of principles and rules of thumb. *Renewable energy*, *32*(14), 2306-2319.

Fudholi, A., Sopian, K., Yazdi, M. H., Ruslan, M. H., Gabbasa, M., & Kazem, H. A. (2014). Performance analysis of solar drying system for red chili. *Solar Energy*, *99*, 47-54.

Fufa, N., Abera, G., & Etissa, E. (2019). Agronomic and economic performance of hot pepper (Capsicum annuum L.) in response to blended fertilizer supply at Asossa, Western Ethiopia. *International Journal of Plant & Soil Science*, 1-11.

Gbaha, P., Andoh, H. Y., Saraka, J. K., Koua, B. K., & Toure, S. (2007). Experimental investigation of a solar dryer with natural convective heat flow. *Renewable energy*, *32*(11), 1817-1829.

Gebretsadik, M. (2016). Reducing land degradation and farmers’ vulnerability to climate change in the highland dry areas of north-western Ethiopia.

Goud, M., Reddy, M. V. V., Chandramohan, V. P., & Suresh, S. (2019). A novel indirect solar dryer with inlet fans powered by solar PV panels: drying kinetics of Capsicum Annum and Abelmoschus esculentus with dryer performance. *Solar Energy*, *194*, 871-885.

Gunjo, D. G. (2018). Thermal Analysis of Solar Flat Plate Collector Coupled with Heat Storage (Doctoral dissertation).

Gupta, S., Sharma, S., Mittal, T., Jindal, S., & Gupta, S. (2018). Effect of Different Drying Techniques on The Quality of Red Chilli Powder. *Indian Journal of Ecology*, *46*(2), 402-405.

Hamdi, I., Kooli, S., & Guizani, A. (2019). Drying of red pepper slices in a solar greenhouse dryer and under open sun: Experimental and mathematical investigations. *Innovative food science & emerging technologies*.

Ikem, I. A., Ibeh, M. I., & John, U. (2017). Estimating the efficiency of okra drying mixed-mode solar dryer. *International Journal of Engineering Research*, *6*(5), 250-254.

Ilori, T. A., Raji, A. O., & Kilanko, O. O. (2018). Some physical properties of selected vegetable. *Journal of Agricultural and Veterinary Sciences*, *2*, 101-109.

Jafarkazemi, F., & Ahmadifard, E. (2013). Energetic and exergetic evaluation of flat plate solar collectors. *Renewable energy*, *56*, 55-63.

Kabeel, A. E., Hamed, M. H., Omara, Z. M., & Kandeal, A. W. (2017). Solar air heaters: Design configurations, improvement methods and applications–A detailed review. *Renewable and Sustainable Energy Reviews*, *70*, 1189-1206.

Kaleemullah, S., & Kailappan, R. (2005). Drying kinetics of red chillies in a rotary dryer. *Biosystems Engineering*, *92*(1), 15-23.

Khalifa, A. J. N., Al-Dabagh, A. M., & Al-Mehemdi, W. M. (2012). An experimental study of vegetable solar drying systems with and without auxiliary heat. *International Scholarly Research Notices*, *2012*.

Koca, A., Oztop, H. F., Koyun, T., & Varol, Y. (2008). Energy and exergy analysis of a latent heat storage system with phase change material for a solar collector. *Renewable Energy*, *33*(4), 567-574.

Kulkarni, K., & Kim, K. Y. (2016). Comparative study of solar air heater performance with various shapes and configurations of obstacles. *Heat and Mass Transfer*, *52*(12), 2795-2811.

Kumar, A., & Kim, M. H. (2017). Solar air-heating system with packed-bed energy-storage systems. *Renewable and Sustainable Energy Reviews*, *72*, 215-227.

Kumar, M., Sansaniwal, S. K., & Khatak, P. (2016). Progress in solar dryers for drying various commodities. *Renewable and Sustainable Energy Reviews*, *55*, 346-360.

Kumar, P., & Singh, D. (2020). Advanced technologies and performance investigations of solar dryers: A review. *Renewable Energy Focus*.

Lakshmi, D. V. N., Muthukumar, P., & Nayak, P. K. (2021). Experimental investigations on active solar dryers integrated with thermal storage for drying of black pepper. *Renewable Energy*, *167*, 728-739.

Lingayat, A. B., Chandramohan, V. P., Raju, V. R. K., & Meda, V. (2020). A review on indirect type solar dryers for agricultural crops–Dryer setup, its performance, energy storage and important highlights. *Applied Energy*, *258*, 114005.

Lingayat, A., Chandramohan, V. P., & Raju, V. R. K. (2017). Design, development and performance of indirect type solar dryer for banana drying. *Energy Procedia*, *109*, 409-416.

Mengesha, T. T. (2020). Performance Evaluation of forced Convection solar dryer under Jimma condition. *International Journal of Science and Research Publications*, 10(6), 264-274.

Menya, E., & Komakech, A. J. (2013). Investigating the effect of different loading densities on selected properties of dried coffee using a GHE dryer. *Agricultural Engineering International: CIGR Journal*, *15*(3), 231-237.

Ministry of Water Irrigation and Energy (MoWIE), (2017) “Ethiopian National Energy Policy (ENEP)” retrieved from http://www.lse.ac.uk/ wp content/uploads/laws.pdf

Miró, L., Barreneche, C., Ferrer, G., Solé, A., Martorell, I., & Cabeza, L. F. (2016). Health hazard, cycling and thermal stability as key parameters when selecting a suitable phase change material (PCM). *Thermochimica acta*, *627*, 39-47.

Mohana, Y., Mohanapriya, R., Anukiruthika, T., Yoha, K. S., Moses, J. A., & Anandharamakrishnan, C. (2020). Solar dryers for food applications: Concepts, designs, and recent advances. *Solar Energy*, *208,* 321-344.

Mohanraj, M., & Chandrasekar, P. (2009). Performance of a forced convection solar drier integrated with gravel as heat storage material for chili drying. *Journal of Engineering Science and technology*, *4*(3), 305-314.

Montero, I., Blanco, J., Miranda, T., Rojas, S., & Celma, A. R. (2010). Design, construction, and performance testing of a solar dryer for agroindustrial by-products. *Energy Conversion and Management*, *51*(7), 1510-1521.

Mursalim, S., & Dewi, Y. S. (2002). Drying of cashew nut in shell using solar dryer. *Science & Technology*, *3*(2), 25-33.

Musembi, M. N., Kiptoo, K. S., & Yuichi, N. (2016). Design and analysis of solar dryer for mid-latitude region. *Energy procedia*, *100,* 98-110.

Muzathik, A. M., Nik, W. B. W., Ibrahim, M. Z., Samo, K. B., Sopian, K., & Alghoul, M. A. (2011). Daily Global Solar Radiation Estimate Based on Sunshine Hours. *International journal of mechanical and materials engineering*, *6*(1), 75-80.

Oberoi, H. S., Ku, M. A., Kaur, J., & Baboo, B. (2005). Quality of red chilli variety as affected by different drying methods. *Journal of Food Science and Technology-Mysore*, *42*(5), 384-387.

Pardhi, C. B., & Bhagoria, J. L. (2013). Development and performance evaluation of mixed-mode solar dryer with forced convection. *International journal of energy and environmental engineering*, *4*(1), 1-8.

Patil, R., & Gawande, R. (2016). Comparative analysis of cabinet solar dryer in natural and forced convection mode for tomatoes. *Int. J Res Sci Innov (IJRSI)*, *3*(7).

Pramanik, R. N., Sahoo, S. S., Swain, R. K., Mohapatra, T. P., & Srivastava, A. K. (2017). Performance analysis of double pass solar air heater with bottom extended surface. *Energy procedia*, *109*, 331-337.

Rabha, D. K., & Muthukumar, P. (2017). Performance studies on a forced convection solar dryer integrated with a paraffin wax–based latent heat storage system. *Solar Energy*, *149*, 214-226.

Rabha, D. K., Muthukumar, P., & Somayaji, C. (2017). Energy and exergy analyses of the solar drying processes of ghost chilli pepper and ginger. *Renewable Energy*, *105*, 764-773.

Rakshamuthu, S., Jegan, S., Benyameen, J. J., Selvakumar, V., Anandeeswaran, K., & Iyahraja, S. (2021). Experimental analysis of small size solar dryer with phase change materials for food preservation. *Journal of Energy Storage*, *33*, 102095.

Ramadan, M. R. I., El-Sebaii, A. A., Aboul-Enein, S., & El-Bialy, E. (2007). Thermal performance of a packed bed double-pass solar air heater. *Energy*, *32*(8), 1524-1535.

Ramani, B. M., Gupta, A., & Kumar, R. (2010). Performance of a double pass solar air collector. *Solar energy*, *84*(11), 1929-1937.

Ravi, R. K., & Saini, R. P. (2016). A review on different techniques used for performance enhancement of double pass solar air heaters. *Renewable and Sustainable Energy Reviews*, *56*, 941-952.

Sahar, N., Arif, S., Iqbal, S., Afzal, Q. U. A., Aman, S., Ara, J., & Ahmed, M. (2015). Moisture content and its impact on aflatoxin levels in ready-to-use red chillies. *Food Additives & Contaminants: Part B*, *8*(1), 67-72.

Shalaby, S. M., & Bek, M. A. (2014). Experimental investigation of a novel indirect solar dryer implementing PCM as energy storage medium. *Energy conversion and management*, *83*, 1-8.

Shalaby, S. M., Bek, M. A., & El-Sebaii, A. A. (2014). Solar dryers with PCM as energy storage medium: A review. *Renewable and Sustainable Energy Reviews*, *33*, 110-116.

Shamekhi-Amiri, S., Gorji, T. B., Gorji-Bandpy, M., & Jahanshahi, M. (2018). Drying behaviour of lemon balm leaves in an indirect double-pass packed bed forced convection solar dryer system. *Case studies in thermal engineering*, *12*, 677-686.

Sharma, S. K., & Kalamkar, V. R. (2015). Thermo-hydraulic performance analysis of solar air heaters having artificial roughness–A review. *Renewable and sustainable energy reviews*, *41*, 413-435.

Singh, I., & Singh, S. (2018). A review of artificial roughness geometries employed in solar air heaters. *Renewable and Sustainable Energy Reviews*, *92*, 405-425.

Soares, N. M. L. (2016). Thermal energy storage with phase change materials (PCMs) for the improvement of the energy performance of buildings (Doctoral dissertation).

Solomon, G., Venkatachalam, C., Bekeleb, A., & Parthibanc, M. (2019). Optimization of Sensible Heat Storage Tank. *Journal of Information and Computational Science,* 9(11), 1325-1334.

Sonar, D. (2021). Renewable energy based trigeneration systems—technologies, challenges and opportunities. In *Renewable-Energy-Driven Future* (pp. 125-168). Academic Press.

Sukontasukkul, P., Sutthiphasilp, T., Chalodhorn, W., & Chindaprasirt, P. (2019). Improving thermal properties of exterior plastering mortars with phase change materials with different melting temperatures: paraffin and polyethylene glycol. *Advances in Building Energy Research*, *13*(2), 220-240.

Tarigan, E., & Tekasakul, P. (2005, November). A mixed-mode natural convection solar dryer with biomass burner and heat storage back-up heater. In *Proceedings of the Australia and New Zealand Solar Energy Society Annual Conference* (pp. 1-9).

Tefera, A., Endalew, W., & Fikiru, B. (2013). Evaluation and demonstration of direct solar potato dryer.

Tesfamichael, A. (2004). Experimental Analysis for Performance Evaluation of Solar Dryer. *Addis Ababa University*.

Tiwari, A. (2016). A review on solar drying of agricultural produce. *Journal of Food Processing and Technology*, *7*(9), 1-12.

Tiwari, G. N., & Tiwari, A. (2016). *Handbook of solar energy*. Singapore: Springer.

Toshniwal, U., & Karale, S. R. (2013). A review paper on solar dryer. *International Journal of Engineering Research and Applications*, *3*(2), 896-902.

Toshniwal, U., & Karale, S. R. (2013). A review paper on solar dryer. *International Journal of Engineering Research and Applications*, *3*(2), 896-902.

Tyagi, H., Agarwal, A. K., Chakraborty, P. R., & Powar, S. (2018). Introduction to applications of solar energy. In *Applications of Solar Energy* (pp. 3-10). Springer, Singapore.

Tyagi, V. V., & Buddhi, D. P. C. M. (2007). PCM thermal storage in buildings: A state of art. *Renewable and sustainable energy reviews*, *11*(6), 1146-1166.

Vengadesan, E., & Senthil, R. (2020). A review on recent developments in thermal performance enhancement methods of flat plate solar air collector. *Renewable and Sustainable Energy Reviews*, *134*, 110315.

Wang, S., & Hong, B. (2015). Optimum design of tilt angle and horizontal direction of solar collectors under Obstacle's shadow for building applications. Journal of Building Construction and Planning Research, 3(2), 60-67.

Yadav, A. S., & Thapak, M. K. (2014). Artificially roughened solar air heater: Experimental investigations. *Renewable and Sustainable Energy Reviews*, *36*, 370-411.

Yadav, S., & Kaushal, M. (2014). Exergetic performance evaluation of solar air heater having arc shape-oriented protrusions as roughness element. *Solar Energy*, *105*, 181-189.

APPENDIX A

Calibration of the Thermocouple Thermometer

A thermocouple is a sensor used to measure temperature by forming a connection between two separate metal wires. One end of the junction is called the measurement (hot) junction and the other end is called the reference (cold) junction. When there is a temperature variation in the joint, a voltage is generated, and this voltage can be converted to temperature using a thermocouple reference table or a datalogger. Thermocouples need to be calibrated to ensure the correct temperature and can be calibrated with a reference thermometer, where a temperature calibration test is performed by comparing the readings of the reference thermometer and the other thermometer. In this study, a four-channel type K thermocouple was used, and waver thermometer was used for calibration.

Figure A. 1 Thermometer calibration (a) Reference thermometer (b) K-type 4-channel thermocouple thermometer

K-type thermocouple specifications

Serial number: HT-9815

Temperature range:0-800℃

Power supply: 9V

Weight: approx. 250g

Table A. 1 Data from thermocouple during calibration.

Time	T_1(Reference thermometer) (℃)	T_2(K-type thermocouple) (℃)	Uncertainty (%) $\frac{(T1 - T2)}{T_1} * 100$
1	23.56	23.3454	0.910866
3	29.64	29.35	0.978408
5	36.86	36.5365	0.877645
7	40.47	40.1427	0.808747
9	48.735	48.399	0.689443
11	60.325	59.787	0.891836
13	65.55	65.0065	0.829138
15	69.445	69.0872	0.515228
17	73.245	72.6934	0.753089
19	77.14	76.4894	0.843402
20	78.09	77.6282	0.591369
24	85.125	84.653	0.554479
26	87.8	86.95	0.968109
28	89.15	88.4	0.841279
29	90.4	89.5	0.995575
30	92.12	91.7	0.455927
Average uncertainty (%)			0.770708

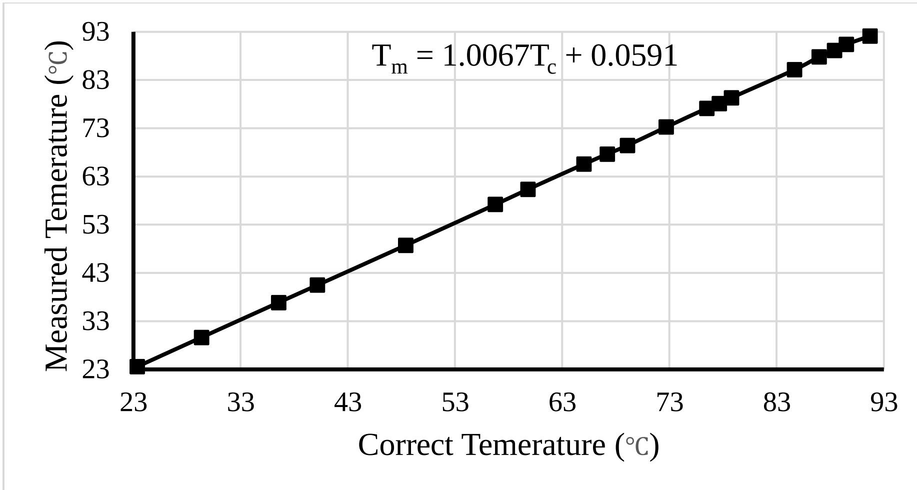

Figure A. 2 Measured vs corrected temperature